THE APPLICATION OF PUMPING INDUCED EBULLITION BASED CARBON DIOXIDE MEASUREMENTS IN NORTHERN WISCONSIN LAKE STUDIES

By

David J. Schueller

A Thesis

Submitted in partial fulfillment of the requirements of the degree

MASTER OF SCIENCE

IN

NATURAL RESOURCES

(WATER CHEMISTRY EMPHASIS)

College of Natural Resources

UNIVERSITY OF WISCONSIN

Stevens Point, Wisconsin

June 2009

APPROVED BY THE GRADUATE COMMITTEE OF:

(died on December 06, 2008)

Dr. Bryant A. Browne, Committee Chairman
Professor of Water and Soil Resources
University of Wisconsin – Stevens Point

Dr. Paul McGinley, Committee Co-Chairman
Associate Professor of Water Resources
University of Wisconsin – Stevens Point

Dr. Ronald L. Crunkilton
Professor of Water Resources
University of Wisconsin – Stevens Point

Dr. Keith W. Rice
Professor of Geography
University of Wisconsin – Stevens Point

Program Authorized to Offer Degree:
UWSP – College of Natural Resources Graduate Program
Date: Tuesday, June 16, 2009

ABSTRACT

Few lake studies have used a method that directly measures dissolved carbon dioxide (CO_2). Direct measurements are dissolved carbon dioxide estimates obtained with an analyzer or sensor, such as the headspace analysis method that uses gas collection syringes and an ion chromatography CO_2 analyzer (Cole and Caraco, 1998). In lake studies summarized in Sobek et al. (2005) for the period 1968 to 2005, the vast majority of estimates of dissolved carbon dioxide were indirectly derived from measurements of pH and dissolved inorganic carbon (DIC) or pH and acid neutralizing capacity (ANC). Traditional direct measurements are difficult to obtain. However, indirect measurements can under or overestimate the carbon dioxide concentration due to uncertainties associated with pH, DIC and ANC.

Recently, a new field based technology called pumping induced ebullition (PIE) was developed for the direct measurement of carbon dioxide (Browne, 2004a). This approach simplifies direct carbon dioxide measurements by using a process that mechanically induces ebullition of a dissolved gas in a water sample, traps the harvested gas within a collection chamber, and measures this harvested gas with an infrared CO_2 gas analyzer (IRGA).

This study explored the potential of this new technology for the collection of field based carbon dioxide data. The accuracy and precision of PIE based measurements of carbon dioxide were characterized using solutions of defined composition. PIE based carbon dioxide measurements were also made in lakes across three trophic classes (eutrophic, mesotrophic, oligotrophic). These results were

compared to traditional direct (headspace) and indirect (pH, ANC; pH, DIC) carbon dioxide measurements.

Carbon dioxide measurements made using PIE showed high precision and accuracy for defined carbon dioxide solutions from 0 to 100 μmol/liter DIC and 0 to 2610 μatm P_{CO2}. Linear regressions between PIE based [$H_2CO_3^*$] and the sodium bicarbonate concentration added to the solutions showed a close relationship with r^2 values of 1.00, RMSE ranging from 0.57 to 1.99 μmol L^{-1} [$H_2CO_3^*$], and coefficients of variation ranging from 1.29 to 4.32 %. PIE's trend with the sodium bicarbonate concentration was also close to the one-to-one line, with slope values ranging from 0.94 to 0.98. PIE based P_{CO2} also proved to be a precise, accurate, and reliable measurement for surface analyses of lake bodies ranging from zero to 2314 μatm P_{CO2} and for depth analyses of lake bodies ranging from 450 to 4250 μatm P_{CO2}.

The PIE method substantially increases the ability to measure carbon dioxide variations in time and space. In a continuous twenty-four hour diurnal pattern, PIE based P_{CO2} and DIC measurements showed the actual respiration and photosynthesis of the lake from day to night and back to day at temporal resolutions inaccessible via traditional indirect and other direct sampling methods. PIE based P_{CO2} and DIC whole lake maps also showed spatial variation of dynamic lake systems at rarely documented spatial resolution. PIE gives researchers direct measurement methods of known quality (accuracy and precision), spatial resolution, and temporal resolution for studying dissolved carbon dioxide, which were inaccessible via traditional sampling methods (indirect and other direct carbon dioxide measurement methods).

ACKNOWLEDGEMENTS

I thank my former advisor, Dr. Bryant Browne, for his guidance and advice throughout the course of this project. I also give thanks to my committee chair, Dr. Paul McGinley, for his guidance, insight, and support to complete this thesis. I also thank Dr. Ronald Crunkilton and Dr. Keith Rice for their suggestions and insight.

TABLE OF CONTENTS

LIST OF TABLES

LIST OF FIGURES

LIST OF EQUATIONS

LIST OF APPENDICES

INTRODUCTION

Dissolved carbon dioxide is an important biogeochemical component in lakes. Dissolved carbon dioxide from ground water, the atmosphere, surface water, and in-lake respiration of dissolved organic matter are important sources of carbon for within lake primary production (Portielje and Lijklema, 1995; Striegl and Michmerhuizen, 1998). Changes in dissolved carbon dioxide concentration can increase or decrease lake pH. These pH changes can lead to the precipitation (higher pH) or dissolution (lower pH) of calcium carbonate (Wetzel, 2001). The biogeochemistry of dissolved carbon dioxide in lakes may also have important consequences for greenhouse gases in the atmosphere. Recent studies of lake metabolism have shown that most of the world's lakes surface waters are supersaturated with dissolved carbon dioxide, suggesting that lakes may be a net source of carbon dioxide emission into the atmosphere (Sobek et al., 2005).

Despite carbon dioxide's central biogeochemical role, few detailed lake studies have used a method to directly measure dissolved carbon dioxide. Direct measurements are defined here as dissolved carbon dioxide estimates obtained by direct measurement with an analyzer or sensor. Direct measurements include headspace analysis that uses gas collection syringes and an ion chromatography CO_2 analyzer (Cole and Caraco, 1998), submersible autonomous moored instrument for CO_2 (SAMI-CO_2) that uses reagent and membrane based optical chemical sensors (Baehr and Degrandpre, 2004), in situ equilibration chamber (ISEC) that uses a gas-permeable membrane, equilibration chamber, and an infrared gas analyzer (IRGA)

(Sellers et al.,1995), or an automated system in Carignan (1998) that uses an equilibration chamber and IRGA. In contrast, indirect measurements are defined here as dissolved carbon dioxide estimates indirectly derived from measurements of pH and dissolved inorganic carbon (DIC) or pH and acid neutralizing capacity (ANC) as used in lake studies of Cole et al. (1994) and Kling et al. (1992).

In supersaturation studies and other lake studies, the vast majority of estimates of dissolved carbon dioxide have been indirect measurements based on pH and DIC or pH and ANC. Of 4902 lakes summarized in Sobek et al. (2005), carbon dioxide was calculated indirectly using thermodynamic equilibrium relationships for at least 1658 lakes (best estimate) based on pH and DIC measurements and for 2876 lakes (best estimate) based on pH and alkalinity or ANC measurements. In less than 439 lakes of 4902 lakes (best estimate) reported within Sobek et al. (2005) was carbon dioxide measured directly. This also holds true with studies by Anderson et al.(1997), Baehr and Degrandpre (2004), Baehr and Degrandpre (2002), Cole and Caraco (1998), Cole et al. (1994), Hope et al. (1996), Jonsson et al. (2003), Kling et al. (1992), Neumann et al. (2001), Sellers et al. (1995), Striegl and Michmerhuizen (1998), and SLU (2000) summarized in Table 1, where out of a total of 4732 lakes studied only 150 lakes had direct carbon dioxide measurements.

Indirect measurements of carbon dioxide can overestimate or underestimate dissolved carbon dioxide due to random or systematic errors in pH, DIC, or ANC (e.g., Cole et al., 1994; Herczeg et al., 1985; Lahav et al., 2001; Neumann et al., 2001; Raymond et al., 1997; Rosich, 2002). However, the nature and effect of these errors

remain somewhat ambiguously defined (Lahav et al., 2001; Rosich, 2002) and the verification of the accuracy and precision against direct measurements remains scarce.

Table 1. Number of lakes with direct and indirect measurements of carbon dioxide.

Data Source	Indirect Measurement by pH & DIC (number of lakes)	Indirect Measurement by pH & ANC or pH & Alkalinity (number of lakes)	Direct Measurement by headspace, SAMI-CO_2, or ISEC (number of lakes)
Anderson et al. (1997)			1
Baehr and Degrandpre (2004)	1*		1*
Baehr and Degrandpre (2002)	1*		1*
Cole and Caraco (1998)	1*		1*
Cole et al. (1994)	1672	59	37
Hope et al. (1996)	27*		27*
Jonsson et al. (2003)			51
Kling et al. (1992)	25*	25*	25*
Neumann et al. (2001)	3*		3*
Sellers et al. (1995)			1
Striegl and Michmerhuizan (1998)			2
SLU (2000)		2851	
subtotal	1672	2910	150
total indirectly measured lakes			4582
total directly measured lakes			150
total lakes studied			4732

*lake measured both directly and indirectly, therefore included in both counts.

Indirect measurements of dissolved carbon dioxide have been more numerous in the literature. This is mainly due to logistical impediments associated with traditional direct in-field measurements. Other factors that affect direct measurements include systematic errors and sensor drift resulting from quality of the colorimetric

indicator reagent, light input to sensor, sensor equilibration, or biological fouling (Degrandpre and Baehr, 1999; Degrandpre et al., 1995; Sellers et al., 1995).

Recently, a new field based technology called pumping induced ebullition (PIE) was developed for the direct measurement of carbon dioxide (Browne, 2004a). This approach simplifies direct carbon dioxide measurements by using a process that mechanically induces ebullition of a dissolved gas in a water sample, traps the harvested gas within a collection chamber, and measures this harvested gas with an infrared CO_2 gas analyzer (IRGA).

This new approach can directly measure carbon dioxide in real time while on a lake, stream, or river. Carbon dioxide data is recorded in real time at one record per second and stored on a data logger for archival purposes or for immediate review of the concentration on a computer display. PIE based measurements can be made continuously or in rapid succession throughout a water body at temporal and spatial resolutions inaccessible via traditional direct (headspace) and indirect (pH and DIC; pH and ANC) dissolved CO_2 measurement methods.

Additionally, this PIE based approach offers quality, time, and labor savings. This new approach avoids the systematic error associated with use of colorimetric indicator reagents, membranes, and equilibration chambers. The PIE based approach also avoids the time involved with the collection, storage, transport, and analysis of a bottle sample. The PIE based approach uses no sample analytical measurement time in the laboratory, whereas traditional direct (headspace) and indirect (pH and DIC; pH and ANC) dissolved CO_2 measurement methods involve many measurement hours.

This study explored the potential of this new technology for the collection of field based carbon dioxide data. The specific objectives were:

1.) Characterize the accuracy and precision of PIE based direct measurements of carbon dioxide using solutions of defined composition.

2.) Apply PIE based direct carbon dioxide measurements in a limited study of lakes across three trophic classes (eutrophic, mesotrophic, oligotrophic) and compare results to traditional direct and indirect carbon dioxide measurements.

3.) Explore the use of PIE measurements for developing whole lake maps of carbon dioxide concentration.

This research is presented in the four chapters that follow. The first chapter is a methods chapter. The *METHODS* chapter starts with the definitions and ideas for the main components of carbonic chemistry. The subsequent sections contain explanations of the direct (PIE; headspace) and indirect (pH and ANC; pH and DIC) dissolved carbon dioxide measurement methods used in this study. This is followed by subsections on *Other Measurement Procedures* and *Data Management, Statistics, and Graphing*.

In the *ACCURACY and PRECISION of PIE* chapter, the accuracy and precision of PIE based measurements were characterized using solutions of defined

composition. PIE based P_{CO2} and $[H_2CO_3^*]$, headspace, DIC, and ANC measurements were compared to known sodium bicarbonate concentrations. PIE based dissolved carbon dioxide measurements were also compared against headspace measurements. Subsections include the methods for the laboratory experiments, results achieved, and conclusions found.

The *TRADITIONAL LAKE STUDIES with PIE* chapter is where PIE based direct carbon dioxide measurements were applied in a limited study of lakes across three trophic classes (eutrophic, mesotrophic, oligotrophic) and compared to traditional direct and indirect carbon dioxide measurements. This is where researchers will learn the importance of how PIE based dissolved carbon dioxide measurements perform in natural systems and traditional lake studies. The first chapter section contains the methods used for the traditional lake studies. In the following chapter sections, (1) PIE based measurements were taken to have a range of carbon dioxide measurements similar to the laboratory experiments; (2) a set of replicate carbon dioxide measurements within a lake were made to investigate variations between PIE and traditional direct and indirect carbon dioxide measurements; (3) PIE based carbon dioxide measurements were compared in a traditional fifty-two lake surface water survey (one surface water sample measurement with each method at each lake); and (4) PIE based carbon dioxide measurements were compared in traditional depth profiles from two lakes. PIE based measurements were also compared against direct (headspace) and indirect (pH and ANC; pH and DIC) measurements. The last section contains the conclusions for the traditional lake studies.

The *TEMPORAL and SPATIAL RESOLUTION of PIE* chapter contains the methods, and results for the temporal and spatial lake experiments. This is where the PIE method was shown to substantially increase the ability to measure carbon dioxide variations in time and space. In a continuous twenty-four hour diurnal pattern, PIE based partial pressure of carbon dioxide (P_{CO2}) and DIC measurements showed the actual respiration and photosynthesis of the lake from day to night and back to day at temporal resolutions inaccessible via traditional indirect and other direct sampling methods. PIE based P_{CO2} and DIC whole lake maps also showed spatial variation of dynamic lake systems at spatial resolution inaccessible via traditional indirect and other direct sampling methods. Several locations on these maps indicated possible ground and/or surface water entry of dissolved carbon dioxide into the lake. These maps also showed the spatial variation of dissolved carbon dioxide over time.

METHODS

This chapter starts with the definitions and ideas for the main components of carbonic chemistry. The subsequent sections contain explanations of the direct (PIE; headspace) and indirect (pH and ANC; pH and DIC) dissolved carbon dioxide measurement methods used in this study. This is followed by subsections on *Other Measurement Procedures* and *Data Management, Statistics, and Graphing*.

Carbonate Chemistry Background

The inorganic carbon in water consists mainly of carbonic acid (H_2CO_3), aqueous carbon dioxide ($CO_{2\,(aq)}$), bicarbonate (HCO_3^-), and carbonate (CO_3^{2-}). Aqueous carbon dioxide ($CO_{2\,(aq)}$) solutions (lakes or open systems) in the presence of atmospheric gaseous carbon dioxide ($CO_{2\,(g)}$) will exchange by the following reversible relationship:

[1] $CO_{2\,(g)} + H_2O_{\,(aq)} \Leftrightarrow CO_{2\,(aq)} + H_2O_{\,(aq)}$

(Stumm and Morgan, 1981). Once dissolved, carbon dioxide ($CO_{2\,(aq)}$) can dissociate in the following manner:

[2] $CO_{2\,(aq)} + H_2O_{\,(aq)} \Leftrightarrow H_2CO_{3\,(aq)}$

where H_2CO_3 is carbonic acid. The total analytical concentration of dissolved carbon dioxide ($[H_2CO_3^*]$) in mol L^{-1} is defined from the following relationship:

[3] $[H_2CO_3^*{}_{(aq)}] = [H_2CO_{3\,(aq)}] + [CO_{2\,(aq)}]$

where $[H_2CO_3]$ is the concentration of carbonic acid and $[CO_{2aq}]$ is the concentration of aqueous carbon dioxide. This convention in Eq. [3] exists even though only about 0.1 % of the solution actually forms as carbonic acid (Mook and de Vries, 1999).

Water has the ability to act as both an acid and a base at the same time. The dissociation of water or equilibrium equation for water (McMurrey and Fay, 2001) is given by:

[4] $$2H_2O_{(aq)} \Leftrightarrow H_3O^+_{(aq)} + OH^-_{(aq)}$$

where H_2O is water, H_3O^+ is the hydronium ion, and OH^- is hydroxyl. The dissociation constant or ion-product constant of water for concentrated solutions (K_W) is defined as:

[5] $$K_W = \{H_3O^+\}\{OH^-\}$$

(McMurrey and Fay, 2001), where the {} indicate activity. The temperature dependent values of K_W used for these studies were obtained from the following relationship (Mook and de Vries, 1999):

[6] $$K_w = e^{(148.9802 - 13847.26/T - (23.6521\ \mathrm{LnT}))}$$

where T is the solution temperature in Kelvin.

Carbonic acid is a polyprotic acid that dissociates in this stepwise manner:

[7] $$H_2CO_{3(aq)} + H_2O_{(aq)} \Leftrightarrow H_3O^+_{(aq)} + HCO^-_{3(aq)}$$

[8] $$HCO^-_{3(aq)} + H_2O_{(aq)} \Leftrightarrow H_3O^+_{(aq)} + CO^{2-}_{3(aq)}$$

(McMurrey and Fay, 2001). Each dissociation step for carbonic acid has its own acidity or dissociation constant. The first dissociation constant of carbonic acid (K_1 , Eq. [9]) and the second dissociation constant of carbonic acid (K_2 , Eq. [10]) are defined as:

[9] $$K_1 = \frac{\{H_3O^+\}\{HCO_3^-\}}{\{H_2CO_3*\}}$$

[10] $$K_2 = \frac{\{H_3O^+\}\{CO_3^{2-}\}}{\{HCO_3^-\}}$$

(McMurrey and Fay, 2001), where the {} indicate activity. The temperature dependent values of K_1 and K_2 used for these studies were obtained from the following relationships (Eqs. [11] and [12], respectively; Mook and de Vries, 1999):

[11] $$K_1 = 10^{-(3404.71/T + 0.032786T - 14.8435)}$$

[12] $$K_2 = 10^{-(2902.39/T + 0.02379T - 6.4980)}.$$

where T is the solution temperature in Kelvin.

The total concentration of dissolved inorganic carbon (DIC; Stumm and Morgan, 1981; Mook and de Vries, 1999) in mol L^{-1} is defined as:

[13] $DIC_{(aq)} = [H_2CO_3^*{}_{(aq)}] + [HCO_3^-{}_{(aq)}] + [CO_3^{2-}{}_{(aq)}]$.

The solubility of a gas in a liquid at a given temperature is directly proportional to the partial pressure of the gas over the solution (McMurrey and Fay, 2001). Increasing the pressure, (e.g. the atmospheric pressure) will increase the solubility of the gas. The concentration of carbon dioxide in the solution is a function

of the temperature of the solution and its partial pressure of carbon dioxide (P_{CO2}) expressed here in atm. It follows that the total analytical concentration of dissolved carbon dioxide ($[H_2CO_3^*]$, Eq. [14]) in mol L^{-1} can be calculated by Henry's law:

[14] $$[H_2CO_3^*] = K_H \times P_{CO2}$$

where K_H in mol L^{-1} atm^{-1} is the temperature dependent Henry's law constant of the solution (Kling et al., 1992; Stumm and Morgan, 1981; Mook and de Vries, 1999). The temperature dependent values of K_H in mol L^{-1} atm^{-1} used for these studies were obtained from the following relationship from Mook and de Vries (1999):

[15] $$K_H = 10^{-((-2622.38/T)-(0.0178471\ T)+15.5873)}$$

where T is the solution temperature in Kelvin.

The acid neutralizing capacity (ANC) concentration in mol L^{-1} is defined here as the capacity of solutes in an aqueous system to neutralize strong acid. In a system with only carbonate species, ANC (Baker et al., 1990; Mook and de Vries, 1999) is defined as:

[16] $$ANC = [HCO_3^-] + 2[CO_3^{2-}] + [OH^-] - [H^+]$$

where $[H^+]$ is the hydrogen ion concentration.

Direct measurement of CO_2 using pumping induced ebullition (PIE)

Ebullition of a dissolved gas in water is the act of a gas leaving the water in the form of a bubble. This process takes place when the partial pressure of the dissolved gas is in excess of the ambient pressure acting on the water. The spontaneous

formation of bubbles can be induced in a water sample simply by pumping sample water through a narrow-diameter tube to mechanically decrease the ambient pressure acting on the water. The frictional losses from the tube and the suction of the pump will mechanically decrease the ambient pressure acting on the water to a pressure near zero. The bubbles buoyancy can then be used to trap them within a gas collection chamber. Figure 1 shows the schematic of the pumping induced ebullition (PIE) device used in this research. After being trapped, the carbon dioxide gas in the PIE gas collection chamber can then be measured with an analyzer via the connected sampling port. A LI-COR LI- 840 infrared CO_2 gas analyzer (IRGA) was used for this study. Note that the PIE device harvests all dissolved gases (e.g. N_2, O_2, Ar, H_2, N_2O, CH_4, CFC_{11}, CFC_{12}, CFC_{113}, SF_6) from the water sample and that any of these other gases in the gas collection chamber could also be measured with an analyzer, via this connected sampling port (Browne, 2004a). Because the mole fraction (X_i) of an individual gas within the harvested gas reflects its X_i within the solution, measurements of X_i can be used to estimate the concentration of dissolved gases in solution via Henry's law (Browne, 2004a).

The partial pressure (P_i) of an individual dissolved gas within the gas collection chamber (Figure 1) can be lower or higher than in the original solution (P_0). This is a function of the solubility of the dissolved gas. The dilution of an individual gas within the gas collection chamber is defined as the fractionation of that gas. This can be adjusted for with a fractionation coefficient. The fractionation coefficient (f_i) for a gas is the ratio of the PIE based mole fraction (X_i) to the original mole fraction

(X_0) (Browne, 2004a and 2004b). These fractionation coefficient values are controlled by the sample temperature, the pumping rate, and the width and length of the narrow-diameter tube used in the ebullition process. A gas with no fractionation would have a fractionation coefficient value of one. Fractionation was assumed to be close to one for carbon dioxide ($f_i \approx 1.20$; Browne, 2004b) and therefore not included in this study.

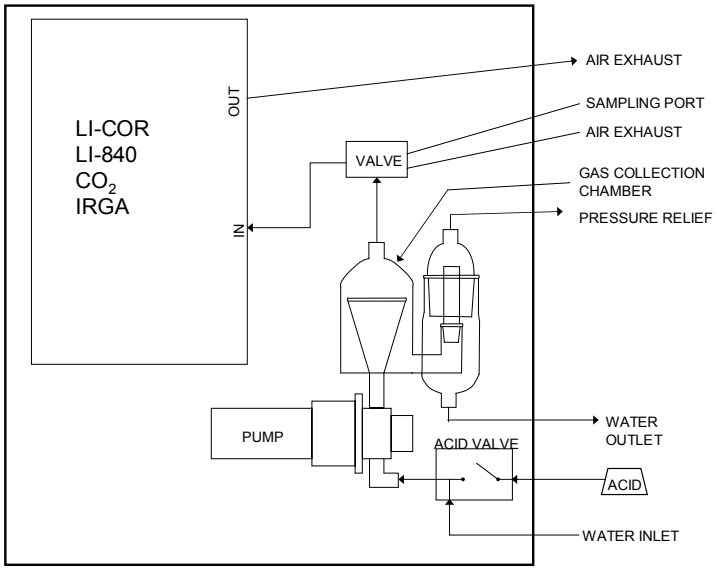

Figure 1. Component diagram of PIE device with LI-COR LI-840 infrared CO_2 gas analyzer (IRGA).

After the PIE device reaches a stable reading (steady-state in the gas collection chamber) one to two minutes after initial start-up, the rate at which a dissolved gas (i) is pumped into the PIE device ($\frac{dn_i}{dt}$) is equal to the rate of bubble formation ($\frac{dn_i^g}{dt}$)

plus the rate at which the remaining dissolved gas exhausts from the water outlet ($\frac{dn_i^s}{dt}$, Figure 1) (Browne, 2004a and 2004b):

$$[17] \qquad \frac{dn_i}{dt} = \frac{dn_i^g}{dt} + \frac{dn_i^s}{dt}$$

where n_i is the total moles of gas i, n_i^g is the total moles in the gas phase, and n_i^s is the total moles in the solution phase. Using Henry's law and the ideal gas law, these rates are defined as follows (Browne, 2004a and 2004b):

$$[18] \qquad \frac{dn_i}{dt} = P_{0,i} K_{H,i} \left(\frac{dV_w}{dt} \right)$$

$$[19] \qquad \frac{dn_i^g}{dt} = \frac{P_i}{RT} \left(\frac{dV_g}{dt} \right)$$

$$[20] \qquad \frac{dn_i^s}{dt} = P_i K_{H,i} \left(\frac{dV_w}{dt} \right)$$

where $\frac{dV_w}{dt}$ is the water pumping rate by volume, $\frac{dV_g}{dt}$ is the rate of bubble accumulation by volume in the gas collection chamber (Figure 1), R is the universal gas constant in L atm mol^{-1} K^{-1}, T is the temperature in Kelvin, and K_H is the Henry's Law constant in mol L^{-1} atm^{-1}. Therefore, the partial pressure (P_i) of an individual dissolved gas within the gas collection chamber is related to its partial pressure in the original solution (P_0) by the following relationship (Browne, 2004a and 2004b):

[21] $$P_i = P_{0,i}\left[\frac{RT\prod K_{H,i}}{1+RT\prod K_{H,i}}\right]$$

where $\prod$ is the ratio of the water pumping rate ($\frac{dV_w}{dt}$) to the bubble accumulation rate ($\frac{dV_g}{dt}$) in the gas collection chamber.

Figures 1 and 2 illustrate the PIE device used in this study. The device was operated in two modes: carbon dioxide (CO_2) and dissolved inorganic carbon (DIC). In CO_2 and DIC mode, the solution was pumped at a rate ($\frac{dV_w}{dt}$) of 1.78 L min^{-1} producing a bubble accumulation rate ($\frac{dV_g}{dt}$) of 5.24 ml min^{-1} in the gas collection chamber for the prototypes used in these studies (Browne, 2004a and 2004b). This gas streamed through a LI-COR model LI-840 infrared H_2O and CO_2 gas analyzer (IRGA), where the response was recorded. The X_{CO_2} values in parts per million by volume (ppmv) were determined by comparing the instrument response to a standard curve (see standardization of the LI-COR model LI-840 with dry gases below).

In CO_2 mode, the PIE based partial pressure of carbon dioxide (P_{CO2}) in μatm was estimated from the X_{CO_2} values in ppmv by:

[22] $$P_{CO2} = \frac{X_{CO_2} \times P}{f_i}$$

where P is the atmospheric barometric pressure in atm and f_i is the fractionation coefficient. As stated above, the fractionation coefficient was assumed to be close to one for carbon dioxide ($f_i \approx 1.20$) based on the work of Browne (2004b) and therefore not included in this study. The concentration of dissolved carbon dioxide ($[H_2CO_3^*]$) was calculated using Henry's law (Eqs. [14] and [15]) and Eq. [22].

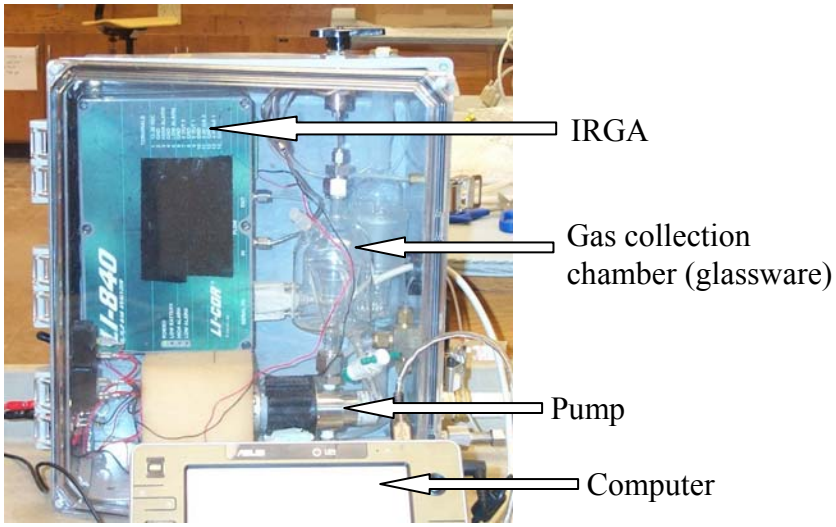

Figure 2. PIE device with LI-COR LI-840 infrared CO_2 gas analyzer (IRGA).

The PIE device was easily switched to DIC mode by turning on the acid valve shown in Figure 1. In DIC mode, phosphoric acid was added to the solution upstream of the pump at a rate of 2 ml min^{-1}. The acid addition causes inorganic carbon species (bicarbonate ($[HCO_3^-]$) and carbonate ($[CO_3^{2-}]$)) to be converted into dissolved carbon dioxide ($[H_2CO_3^*]$). The PIE based concentration of DIC in μmol L^{-1} was calculated by:

[23] $[\text{DIC}] = K_H \times P_{CO2}$

where the temperature dependent value of K_H in mol L^{-1} atm^{-1} was from Eq. [15] and the P_{CO2} (Eq. [22]) in μatm was estimated from the DIC mode X_{CO_2} value in ppmv.

PIE sample readings in CO_2 and /or DIC mode were recorded in succession using one PIE device (Figures 1 and 2) or simultaneously with two PIE devices. The PIE device was equipped with a LI-COR model LI-840 infrared H_2O and CO_2 gas analyzer (IRGA) with water vapor and pressure correction. Unless specifically stated differently in an experiment, a two-minute average measurement (after the PIE device stabilization) was used to estimate P_{CO2}. This two-minute average was only chosen to set a sampling protocol. Therefore, any other protocol could have been used. Readings were returned at 1-Hz. (one record/second) and stored on an ASUSTeK Computer Inc, ASUS R2H ultra mobile tablet personal computer. This computer was chosen for cost, compactness, and memory size. (Note that the PIE device has the ability to observe both numerical and graphical results in real time with this computer.)

Water temperature measurements for the PIE based measurements were made either with a Fluke® temperature probe (resolution = 0.0001 ± 0.0015 °C) in the gas collection chamber (Figure 1) or with a YSI sonde temperature probe (resolution = 0.01 ± 0.15 °C) at the water outlet (Figure 1) of the gas collection chamber. These water temperature measurements were based on factory calibrations of these probes.

The LI-COR model LI-840 was calibrated with NIST traceable dry gas standards of known mole fractions (X_{CO_2}), ranging from 0 to 79980 parts per million

volume (ppmv). Three calibration curve equations were developed for the PIE device in each experiment in X_{CO_2} ranges of 0 to 2953, 2953 to 19970, and 19970 to 79980 ppmv. For most experiments, the PIE device response was fit with a linear function, third order polynomial, and fourth order polynomial for ranges of 0 to 2953, 2953 to 19970, and 19970 to 79980 ppmv, respectively. The atmospheric barometric pressures present during the calibration process may influence this fit.

The PIE device had problems with the non-linear portion (above 5000 ppmv) of the calibration curves obtained with dry gas standardization. Within this non-linear response range, the internal pressure compensation function of the LI-COR model LI-840 has failed as a reliable algorithm for mole fraction (X_{CO2}) estimates (Figure 3; unpublished data from a Browne and Schueller (2007) UWSP and Seattle, WA experiment). With dry gas standardization, the PIE device was calibrated under the atmospheric pressure (cell pressure) present at the time of calibration. The internal pressure compensation function of the LI-COR model LI-840 was designed to compensate for shifts in the atmospheric pressure (cell pressure). However, under conditions of fluctuating atmospheric barometric pressures (Figure 3), shifts in response had lead to incorrect mole fraction (X_{CO2}) estimates when using dry gas standardization. (See McDermitt et al.(1993a and 1993b) for further discussion on water vapor and pressure influence on infrared gas analyzer (IRGA) measurements of CO_2 gas and corrections for this by the LI-COR model LI-840.) To overcome this potential for incorrect determinations of X_{CO2} estimates using dry gas standardization, an aqueous standardization was used to develop empirical response relationships.

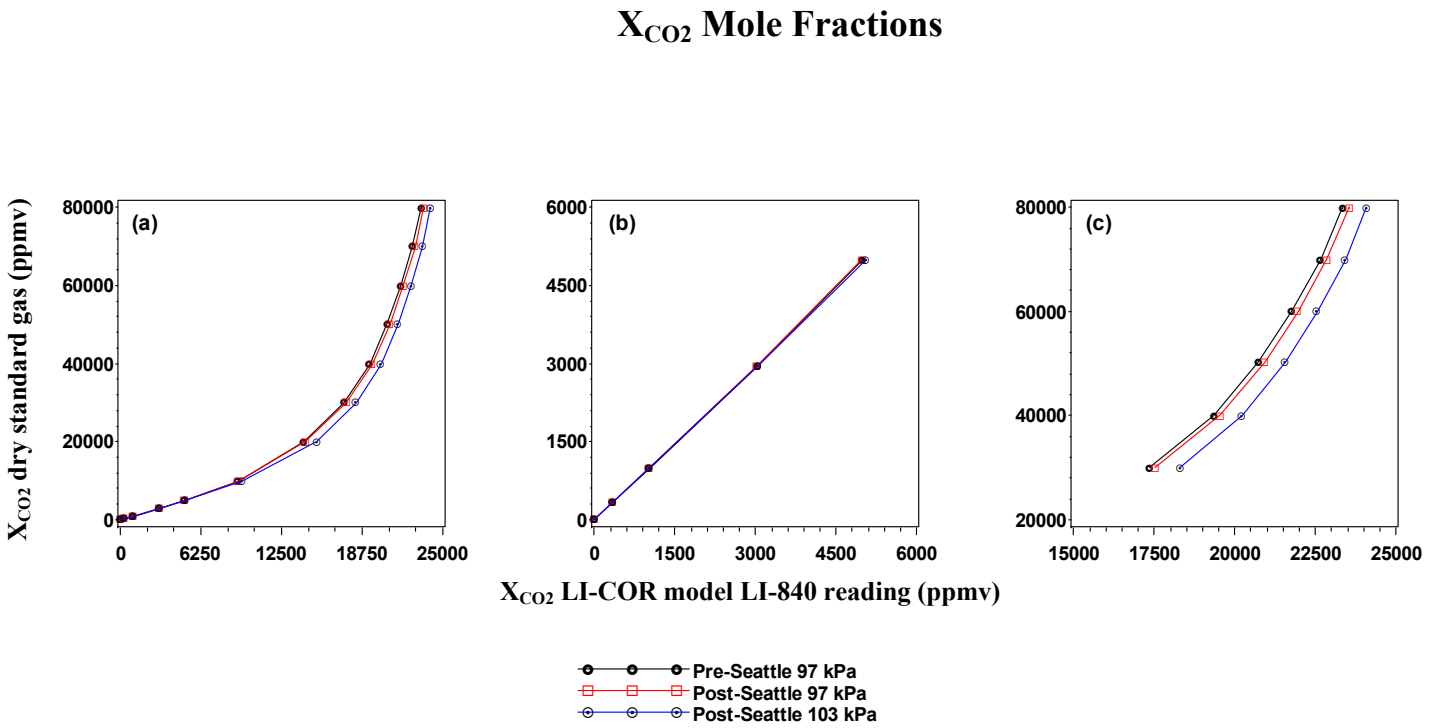

Figure 3. PIE based DIC calibration curves (dry gas standardization; unpublished data from a Browne and Schueller (2007) UWSP and Seattle, WA experiment) with response to shifts in the atmospheric barometric pressure. PIE based DIC LICOR 840 standard curves for 97 kPa (ambient conditions UWSP) and 103 kPa (ambient conditions Seattle, WA) cell pressures. Pressure compensation function of LICOR 840 breaks down at high mole fractions (a) Entire standard curve showing pressure compensation failure at high mole fractions. (b) Isolation of linear portion of curve shows no effect of pressure compensation. (c) Close-up of the pressure compensation departure in the upper curve. Notice that the curve shifts to the right (c) from the increase in atmospheric barometric pressure. Differences in 97 kPa curves may reflect effect of small atmospheric barometric pressure differences (e.g., 96.5 kPa v. 97.2 kPA) and shows need to standardize frequently for the upper end of the curve.

These aqueous standardizations were performed with water sample measurements (DIC, ANC, and $[H_2CO_3^*]$) from the same location, depth, temperature, and time of the PIE based carbon dioxide measurements.

Laboratory ANC, laboratory DIC, and Henry's law were used to develop an empirical response relationship for PIE based P_{CO2}. The expected mole fraction response (X_{E1}) of the LI-COR model LI-840 for the sample was calculated by:

[24] $$[H_2CO_3^*]_{calc} \approx [DIC] - [ANC]$$

[25] $$X_{E1} = \frac{[H_2CO_3^*]_{calc}}{K_H \times P}$$

where $[H_2CO_3^*]_{calc}$ is the calculated concentration of dissolved carbon dioxide, [DIC] is the laboratory DIC concentration in μmol L^{-1}, [ANC] is the ANC concentration by Gran titration in μmol L^{-1}, P is the atmospheric barometric pressure in atm, and K_H is the Henry's law constant in mol L^{-1} atm^{-1} at the sample temperature. Note that the relationship in Eq. [24] is true when the carbonate, hydroxyl, and hydrogen ion species are small. The expected mole fraction response (X_{E1}) was then graphed versus the measured PIE based X_{CO2} values for the sample to develop the empirical response relationship for PIE based P_{CO2} and for each PIE device.

Laboratory ANC, PIE based $[H_2CO_3^*]$, and Henry's law were also used to develop an empirical response relationship for PIE based DIC. The expected mole fraction response (X_{E2}) of the LI-COR model LI-840 for the sample was calculated by:

[26] $$[DIC]_{calc} \approx [ANC] + [H_2CO_3^*]$$

[27] $$X_{E2} = \frac{[DIC]_{calc}}{K_H \times P}$$

where $[DIC]_{calc}$ is the calculated DIC concentration in μmol L^{-1}, [ANC] is the ANC concentration by Gran titration in μmol L^{-1}, $[H_2CO_3^*]$ is the PIE based concentration of dissolved carbon dioxide in μmol L^{-1}, P is the atmospheric barometric pressure in atm, and K_H is the Henry's law constant in mol L^{-1} atm^{-1} at the sample temperature. Note that the relationship in Eq. [26] is true when the carbonate, hydroxyl, and hydrogen ion species are small. The expected mole fraction response (X_{E2}) was then graphed versus the measured PIE based X_{CO2} values for the sample to develop the empirical response relationship for PIE based DIC and for each PIE device.

Direct measurement of CO_2 using headspace analysis

The headspace method used was based on a modified procedures of Cole and Caraco, (1998) and Loftfield et al. (1997). An insulated modified Supelco® 1000-ml gas collection headspace vessel (Figures 4 and 5) with two PTFE stopcocks and one Thermogreen® cylindrical half hole septum was placed vertical with both top and bottom valves open. A water sample was pumped though the sampling line and headspace vessel (Figures 4 and 5) until flushed with six times the combined volume of the sampling line and vessel. Both headspace vessel valves were then closed. Next, two gas tight 60-ml collection syringes (Monoject®) were filled with headspace gas (ambient air) (care was taken to avoid contamination with carbon dioxide from breath during collection). One of these syringes with the 60-ml of headspace gas (ambient air) was then introduced into the headspace vessel through septum in side of headspace

Figure 4. Insulated modified Supelco® 1000-ml gas collection vessel (tube).

vessel, replacing the 60-ml of sample water exiting through the now opened bottom valve. With both top and bottom valves now closed, the 940-ml of sample water was equilibrated with the 60-ml of headspace gas by vigorously shaking vessel for one

minute. This shaking is approximately twice the time required to equilibrate the air and water phases of the CO_2 (Cole and Caraco, 1998). The equilibrated headspace gas was then transferred to a gas tight 60-ml collection syringe (Monoject®). This

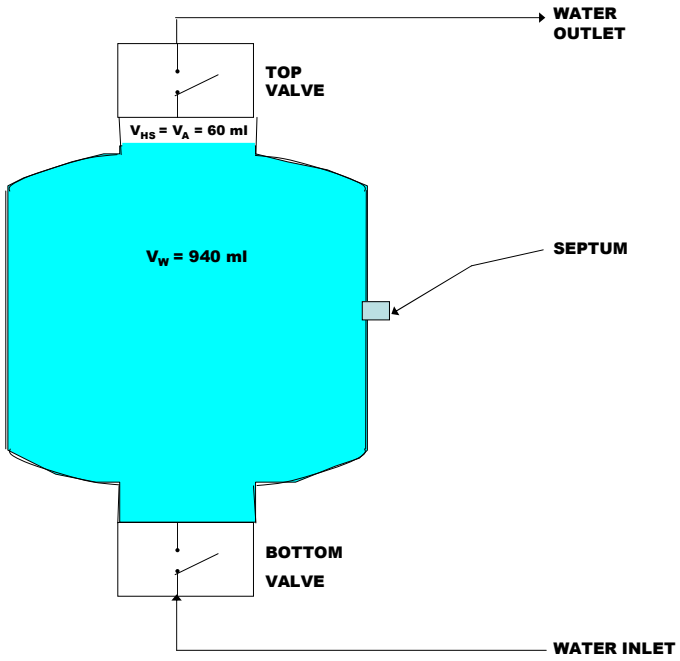

Figure 5. Component diagram of the insulated modified Supelco® 1000-ml gas collection vessel. Sample water entered through the bottom water inlet and valve and exited via a water outlet and valve at the top of the vessel. Gas collection was through septum visible on side of vessel.

equilibrated headspace gas and the gas of ambient air in the other syringe were injected into separate pre-evacuated 10-ml septum sample bottles sealed with Bellco® 20-mm stoppers. (Gas mole fractions within these septum sample bottles (Browne, 2004b) have been shown to be stable for greater than six weeks.) Mole fractions of

CO_2 in the headspace gas and ambient air were measured in the lab with a SRI 8610C gas chromatograph (SRI) equipped with a methanizer, flame ionization detector (FID), and a customized pressure controlled auto-sampler designed to accept 10-ml septum sample bottles sealed with Bellco® 20-mm stoppers. Temperatures for the ambient air and sample vessel water were measured with a Traceable® thermometer.

The concentration of dissolved carbon dioxide ($[H_2CO_3^*]$) in μmol L^{-1} was calculated using:

$$[28] \quad [H_2CO_3^*] = \frac{n_{TOTAL}}{V_W} = \frac{n_W + n_{HS} - n_A}{V_W}$$

where n_{TOTAL} is the total μmoles of CO_2 initially present in the 940-ml of water (V_W) added to the headspace analysis equilibrator, n_w is the total μmoles of CO_2 present in V_w after headspace equilibration, n_{HS} is the total μmoles of CO_2 present in the 60-ml of headspace gas (V_{HS}) after headspace equilibration, and n_A is the total μmoles of CO_2 present in the 60-ml of the initial headspace gas (V_A) before headspace equilibration.

The estimate for n_w (Eq. [29]) in μmol was obtained from the Henry's law relationship (Mook and de Vries, 1999):

$$[29] \quad n_W = K_H \times X_{CO_2}^{HS} \times P \times V_W$$

where temperature dependent values of K_H in mol L^{-1} atm^{-1} were from Eq. [15] at the headspace sample vessel water temperature after equilibration, $X_{CO_2}^{HS}$ in ppmv is the measured mole fraction of CO_2 in the headspace gas after equilibration of the sample, and P is the atmospheric barometric pressure in atm.

The estimate for n_{HS} (Eq. [30]) in μmol was obtained from the ideal gas law:

$$[30] \qquad n_{HS} = \frac{X_{CO_2}^{HS} \times P \times V_{HS}}{R \times T_w}$$

where V_{HS} is the volume of the headspace gas (60-ml) after equilibration of the sample, R is the universal gas constant (0.08206 L atm mol^{-1} K^{-1}), and T_W is the headspace sample vessel water temperature in Kelvin after equilibration.

The estimate for n_A (Eq. [31]) in μmol was also obtained from the ideal gas law:

$$[31] \qquad n_A = \frac{X_{CO_2}^{A} \times P \times V_A}{R \times T_A}$$

where $X_{CO_2}^{A}$ in ppmv is the measured mole fraction of CO_2 in the headspace gas before equilibration of the sample, V_A is the volume of the headspace gas (60-ml) before sample equilibration, and T_A is the headspace ambient air temperature in Kelvin before equilibration of the sample.

The headspace partial pressure of carbon dioxide (P_{CO2}) in μatm was estimated using a rearrangement of Eq. [14], where [H_2CO_3*] in μmol L^{-1} was from Eq. [28] and the temperature dependent value of K_H in mol L^{-1} atm^{-1} was from Eq. [15].

Indirect estimation of CO_2 using pH and ANC

There are several traditional ways to indirectly measure carbon dioxide. Indirect measurements are defined here as dissolved carbon dioxide estimates indirectly derived from measurements of pH and dissolved inorganic carbon (DIC) or

pH and acid neutralizing capacity (ANC). ANC and DIC were originally used for estimating carbon dioxide, because they were common measurements taken in lakes, streams, and rivers. To estimate carbon dioxide, all the indirect measurement methods require knowledge of appropriate equilibrium constants.

One indirect estimate of the partial pressure of carbon dioxide (P_{CO2}, Eq. [32]) in μatm was obtained using thermodynamic equilibrium relationships based on pH and acid neutralizing capacity (ANC) measurements with corrections for ionic strength and activity coefficients (Baker et al., 1990; Stumm and Morgan, 1981; Mook and de Vries, 1999):

$$[32] \qquad P_{CO2} = \frac{\text{ANC} - 10^{(\text{pH}-K_w)} + 10^{-\text{pH}}}{\left(\frac{K_1 K_H 10^{\text{pH}}}{\gamma_1}\right) + \left(\frac{2K_1 K_2 K_H 10^{2\text{pH}}}{\gamma_2}\right)}$$

where ANC is in μmol L^{-1}, K_W is the dissociation constant of water, K_1 is the first dissociation constant of carbonic acid, K_2 is the second dissociation constant of carbonic acid, γ_1 is the activity coefficient of bicarbonate, and γ_2 is the activity coefficient of carbonate. The temperature dependent values of K_W, K_1, K_2, and K_H were obtained from Eqs. [6], [11], [12], and [15], respectively. The activity coefficients for bicarbonate (γ_1) and carbonate (γ_2) were based on the Lewis and Randall concept of ionic strength (Stumm and Morgan, 1981) and the extended Debye-Huckel limiting law (Stumm and Morgan, 1981).

The acid neutralizing capacity (ANC) was measured by Gran titration (Baker et al., 1990; Rounds, 2006). Water samples were collected in headspace-free 125-ml bottles and titrated to a pH around 3.0. The pH was measured with an Orion ROSS Sure-Flow glass electrode (resolution = 0.001 ± 0.010 units). The F_1 Gran function (F_1) was measured, calculated, and plotted versus the volume of the titrant (V_1):

[33] $$F_1 = (V_1 + V_2) \times (10^{-pH})$$

where V_2 is the volume of the sample in ml and pH is the sample pH at each V_1 addition. The upper right-most linear portion of the F_1 curve was then extrapolated downward to determine the titrant volume (V_E) at the bicarbonate equivalence point (Baker et al., 1990). The ANC in μmol L^{-1} was estimated from the following relationship (Baker et al., 1990; Rounds, 2006; Stumm and Morgan, 1981):

[34] $$ANC = \frac{C_1 \times V_E}{V_2} \times (1 \times 10^6)$$

where C_1 is the normality of the titrant.

Acid neutralizing capacity (ANC) by C_B and C_A is another common method for measuring the ANC. The ANC by C_B and C_A samples were collected in headspace-free 125-ml bottles and transported to the laboratory for measurement of non-acidic cation concentrations (C_B, basic cations, Eq. [35]) and mineral acid anion concentrations (C_A, Eq. [36]) by Dionex ion chromatography (Baker et al., 1990; Neumann et al., 2001):

[35] $$C_B = [Na^+] + [K^+] + 2[Ca^{2+}] + 2[Mg^{2+}] + [NH_4^+] + 3[Al^{3+}] + 2[Fe^{2+}] + 2[Mn^{2+}]$$

[36] $$C_A = [Cl^-] + [NO_3^-] + 2[SO_4^{2-}] + [NO_2^-] + [F^-]$$

where $[Na^+]$ is sodium, $[K^+]$ is potassium, $[Ca^{2+}]$ is calcium, $[Mg^{2+}]$ is magnesium, $[NH_4^+]$ is ammonium, $[Al^{3+}]$ is aluminum, $[Fe^{2+}]$ is iron, $[Mn^{2+}]$ is manganese, $[Cl^-]$ is chloride, $[NO_3^-]$ is nitrate, $[SO_4^{2-}]$ is sulfate, $[NO_2^-]$ is nitrite, and $[F^-]$ is fluoride.

Using electroneutrality (Eqs. [37] and [38]) and ANC (Eq. [16]), the sum of the non-acidic cation concentrations (C_B, Eq. [35]) minus the sum of the mineral acid anion concentrations (C_A, Eq. [36]) is equal to the ANC (Eq. [39]; Baker et al., 1990; Mook and de Vries, 1999; and Stumm and Morgan, 1981):

[37] $$[Na^+] + [K^+] + 2[Ca^{2+}] + 2[Mg^{2+}] + [NH_4^+] + 3[Al^{3+}] + 2[Fe^{2+}] + 2[Mn^{2+}] + [H^+] = [Cl^-] + [NO_3^-] + 2[SO_4^{2-}] + [NO_2^-] + [F^-] + [HCO_3^-] + 2[CO_3^{2-}] + [OH^-]$$

[38] $$C_B + [H^+] = C_A + [HCO_3^-] + 2[CO_3^{2-}] + [OH^-]$$

[39] $$ANC = C_B - C_A.$$

The ANC calculated above using C_B and C_A measurements is equivalent to the ANC measured by Gran titration.

Indirect estimation of CO_2 using pH and DIC

A second indirect estimate of the partial pressure of carbon dioxide (P_{CO2}, Eq. [40]) in µatm was obtained using thermodynamic equilibrium relationships based on pH and laboratory DIC measurements with corrections for ionic strength and activity coefficients (Stumm and Morgan, 1981; Mook and de Vries, 1999):

[40] $$P_{CO2} = \frac{DIC}{K_H + \left(\frac{K_1 K_H 10^{pH}}{\gamma_1}\right) + \left(\frac{K_1 K_2 K_H 10^{2pH}}{\gamma_2}\right)}$$

where DIC is in μmol L^{-1} and the temperature dependent values of K_W, K_1, K_2, and K_H were obtained from Eqs. [6], [11], [12], and [15], respectively. The activity coefficients for bicarbonate (γ_1) and carbonate (γ_2) were based on the Lewis and Randall concept of ionic strength (Stumm and Morgan, 1981) and the extended Debye-Huckel limiting law (Stumm and Morgan, 1981).

The laboratory dissolved inorganic carbon measurements were performed using a Shimadzu Corp. non-dispersive infrared gas analyzer (NDIR) model TOC-5000A (e.g., Baehr and DeGrandpre, 2002) in conjunction with the methods described in Shimadzu Corp. (1994). Headspace-free water samples were collected in 125-ml bottles as described above and stored for analysis. The water samples were then auto injected into an inorganic carbon (IC) reactor vessel and acidified. The acid converts inorganic carbon species ($[HCO_3^-]$ and $[CO_3^{2-}]$) into dissolved carbon dioxide ($[H_2CO_3^*]$), allowing the total DIC (Eq. [13]) in μmol L^{-1} to be measured by the NDIR.

Other Measurement Procedures.

The water temperature, atmospheric barometric pressure, and specific conductivity measurements required for the carbon dioxide estimates were performed with an YSI 600 MDS equipped with a 600XL multi-parameter sonde. Additionally, pH measurements required for the indirect carbon dioxide estimates were performed with either a YSI 600 MDS equipped with a 600XL multi-parameter sonde pH probe (resolution = 0.01 ± 0.20 units) or an Orion ROSS electrode pH probe (resolution =

0.001 ± 0.010 units) using the methods described in Rosich (2002), and Wilde et al. (2006). The sonde and Orion electrode pH probe were calibrated with two buffers (e.g., 4 and 7 pH or 7 and 10 pH), thoroughly rinsed, and allowed to equilibrate with a representative sample of solution for 30 minutes before they were used for pH measurement (Rosich, 2002; Wilde et al., 2006). To measure pH, the probes were placed in a sample and then the first reasonably stable measurement of pH was taken (i.e. with its unsaturated partial pressure of carbon dioxide value intact). Measurements of pH were recorded within the first minute to accurately reflect the true pH values (Rosich, 2002; Wilde et al., 2006). When the Orion electrode pH was used, the YSI sonde pH was also measured at the same time for comparison. The water temperature, atmospheric barometric pressure, and specific conductivity measurements from the YSI sonde were based on factory calibrations.

Data Management, Statistics, and Graphing

Several personal computer based programs were used to collect, download data from data loggers, store, compile, manipulate, and display the data. Ecowatch by InstallShield Software Corp. was used to download all YSI sonde data. LI-1400 by LI-COR Biosystems or LI-840 by LI-COR Biosciences was used to record and download all LI-COR model LI-840 infrared H_2O and CO_2 gas analyzer (IRGA) data. Data collection, storage, compilation, manipulation, statistics, and graphing were completed with Microsoft Excel (Microsoft Corporation) and SAS (SAS Institute Inc.).

Accuracy and precision were reported using box plots and analyses of regression with statistical parameters of root mean square error (RMSE), coefficient of variation (CV), mean (x-bar), median, square of the correlation (r^2), standard deviation, slope, and p-values. The root mean square error (RMSE) is the standard deviation of the error term and defined as the square root of the mean square residual or error. The coefficient of variation (CV) is the relative standard deviation as a percent and defined as the standard deviation divided by the mean of the dependent variable. In analyses of regression using SAS, the coefficient of variation is defined as the RMSE divided by the mean of the dependent variable. The CV measures the relative scatter of two or more samples about their means. The CV is useful for making comparisons between distributions and / or regressions that have different means, standard deviations, RMSE's, and / or units of measure. The square of the correlation (r^2) is the fraction of variation in the values of y that is explained by the least squares regression of y on x. The r^2 can also be described as the proportion of variance in the dependent variable which can be predicted from the independent variable. The slope term for the regression is the parameter estimate of the independent variable. The square of the correlation and the slope term are a measure of the strength of association between the variables for the regression.

ACCURACY and PRECISION of PIE

In this chapter, the accuracy and precision of PIE based measurements were characterized using solutions of defined composition. PIE based P_{CO2} and $[H_2CO_3^*]$, headspace, DIC, and ANC measurements were compared to known sodium bicarbonate concentrations. PIE based dissolved carbon dioxide measurements were also compared against headspace measurements. Subsections include the methods for the laboratory experiments, results achieved, and conclusions found.

Methods - Accuracy and Precision of PIE

The accuracy and precision were assessed using solutions of known carbon dioxide composition. These solutions were prepared in 119.46 ± 0.46-liter Rubbermaid® containers by acidification of known concentrations of sodium bicarbonate with 1N sulfuric or 36N phosphoric acid. The sodium bicarbonate mass for these known concentrations were measured on an analytical scale (resolution = 0.0001 grams), after which the mass was used to calculate the known concentrations of sodium bicarbonate. The bicarbonate is converted to carbonic acid and dissolved carbon dioxide when acidified (Eqs. [2] and [7]). Because the experiments were of short duration (less than two days), solutions were closed (capped) to the atmosphere, and solutions had little headspace, the total analytical concentration of dissolved carbon dioxide ($[H_2CO_3^*]$) was assumed equal to the added bicarbonate concentration and initial carbon dioxide (present in the deionized water used to make the solutions) or equal to the quantity of bicarbonate concentration acidified plus any initial

[$H_2CO_3^*$]. Table 2 shows the experimental range of dissolved carbon dioxide concentrations for these laboratory experiments.

Table 2. Summary of Experiments 1 through 7.

Experiment	Solution prep. date	Sampling date	dissolved carbon dioxide conc. (μmol/L)	dissolved carbon dioxide conc. as P_{CO2} (μatm)	Number of solutions measured	36N H_3PO_4 added (mL)	1N H_2SO_4 added (mL)
1	1/4/2008	1/5/2008	0,10-100		12	1	
2	1/2/2008	1/3/2008	0,1-10		12	1	
3	1/7/2008	1/8/2008	0,10-100		14	4	
4	1/9/2008	1/10/2008	0,10-100		14	4	
5	1/16/2008	1/17/2008	0,10-100		13	4	
6	2/9/2008	2/10/2008	0,100	0-2610	14		incrementally
7	2/23/2008	2/24/2008	0,100	0-2610	14		incrementally

The first five experiments used bulk solutions prepared by addition of sodium bicarbonate to deionized water. The concentration for these sodium bicarbonate solutions ranged from one to one-hundred μmol L^{-1} (Table 2). Blanks were prepared as bulk solutions of deionized water alone. Once prepared, blanks and sodium bicarbonate solutions were allowed to sit overnight. The next day the mole fraction of carbon dioxide was measured immediately before and immediately after solution acidification. The total solution acidification caused a conversion of all bicarbonate to dissolved carbon dioxide (Eqs. [2] and [7]). The amount of time between pre- and post-acidification measurements was around 10 to17 minutes for Experiments 1 through 3 and around 22 to 33 minutes for Experiments 4 and 5.

The pre-acidification PIE based carbon dioxide measurement only measured the background [$H_2CO_3^*$] present in the pre-acidified solution. The post-acidification PIE based carbon dioxide measurement contained the sum of all carbon species (Eq. [13]), including the sodium bicarbonate concentration added to the solution plus the background DIC.

Concurrent measurements included YSI sonde temperature, specific conductivity, and barometric pressure. Additionally, in Experiments 4 and 5, measurements for laboratory DIC, ANC, and headspace were compared against the sodium bicarbonate concentration; pH by YSI sonde was also measured.

Experiments 6 and 7 also used bulk solutions prepared by addition of sodium bicarbonate to deionized water. These solutions were prepared with one-hundred μmol L^{-1} [$NaHCO_3$] (Table 2) and allowed to sit overnight. The next day they were acidified with sulfuric acid. Immediately after the pH stabilized, the mole fraction of carbon dioxide was measured. The amount of acid added would be equal to the amount of bicarbonate concentration that would be converted to dissolved carbon dioxide. Acid additions were used to obtain a known range spanning from three to one-hundred μmol L^{-1} [$H_2CO_3^*$]. Concurrent measurements include pH by Orion electrode and pH, water temperature, specific conductivity, and barometric pressure by YSI sonde.

Results and Discussion - Accuracy and Precision of PIE

The results from all of the experiments evaluating the accuracy and precision of PIE are summarized in Table 3. Results from Experiment 4 are presented in detail here to summarize the findings from this part of the study. In Experiment 4, PIE, headspace, DIC, and ANC measurements were compared against known sodium bicarbonate concentrations. PIE based dissolved carbon dioxide measurements were also compared against headspace measurements. Table 3 shows PIE based P_{CO2} and $[H_2CO_3^*]$ measurements taken immediately before and immediately after total solution acidification regressed against the sodium bicarbonate concentration added to the solutions. (Solution temperatures ranged from 19.89 to 22.15 °C.) Pre-acidification P_{CO2} did not have a statistically significant relationship to the sodium bicarbonate concentration ($p = 0.1921$, $r^2 = 0.1374$, slope = 0.3501 ± 0.2533 atm L mol^{-1}, Table 3). Thus, similar to Experiments 1 and 3, pre-acidification P_{CO2} (Table 3) did not decrease systematically with the sodium bicarbonate concentration. Post-acidification P_{CO2} increased systematically with sodium bicarbonate concentration ($p < 0.0001$, $r^2 = 0.9979$, slope = 27.0937 ± 0.3574 atm L mol^{-1}, Table 3).

Corresponding concentrations of $[H_2CO_3^*]$, estimated by Henry's law, illustrate similar trends (Table 3). As in Experiments 1 and 3, pre-acidification PIE based $[H_2CO_3^*]$ did not exhibit a statistically significant trend with the sodium bicarbonate concentration ($p = 0.13$, $r^2 = 0.18$, slope = 0.01 ± 0.01, Table 3). However, post-acidification PIE based $[H_2CO_3^*]$ increased systematically with sodium bicarbonate concentration ($p < 0.0001$, $r^2 = 1.00$, slope = 0.98 ± 0.01, Table 3).

A comparison of PIE based P_{CO2} versus sodium bicarbonate concentration (Table 3) and $[H_2CO_3^*]$ versus sodium bicarbonate concentration (Table 3) showed a slight improvement in the $[H_2CO_3^*]$ versus sodium bicarbonate concentration relationship ($r^2 = 0.9979$ and $r^2 = 0.9994$, respectively). The use of Henry's law to calculate $[H_2CO_3^*]$ adjusts for variation due to temperature (19.89 to 22.15 °C), effectively improving the measurements overall. This adjustment for temperature would have likely been more evident for a broader temperature range.

In Figure 6, the PIE based $[H_2CO_3^*]$ data were regressed against the sodium bicarbonate concentration after excluding the background $[H_2CO_3^*]$ present in the pre-acidified solutions:

[41] $$\left[H_2CO_3*\right]_{\text{adjusted}} = \left[H_2CO_3*\right]_{\text{post}} - \left[H_2CO_3*\right]_{\text{pre}}.$$

Adjustment of the post-acidification data for the background $[H_2CO_3^*]$ brought the association between $[H_2CO_3^*]$ and the sodium bicarbonate concentration to a slightly closer relationship. The association between $[H_2CO_3^*]$ and the sodium bicarbonate concentration was close to a one-to-one relationship ($r^2 = 1.00$, slope = 0.97 ± 0.01, Table 3). Similar results were also found in Experiments 1 through 3 and Experiments 5 through 7. All results for Experiments 1 through 7 are reported in Table 3.

As in Experiments 1 through 3, the y-intercept of 1.14 ± 0.39 μmol L^{-1} $[H_2CO_3^*]$ likely reflects the presence of background carbonic acid and bicarbonate above the amount of HCO_3^- added to the solution.

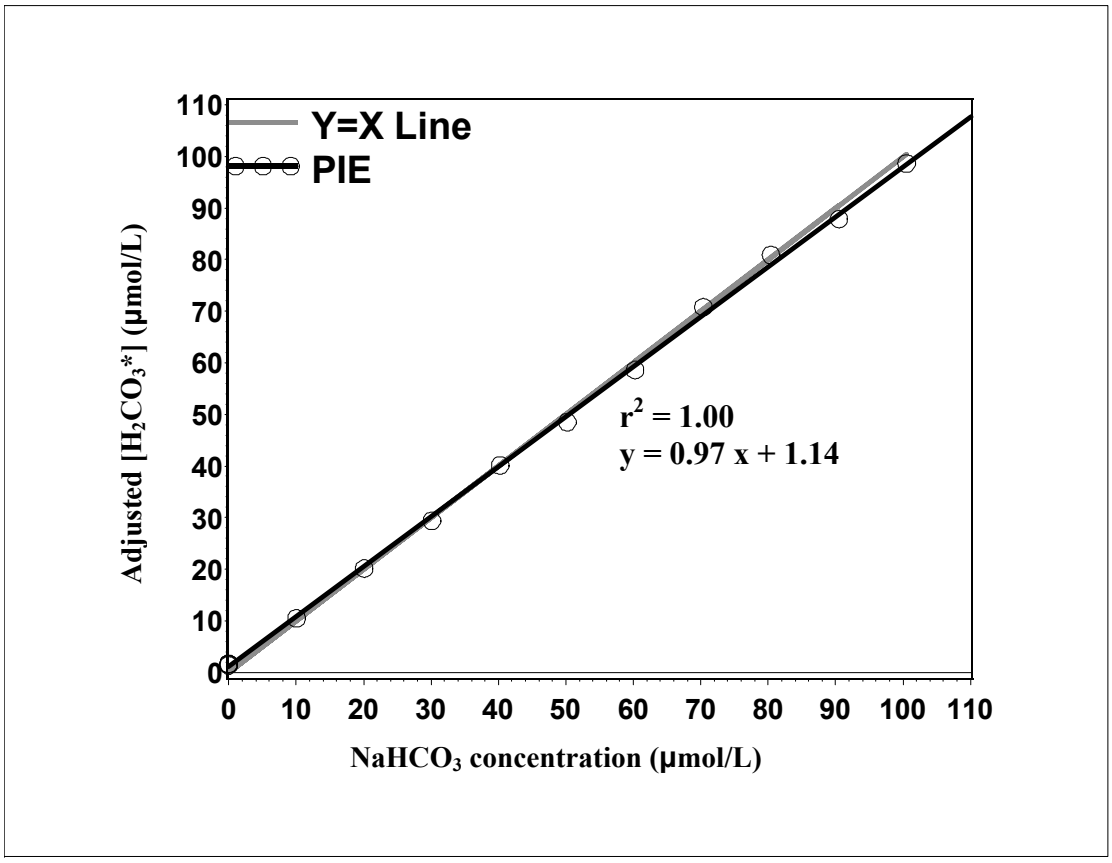

Figure 6. Experiment 4 (N=14), adjusted PIE based [H_2CO_3*] values (Eq. [41]) versus sodium bicarbonate concentration in acidified samples.

There are several sources of background dissolved carbon dioxide. The deionized water used for the experiment always contained some dissolved carbon dioxide, regardless how long we ran the deionized water tap. The containers used in the experiments were closed. However, the covers did not completely seal the containers from atmospheric interaction. Although complete equilibration with the atmosphere would take time, some transfer with the atmosphere likely occurred. None

of the solutions in Experiments 1 through 7 had time to equilibrate completely with the atmosphere.

The inverse of the slope of the regression line of the post-acidification PIE data in Experiment 4, Table 3, was used to estimate the average Henry's law constant (K_H). The inverse of the slope of the regression line (0.0369 ± 0.0005 mol L^{-1} atm^{-1}) was not significantly different from the average Henry's law constant (K_H = 0.0379 ± 0.0010 mol L^{-1} atm^{-1}) at the p = 0.4602 significance level. This means that the inverse of the slope of the regression line was nearly equal to the average Henry's law constant.

In Figure 7, Headspace based [$H_2CO_3^*$] measurements taken immediately after total solution acidification were regressed against the sodium bicarbonate concentration added to the solutions. There was a strong correlation between [$H_2CO_3^*$] and the sodium bicarbonate concentration (r^2 = 0.99, slope = 0.97 ± 0.03, Table 3). However, the headspace measurements overestimate the sodium bicarbonate concentration. This overestimation and y-intercept of 8.55 ± 1.75 μmol L^{-1} [$H_2CO_3^*$] likely reflect the presence of background carbonic acid and bicarbonate above the amount of HCO_3^- added to the solution.

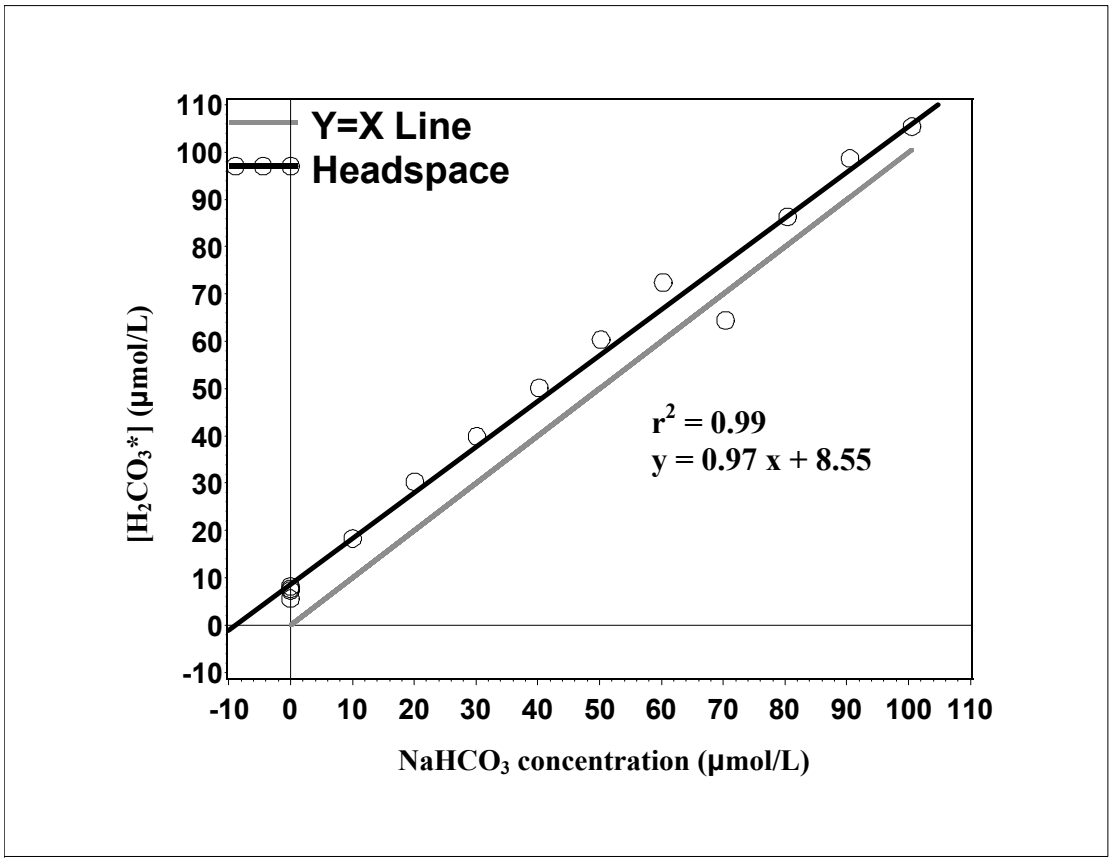

Figure 7. Experiment 4 (N=14), headspace based $[H_2CO_3^*]$ post-acidification values (Eq. [28]) versus sodium bicarbonate concentration.

In Figure 8, the PIE based $[H_2CO_3^*]$ post-acidification measurements were also compared against the headspace based $[H_2CO_3^*]$ post-acidification measurements. PIE based post-acidification $[H_2CO_3^*]$ increased systematically with headspace based $[H_2CO_3^*]$ measurements (r^2 = 0.99, slope = 1.00 ± 0.03, Table 3). There was a close one-to-one relationship.

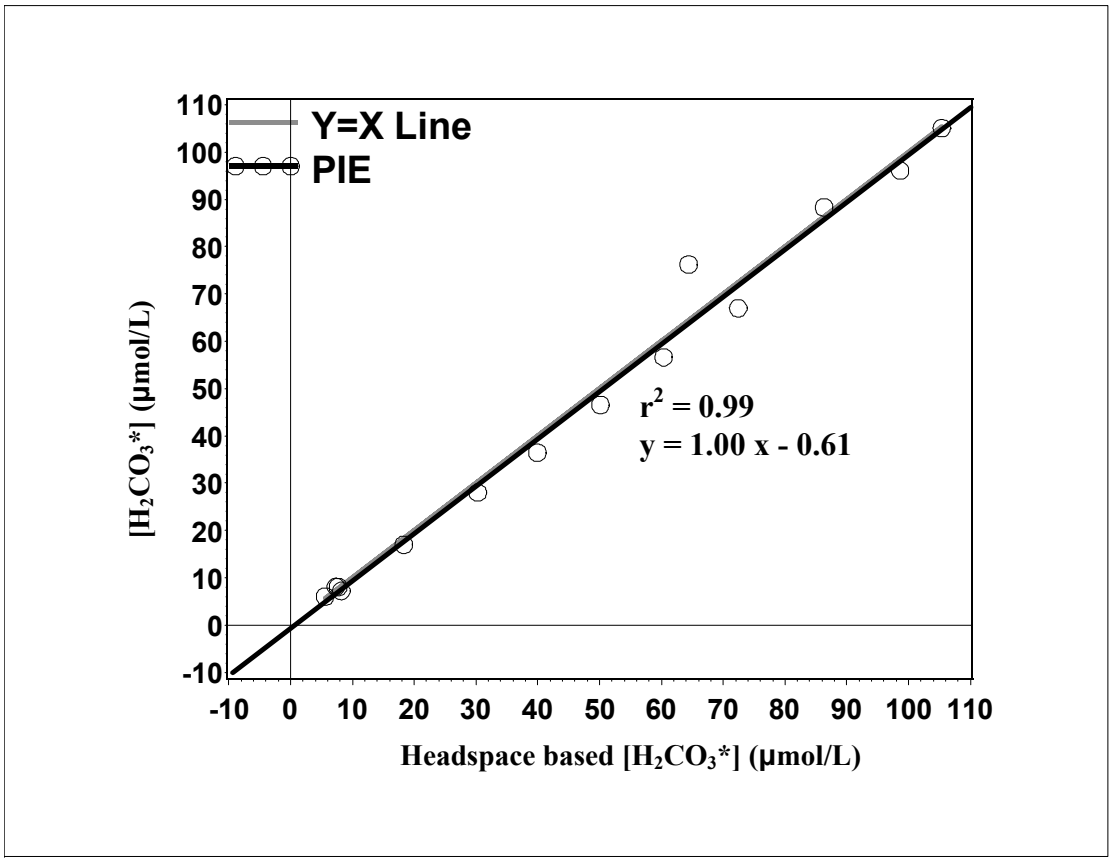

Figure 8. Experiment 4 (N=14), PIE based [H_2CO_3*] post-acidification values (Eq. [14]) versus headspace based [H_2CO_3*] post-acidification values (Eq. [28]).

Laboratory based DIC measurements taken immediately before total solution acidification were regressed against the sodium bicarbonate concentration added to the solutions. Figure 9 shows a strong correlation between the laboratory based DIC pre-acidification measurements and the sodium bicarbonate concentration (r^2 = 1.00, slope = 0.95 ± 0.02, Table 3). However, the laboratory based DIC clearly underestimated the sodium bicarbonate concentration.

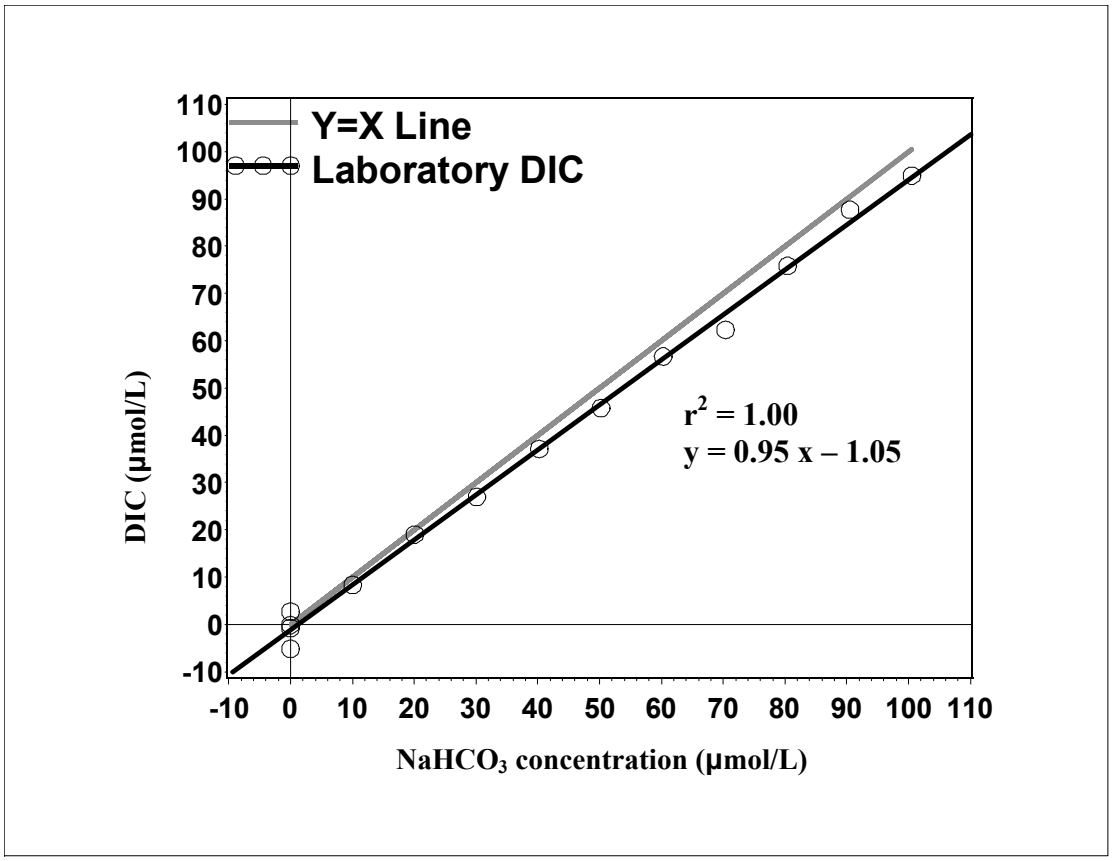

Figure 9. Experiment 4 (N=14), laboratory based DIC pre-acidification values versus sodium bicarbonate concentration.

All the laboratory and lake experiments had problems with the laboratory based DIC measurements. Laboratory based DIC measurements (Experiments 4 and 5) were taken immediately before total solution acidification, in order reduce of loss of $[H_2CO_3^*]$ during sampling and/or analyses. However, the laboratory based DIC pre-acidification measurements y-intercepts (Experiments 4 and 5) are shifted below the origin, unlike the headspace based $[H_2CO_3^*]$ post-acidification measurements (Experiments 4 and 5) and the PIE based $[H_2CO_3^*]$ post-acidification measurements

(Experiments 4 and 5). Therefore, we suspect that the y-intercepts of -1.0 ± 0.25 and -5.84 ± 0.85 μmol L^{-1} DIC for Experiments 4 and 5 (Table 3), respectively, likely reflect the loss of [$H_2CO_3^*$] during sampling and/or analyses. Other lake and laboratory studies have also reported this [$H_2CO_3^*$] loss during sampling and/or analyses.

Results from replicate laboratory based DIC pre-acidification measurements, which had been performed in conjunction with the laboratory experiments, also showed this [$H_2CO_3^*$] loss during sampling and/or analyses. Results showed large variations in the laboratory based DIC concentrations of the (triplicate) replicate samples. The first replicate set measured by the gas chromatograph had better results than the following sets. The variations had no specific pattern for the measured DIC range (0 to 100 μmol L^{-1}) other than a decrease in DIC concentrations (5 to 20 μmol L^{-1}) recorded over the time of measurement by the gas chromatograph. It was suspected that some samples had built up gas pressure, were supersaturated with respect to the atmosphere, and had subsequent loss of carbon dioxide to the atmosphere. Other studies also have found that built up gas pressure (Portielje and Lijklema, 1995), biotic activity (Neumann et al., 2001; Portielje and Lijklema, 1995; and Rounds, 2006), warming (Neumann et al., 2001), and leakage during sampling, storage, transport, and measurement (Rosich, 2002) can alter the bicarbonate and $H_2CO_3^*$ concentration and subsequently the DIC concentration.

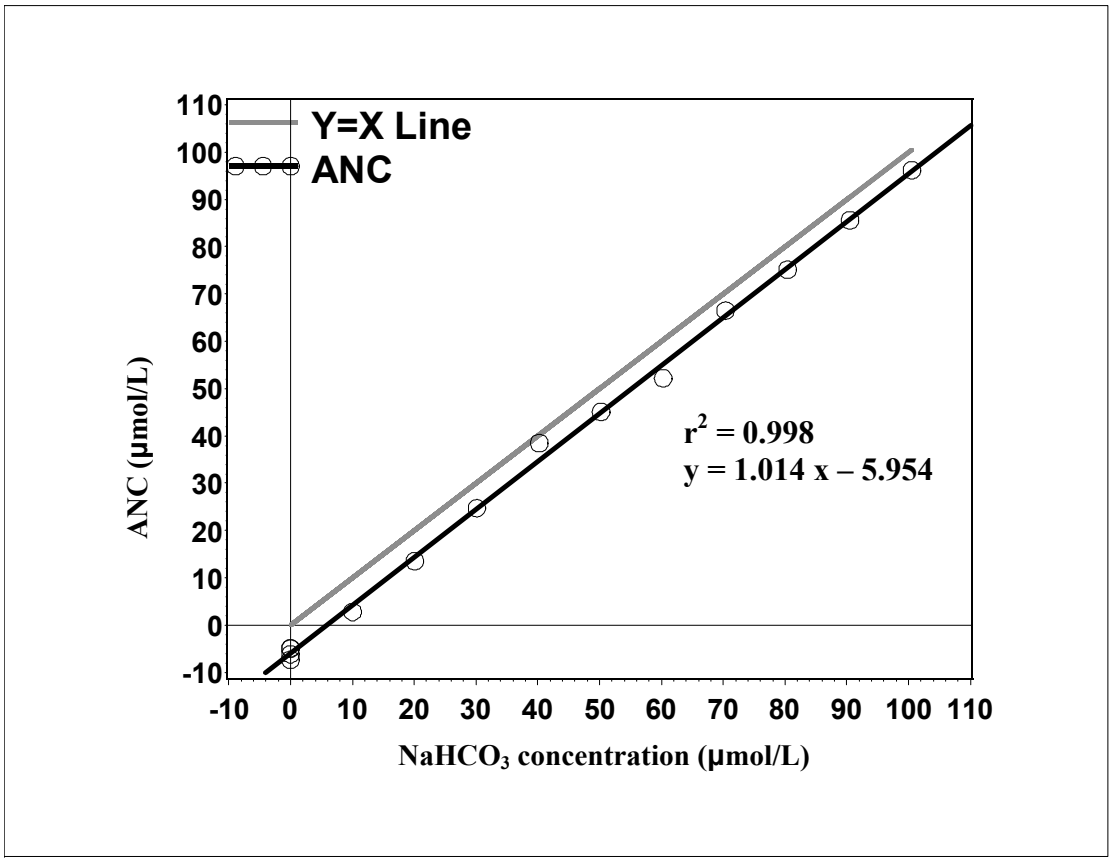

Figure 10. Experiment 4 (N=14), ANC (by Gran titration) pre-acidification values versus sodium bicarbonate concentration.

ANC measurements (by Gran titration) taken immediately before total solution acidification were regressed against the sodium bicarbonate concentration added to the solutions. As shown in Figure 10, the ANC pre-acidification measurements are strongly correlated with the sodium bicarbonate concentration ($r^2 = 0.998$, slope = 1.014 ± 0.012, Table 3). However, the ANC measurements y-intercept is shifted below the origin. The y-intercept of -5.954 ± 0.643 µmol L^{-1} ANC (Table 3) likely reflects the presence of background negative ANC in the pre-acidified solutions.

Table 3. Results for Experiments 1 through 7.

Experiment	Figure	Dependent variable (y)	Indep. variable (x)	N	RMSE	dep. mean	coeff. of variation (CV, %)	r^2	Adj. r^2	slope	std error slope	y-int.	std error y-int.	p-value
1		PIE P_{CO2} (pre-acidification)	$NaHCO_3$ conc.	12	22.0306	188.0271	11.7167	0.0786	-0.0135	-0.1760	0.1905	196.1156	10.8235	0.3775
1		PIE P_{CO2} (post-acidification)	$NaHCO_3$ conc.	12	33.9702	1405.8819	2.4163	0.9986	0.9985	25.1094	0.2938	251.5763	16.6895	< 0.0001
1		PIE $[H_2CO_3]$ (pre-acidification)	$NaHCO_3$ conc.	12	0.66	6.95	9.54	0.02	-0.08	-0.002	0.006	7.06	0.33	0.68
1		PIE $[H_2CO_3]$ (post-acidification)	$NaHCO_3$ conc.	12	0.51	52.57	0.98	1.00	1.00	0.97	0.004	8.09	0.25	< 0.0001
1		PIE $[H_2CO_3]$ (adjusted)	$NaHCO_3$ conc.	12	0.59	45.63	1.29	1.00	1.00	0.97	0.005	1.04	0.29	< 0.0001
2		PIE P_{CO2} (pre-acidification)	$NaHCO_3$ conc.	11	15.6353	169.7337	9.2116	0.6340	0.5933	-5.8891	1.4916	199.2343	8.8349	0.0034
2		PIE P_{CO2} (post-acidification)	$NaHCO_3$ conc.	11	7.7794	331.9466	2.3436	0.9844	0.9826	17.6719	0.7422	243.4226	4.3958	< 0.0001
2		PIE $[H_2CO_3]$ (pre-acidification)	$NaHCO_3$ conc.	11	0.55	6.43	8.55	0.54	0.49	-0.17	0.05	7.28	0.31	0.01
2		PIE $[H_2CO_3]$ (post-acidification)	$NaHCO_3$ conc.	11	0.23	12.68	1.83	0.99	0.99	0.78	0.02	8.77	0.13	< 0.0001
2		PIE $[H_2CO_3]$ (adjusted)	$NaHCO_3$ conc.	11	0.58	6.24	9.30	0.97	0.97	0.95	0.06	1.49	0.33	< 0.0001
3		PIE P_{CO2} (pre-acidification)	$NaHCO_3$ conc.	14	31.0241	209.4629	14.8113	0.0904	0.0146	0.2591	0.2372	199.2227	12.5158	0.2962
3		PIE P_{CO2} (post-acidification)	$NaHCO_3$ conc.	14	49.9771	1305.6411	3.8278	0.9976	0.9974	27.0224	0.3822	237.7201	20.1618	< 0.0001
3		PIE $[H_2CO_3]$ (pre-acidification)	$NaHCO_3$ conc.	14	0.98	7.49	13.11	0.14	0.07	0.01	0.01	7.08	0.40	0.19
3		PIE $[H_2CO_3]$ (post-acidification)	$NaHCO_3$ conc.	14	0.85	46.97	1.82	1.00	1.00	0.98	0.01	8.40	0.34	< 0.0001
3		PIE $[H_2CO_3]$ (adjusted)	$NaHCO_3$ conc.	14	0.57	39.48	1.45	1.00	1.00	0.97	0.004	1.32	0.23	< 0.0001

Table 3. (continued).

Experiment	Figure	Dependent variable (y)	Indep. variable (x)	N	RMSE	dep. mean	coeff. of variation (CV, %)	r^2	Adj. r^2	slope	std error slope	y-int.	std error y-int.	p-value
4		PIE P_{CO2} (pre-acidification)	$NaHCO_3$ conc.	14	33.0996	189.6421	17.4537	0.1374	0.0655	0.3501	0.2533	175.8117	13.3551	0.1921
4		PIE P_{CO2} (post-acidification)	$NaHCO_3$ conc.	14	46.7055	1282.3376	3.6422	0.9979	0.9977	27.0937	0.3574	211.9259	18.8449	< 0.0001
4		PIE $[H_2CO_3]$ (pre-acidification)	$NaHCO_3$ conc.	14	1.05	6.80	15.50	0.18	0.11	0.01	0.01	6.28	0.43	0.13
4		PIE $[H_2CO_3]$ (post-acidification)	$NaHCO_3$ conc.	14	0.87	46.23	1.89	1.00	1.00	0.98	0.01	7.43	0.35	< 0.0001
4	6	PIE $[H_2CO_3]$ (adjusted)	$NaHCO_3$ conc.	14	0.97	39.43	2.45	1.00	1.00	0.97	0.01	1.14	0.39	< 0.0001
5		PIE P_{CO2} (pre-acidification)	$NaHCO_3$ conc.	13	32.1023	193.0650	16.6277	0.2412	0.1722	0.4911	0.2626	172.4823	14.1572	0.0883
5		PIE P_{CO2} (post-acidification)	$NaHCO_3$ conc.	13	53.5492	1328.3607	4.0312	0.9971	0.9969	27.0185	0.4380	195.8765	23.6153	< 0.0001
5		PIE $[H_2CO_3]$ (pre-acidification)	$NaHCO_3$ conc.	13	1.11	6.84	16.29	0.25	0.19	0.02	0.01	6.10	0.49	0.08
5		PIE $[H_2CO_3]$ (post-acidification)	$NaHCO_3$ conc.	13	1.71	47.23	3.62	1.00	1.00	0.96	0.01	6.93	0.75	< 0.0001
5		PIE $[H_2CO_3]$ (adjusted)	$NaHCO_3$ conc.	13	1.08	40.39	2.67	1.00	1.00	0.94	0.01	0.83	0.48	< 0.0001
4	7	headspace $[H_2CO_3]$	$NaHCO_3$ conc.	14	4.33	46.82	9.26	0.99	0.99	0.97	0.03	8.55	1.75	< 0.0001
4	8	PIE $[H_2CO_3]$ (post-acidification)	headspace $[H_2CO_3]$	14	4.31	46.23	9.32	0.99	0.99	1.00	0.03	-0.61	1.97	< 0.0001
5		headspace $[H_2CO_3]$	$NaHCO_3$ conc.	13	2.68	49.78	5.39	0.99	0.99	0.99	0.02	8.37	1.18	< 0.0001
5		PIE $[H_2CO_3]$ (post-acidification)	headspace $[H_2CO_3]$	13	2.31	47.23	4.90	1.00	1.00	0.97	0.02	-1.05	1.15	< 0.0001

Table 3. (continued).

Experiment	Figure	Dependent variable (y)	Indep. variable (x)	N	RMSE	dep. mean	coeff. of variation (CV, %)	r^2	Adj. r^2	slope	std error slope	y-int.	std error y-int.	p-value
4	9	Laboratory DIC	$NaHCO_3$ conc.	14	2.14	36.56	5.84	1.00	1.00	0.95	0.02	-1.05	0.25	< 0.0001
4		PIE [H_2CO_3] (post-acidification)	Laboratory DIC	14	1.93	46.23	4.18	1.00	1.00	1.03	0.02	8.61	0.77	< 0.0001
5		Laboratory DIC	$NaHCO_3$ conc.	13	1.92	35.30	5.45	1.00	1.00	0.98	0.02	-5.84	0.85	< 0.0001
5		PIE [H_2CO_3] (post-acidification)	Laboratory DIC	13	0.88	47.23	1.87	1.00	1.00	0.98	0.007	12.67	0.36	< 0.0001
4	10	ANC by Gran titration	$NaHCO_3$ conc.	14	1.592	34.093	4.671	0.998	0.998	1.014	0.012	-5.954	0.643	< 0.0001
4		PIE [H_2CO_3] (adjusted)	ANC by Gran titration	14	1.59	39.43	4.02	1.00	1.00	0.95	0.01	6.88	0.59	< 0.0001
5		ANC by Gran titration	$NaHCO_3$ conc.	13	2.485	37.002	6.715	0.995	0.995	0.966	0.020	-3.482	1.096	< 0.0001
5		PIE [H_2CO_3] (adjusted)	ANC by Gran titration	13	2.81	40.39	6.95	0.99	0.99	0.97	0.02	4.42	1.17	< 0.0001

Table 3. (continued).

Experiment	Figure	Dependent variable (y)	Indep. variable (x)	N	RMSE	dep. mean	coeff. of variation (CV, %)	r^2	Adj. r^2	slope	std error slope	y-int.	std error y-int.	p-value
6		PIE P_{CO2} (post-acidification)	$NaHCO_3$ P_{CO2}	12	53.1768	1235.0678	4.3056	0.9970	0.9967	0.9848	0.0172	138.7984	24.5465	<.0001
6		PIE [H_2CO_3] (post-acidification)	$NaHCO_3$ conc.	12	1.99	45.96	4.32	1.00	1.00	0.98	0.02	5.21	0.92	<.0001
7		PIE P_{CO2} (post-acidification)	$NaHCO_3$ P_{CO2}	12	26.9727	1261.0537	2.1389	0.9992	0.9991	0.9611	0.0085	164.3779	12.4503	<.0001
7		PIE [H_2CO_3] (post-acidification)	$NaHCO_3$ conc.	12	1.04	45.87	2.26	1.00	1.00	0.95	0.01	6.13	0.48	<.0001
6		headspace [H_2CO_3]	$NaHCO_3$ conc.	12	3.18	45.86	6.93	0.99	0.99	0.97	0.03	5.60	1.48	<.0001
6		PIE [H_2CO_3] (post-acidification)	headspace [H_2CO_3]	12	1.59	45.96	3.46	1.00	1.00	1.01	0.01	-0.30	0.80	<.0001
7		headspace [H_2CO_3]	$NaHCO_3$ conc.	12	2.12	46.71	4.53	1.00	1.00	0.92	0.02	8.19	0.98	<.0001
7		PIE [H_2CO_3] (post-acidification)	headspace [H_2CO_3]	12	1.37	45.87	2.99	1.00	1.00	1.03	0.01	-2.22	0.72	<.0001

Conclusion – Accuracy and Precision of PIE

For Experiment 1 and Experiments 3 through 7, the PIE based measurements had high accuracy and precision. The PIE based [$H_2CO_3^*$] measurements are strongly correlated with the sodium bicarbonate concentration added to the solutions. The r^2 values were 1.00. The root mean square errors (RMSE) were low and ranged from 0.57 to 1.99 μmol L^{-1} [$H_2CO_3^*$] and the mean RMSE was 1.04 μmol L^{-1} [$H_2CO_3^*$]. The coefficients of variation (CV) were also low and ranged from 1.29 to 4.32 % and the mean CV was 2.41 %. The PIE based [$H_2CO_3^*$] measurements trend with the sodium bicarbonate concentration added to the solutions was close to the one-to-one line. These slope values ranged from 0.94 to 0.98 with a mean slope of 0.96.

This chapter has characterized and examined the accuracy and precision of PIE based direct measurements of carbon dioxide using solutions of defined composition. With this verification, researchers now have a PIE based direct measurement with known precision and accuracy that can be applied to laboratory and lake studies.

TRADITIONAL LAKE STUDIES with PIE

In this chapter, PIE based direct carbon dioxide measurements were applied in a limited study of lakes across three trophic classes (eutrophic, mesotrophic, oligotrophic) and compared to traditional direct and indirect carbon dioxide measurements. This is where researchers will learn the importance of how PIE based dissolved carbon dioxide measurements perform in natural systems and traditional lake studies. The first chapter section contains the methods used for the traditional lake studies. In the following chapter sections, (1) PIE based measurements were taken to have a range of carbon dioxide measurements similar to the laboratory experiments; (2) a set of replicate carbon dioxide measurements within a lake were made to investigate variations between PIE and traditional direct and indirect carbon dioxide measurements; (3) PIE based carbon dioxide measurements were compared in a traditional fifty-two lake surface water survey (one surface water sample measurement with each method at each lake); and (4) PIE based carbon dioxide measurements were compared in traditional depth profiles from two lakes. PIE based measurements were also compared against direct (headspace) and indirect (pH and ANC; pH and DIC) measurements. The last section contains the conclusions for the traditional lake studies.

Methods –Traditional Lake Studies with PIE

The fifty-two study lakes (Figure 11; Appendices B and C) for the traditional lake studies were located in Vilas and Oneida Counties of Northern Wisconsin. These lakes had a wide range of geologic, hydrologic, watershed, and landscape position characteristics. See Appendices B and C for lake names, lake numbers, and other characteristics. Three broad trophic classes (oligotrophic, N = 17; mesotrophic, N = 18; and eutrophic, N =17) were represented.

Since there was little or no available data for selecting these lakes, these study lakes were chosen using Remote Sensing (Landsat satellite) estimates of the water clarity (Secchi disk transparency) of these lakes (Chipman et al., 2004) to derive the Wisconsin trophic state index Secchi disk transparency (WTSI (SDT)) (Carlson, 1977; Chipman et al., 2004; Lillie et al., 1993). Secchi disk transparency (SDT) is an estimate of the amount of nutrients in the water, growth of algae and plankton, and distance you can see down into the water. The greater the Secchi disk transparency, the deeper you can see into the water (Tyler, 1968). The WTSI (SDT) was used because it was specifically designed for the morphology of Wisconsin lakes (Lillie et al., 1993). Trophic class breakpoints were above fifty for eutrophic lakes, between forty to fifty for mesotrophic lakes, and below forty for oligotrophic lakes (Figure 11). After selection by trophic class, lakes were additionally chosen by accessibility (navigable boat ramp) and logistics (route between lakes). The fifty-two study lakes in Figure 11 were mapped using ESRI ArcGIS ArcMAP. For proper registration, this map was geo-referenced to the Wisconsin Transverse Mercator (WTM83/91)

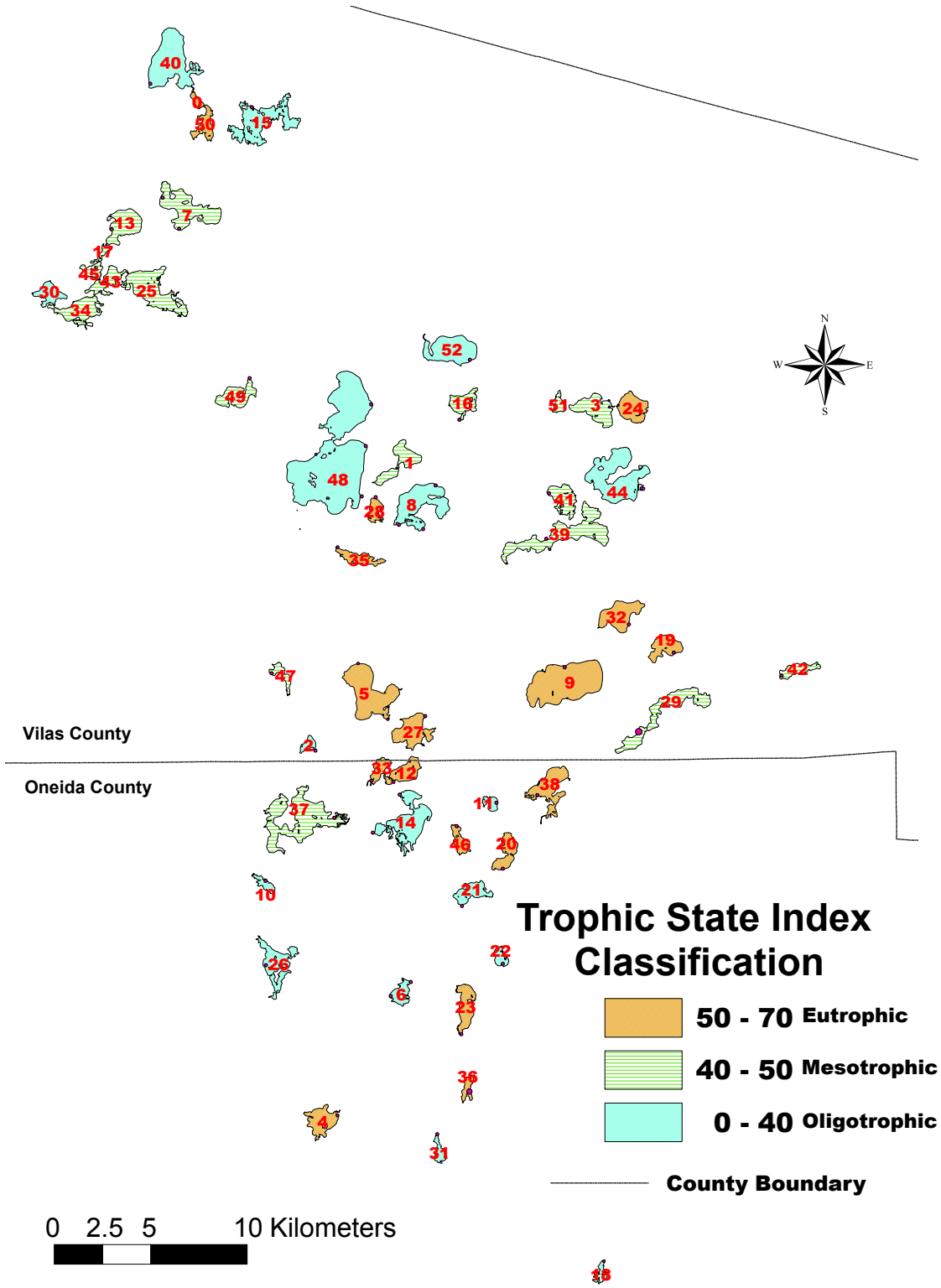

Figure 11. This ESRI ArcGIS ArcMAP lake clarity map of the 52 lakes (Appendices B and C) in this study was based on Secchi disk transparency and classified with the Wisconsin trophic state index Secchi disk transparency (Carlson, 1977; Chipman et al., 2004; Lillie et al., 1993).

geographic coordinate system (meters) and North American 1983 HARN geographic projection system.

Lake samples were collected from a 17-foot boat. The boat was secured with two anchors at each sampling point. For the lake study with a similar carbon dioxide range to the laboratory studies, thirty-five near-shore surface water, deep-water surface water, and depth profile samples were taken throughout one lake. (The surface water samples were taken at a one-half meter depth or at least 30 cm above the sediment. The depth profile samples were taken at one-half to one-meter intervals starting at less than one-half meter below the surface water-atmosphere interface down to just above the lake sediment.) For the replicate sample lake study, ten P_{CO2} replicate measurements were taken from one point and 0.5m depth during a six-hour period on one lake. For the fifty-two lake surface-water lake study, near-surface water lake samples (0.5 m depth) were taken near the deepest point of lakes with known bathymetry or otherwise at a point near the middle of the lake and at least 100 meters from shore. For the depth profile lake studies, depth profiles were taken near the deepest point of two lakes at one-half to one-meter intervals starting at less than one-half meter below the surface water-atmosphere interface down to just above the lake sediment. A Trimble GeoExplorer Geo (CE) XT Global Positioning System (GPS) was used to record each surface water sampling point on these lakes. These points were geo-referenced to the Wisconsin Transverse Mercator (WTM83/91) geographic coordinate system (meters) and North American 1983 HARN geographic projection system. See Appendices B and C for the sampling point coordinates for the fifty-two

lake study, carbon dioxide replicate study, diurnal pattern study, and depth profile studies.

Samples for PIE, headspace, laboratory DIC, and ANC were obtained at the same time by lowering three polyethylene-sampling lines attached to a YSI multi-parameter sonde to the sampling depth. All PIE based carbon dioxide measurements were obtained with one sampling line and peristaltic pump. Headspace based carbon dioxide measurements and Orion ROSS electrode pH were obtained with the second sampling line and peristaltic pump. This pH was measured using an Orion electrode pH probe in a modified beaker that had been flushed with sample via the sampling line. The flow was then stopped for this Orion electrode pH measurement. All the other water samples for ANC and DIC were taken through the same third sampling line and peristaltic pump. The YSI 600 MDS equipped with a 600XL multi-parameter sonde attached to these three sampling lines was used to record depth, temperature, oxygen, pH, atmospheric barometric pressure, and specific conductivity measurements for each sampling position. Air temperatures measurements were also made with a Traceable® thermometer.

Results and Discussion – Traditional Lake Studies with PIE

Comparison of PIE to traditional methods on Allequash Lake. PIE based measurements were compared against direct (headspace) and indirect (P_{CO2} by pH and ANC) measurements. These carbon dioxide measurements (0 to 2314 μatm; 0 to 93 μmol L^{-1}) were taken to have a range of carbon dioxide measurements similar to the laboratory experiments (0 to 2610 μatm; 0 to 100 μmol L^{-1}). These measurements were composed of near-shore surface water, deep-water surface water, and depth profile samples.

Thirty-five P_{CO2} measurements were made at Allequash Lake from 06/06/2008 to 06/10/2008 with PIE. They were regressed against the headspace measured P_{CO2}. There was a strong correlation between PIE based P_{CO2} and headspace based P_{CO2} (r^2 = 0.9778, slope = 0.9067 ± 0.0238, Table 4). (These measurements were made at different locations and depths throughout the northern bay of Allequash Lake, where lake temperatures ranged from 15.47 to 20.21 °C.)

Corresponding concentrations of [$H_2CO_3^*$], estimated by Henry's law, illustrate similar trends. There was a strong correlation between PIE based [$H_2CO_3^*$] (Figure 12) and headspace based [$H_2CO_3^*$] (r^2 = 0.98, slope = 0.87 ± 0.02, Table 4).

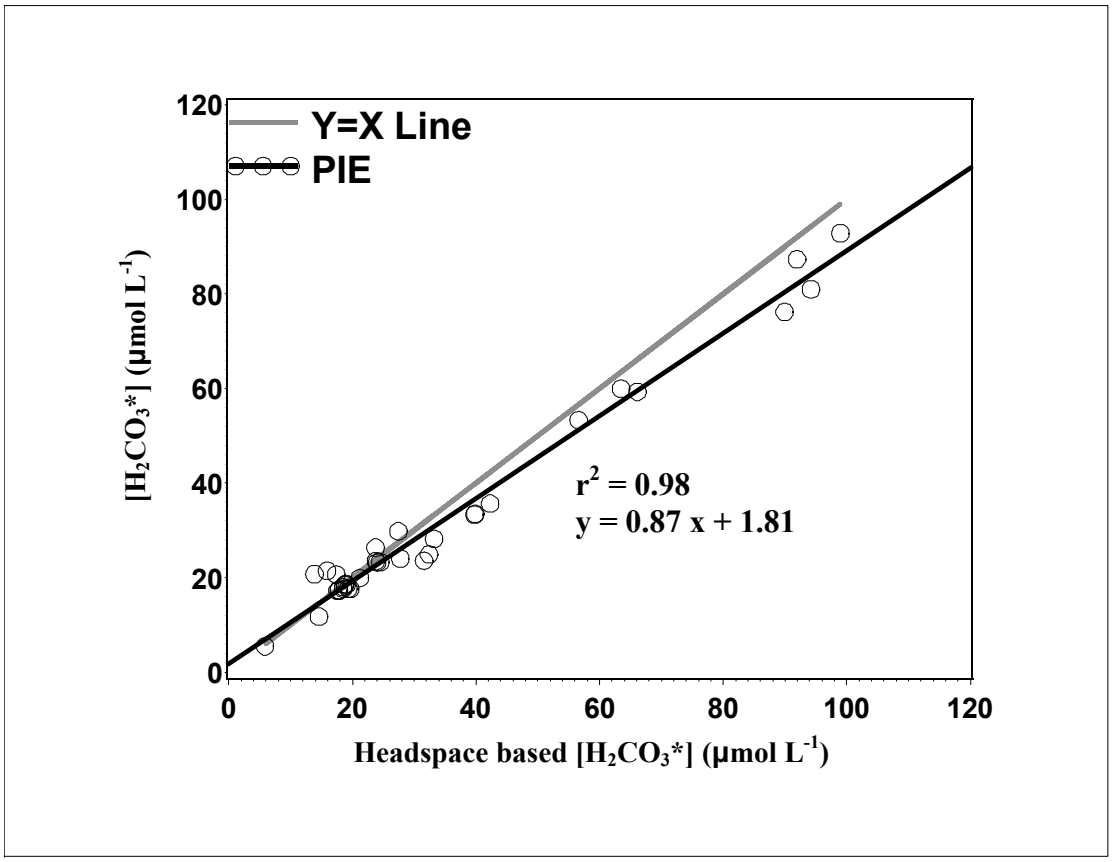

Figure 12. Comparison of PIE to traditional methods on Allequash Lake (N = 35), PIE based $[H_2CO_3^*]$ versus headspace based $[H_2CO_3^*]$.

PIE based P_{CO2} (Figure 13) were also regressed against the P_{CO2} by pH and ANC (Gran titration) measurements. There was a strong correlation between PIE based P_{CO2} and P_{CO2} by pH and ANC ($r^2 = 0.9797$, slope = 1.0882 ± 0.0272, Table 4).

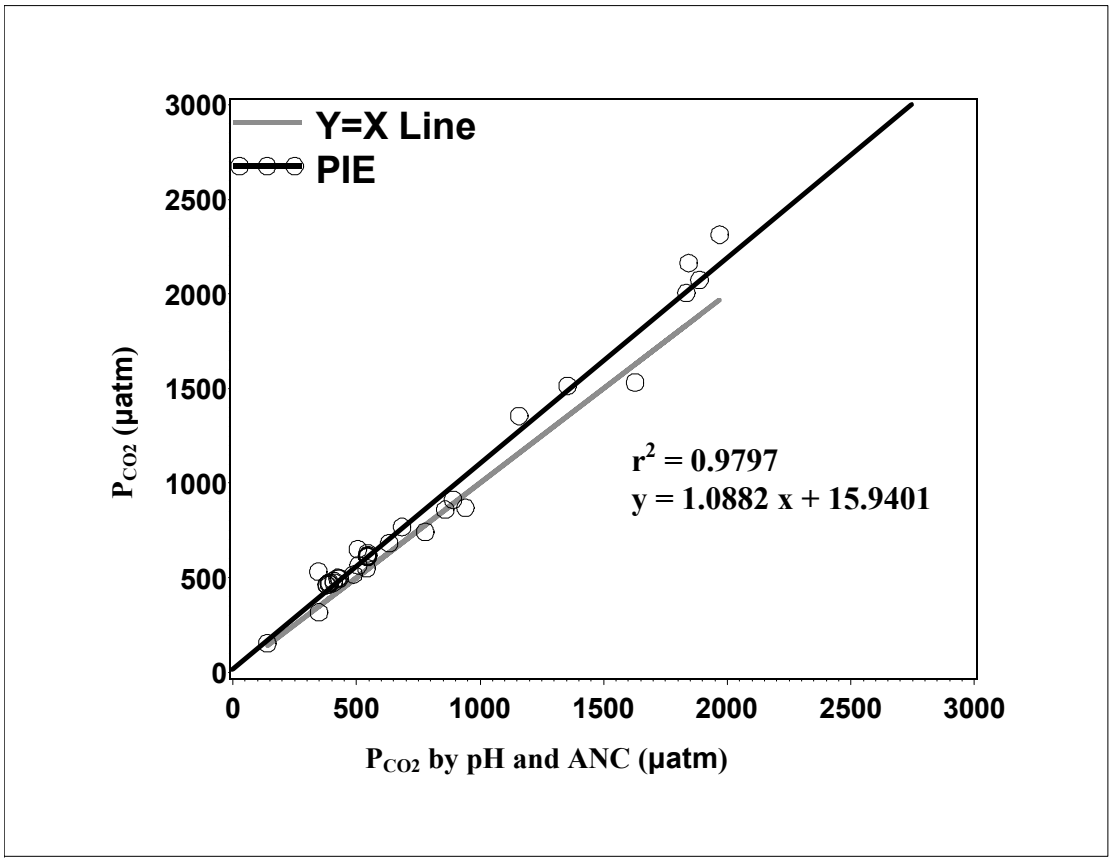

Figure 13. Comparison of PIE to traditional methods on Allequash Lake (N = 35), PIE based P_{CO2} versus P_{CO2} by pH and ANC (Gran titration).

Table 4. Comparison of PIE to traditional methods on Allequash Lake.

Experiment	Figure	Dependent variable (y)	Indep. variable (x)	N	RMSE	dep. mean	coeff. of variation (CV, %)	r^2	Adj. r^2	slope	std error slope	y-int.	std error y-int.	p-value
Allequash's range		PIE P_{CO2}	headspace P_{CO2}	35	84.9812	827.6831	10.2674	0.9778	0.9771	0.9067	0.0238	39.6870	25.1656	<.0001
Allequash's range	12	PIE $[H_2CO_3^*]$	headspace $[H_2CO_3^*]$	35	3.15	31.98	9.84	0.98	0.98	0.87	0.02	1.81	0.90	<.0001
Allequash's range		headspace $[H_2CO_3^*]$	PIE $[H_2CO_3^*]$	35	3.57	34.50	10.33	0.98	0.98	1.12	0.03	-1.37	1.06	<.0001
Allequash's range	13	PIE P_{CO2}	P_{CO2} by pH and ANC (Gran tit.)	35	81.1889	827.6831	9.8092	0.9797	0.9791	1.0882	0.0272	15.9401	24.5168	<.0001

PIE based replicate measurements on Allequash Lake. A set of replicate P_{CO2} measurements within a lake were made to investigate variations between PIE and traditional direct and indirect carbon dioxide measurements. Ten measurements were taken at one surface water point and 0.5 m depth over a six hour period on Allequash Lake. These measurements were made from 1133 to 1738 hours (CST) on 06/10/2008 in the middle of summer stratification. Figure 14 compares PIE based P_{CO2} measurements against direct (headspace based P_{CO2}) and indirect (P_{CO2} by pH and ANC) measurements. A dashed line was drawn at the extreme minimum and maximum values of the PIE based P_{CO2} method in order to show the spread of values in comparison to the other methods. (These Allequash Lake temperature measurements only ranged from 18.84 to 19.10 °C.)

PIE based P_{CO2} (Figure 14) measurements more closely matched the spread, median, and mean of the direct (headspace based P_{CO2}) measurements than the indirect (P_{CO2} by pH and ANC) measurements. The PIE based P_{CO2} (mean = 479.1384 ± 14.4888 µatm, Table 5) was not significantly different from the headspace based P_{CO2} (mean = 493.75 ± 18.37 µatm, Table 5) at the $p = 0.21$ significance level. However, the PIE based P_{CO2} (mean = 479.1384 ± 14.4888 µatm, Table 5) was significantly different from the P_{CO2} by pH and ANC (mean = 403.33 ± 19.70 µatm, Table 5) at the $p = 0.0002$ significance level. All the methods have very low coefficients of variation with PIE based P_{CO2} having the lowest CV at 3.0239 %. The indirect P_{CO2} by pH and ANC measurements (ranging from 379 to 431 µatm) were also different from the direct measurements for having some measurements close to the June 2008 ambient

atmospheric global average of 362 µatm P_{CO2} (385 ppmv P_{CO2}; Tans, 2008). The indirect measurement seems to be going through some biotic or temperature induced carbon species change during sampling, transport, or measurement, which lead to net loss of ANC.

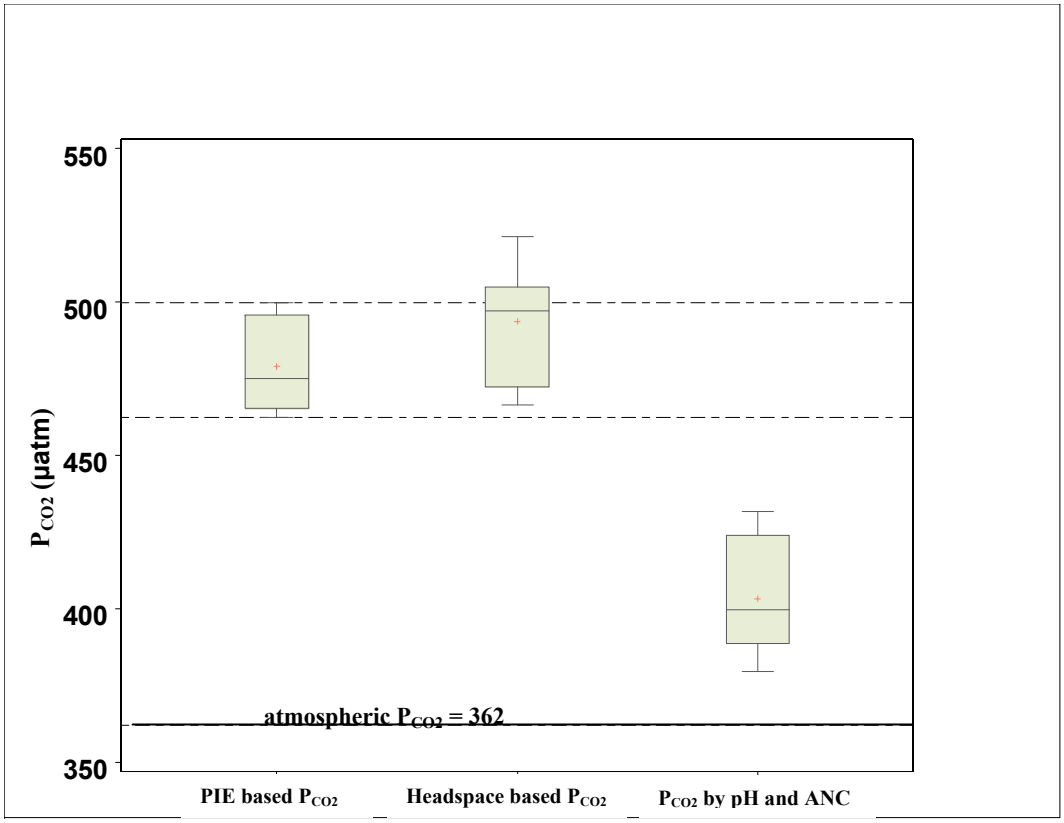

Figure 14. Box plots for PIE based replicate measurements on Allequash Lake (box plot close-up starts at 350 µatm, N = 10). P_{CO2} quartiles with horizontal line median and plus sign (+) mean. Measured P_{CO2} by method, including PIE based P_{CO2}, headspace based P_{CO2}, and P_{CO2} by pH and ANC (Gran titration). A dashed line was drawn at the extreme minimum and maximum values of the PIE based P_{CO2} method in order to show the spread of values in comparison to the other methods.

Table 5. PIE based replicate measurements on Allequash Lake.

Experiment	Figure	Method	N	dep. Mean (µatm)	Median (µatm)	Standard Deviation	coeff. of variation (CV, %)
Allequash's replicates	14	PIE P_{CO2}	**10**	**479.1384**	**475.0387**	**14.4888**	**3.0239**
Allequash's replicates	14	headspace P_{CO2}	**10**	**493.75**	**497.10**	**18.37**	**3.72**
Allequash's replicates	14	P_{CO2} by pH and ANC (Gran tit.)	**10**	**403.33**	**399.80**	**19.70**	**4.88**

PIE in a fifty-two lake surface water survey. Figure 15 shows a comparison between fifty-two surface water PIE based and headspace based P_{CO2} measurements made on lakes throughout Vilas and Onieda Counties (07/09/2007 to 07/22/2007). See Appendices B and C for temperature, lake name, GPS position, and other characteristics of these lakes. There was a strong correlation between PIE based P_{CO2} (Figure 15) and headspace based P_{CO2} ($r^2 = 0.8984$, slope = 0.9093 ± 0.0432, Table 6).

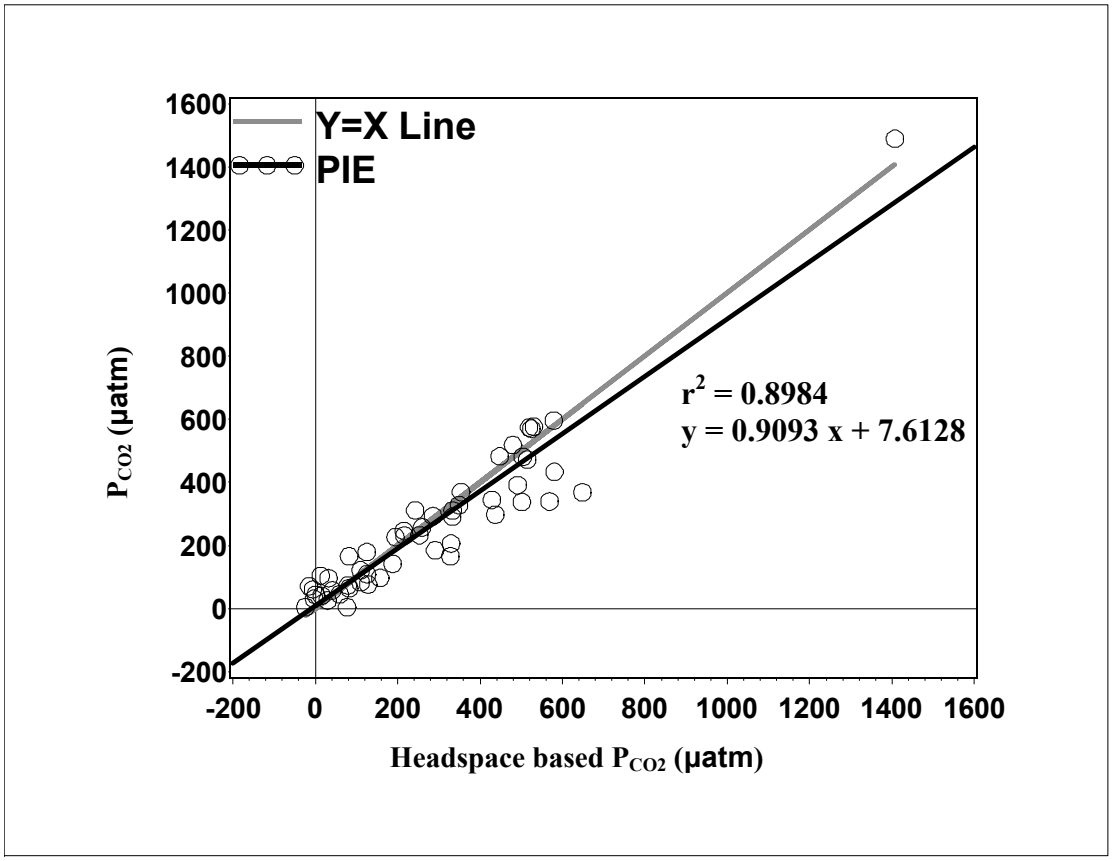

Figure 15. PIE in a fifty-two lake surface water survey (N = 52), PIE based P_{CO2} versus headspace based P_{CO2}.

In Figure 16, PIE based P_{CO2} were regressed against the P_{CO2} by pH and DIC measurements. There was a strong correlation between PIE based P_{CO2} (Figure 16) and P_{CO2} by pH and DIC ($r^2 = 0.9335$, Table 6). However, the slope (1.4850 ± 0.0561, Table 6) was significantly different from one ($p = 0.0002$).

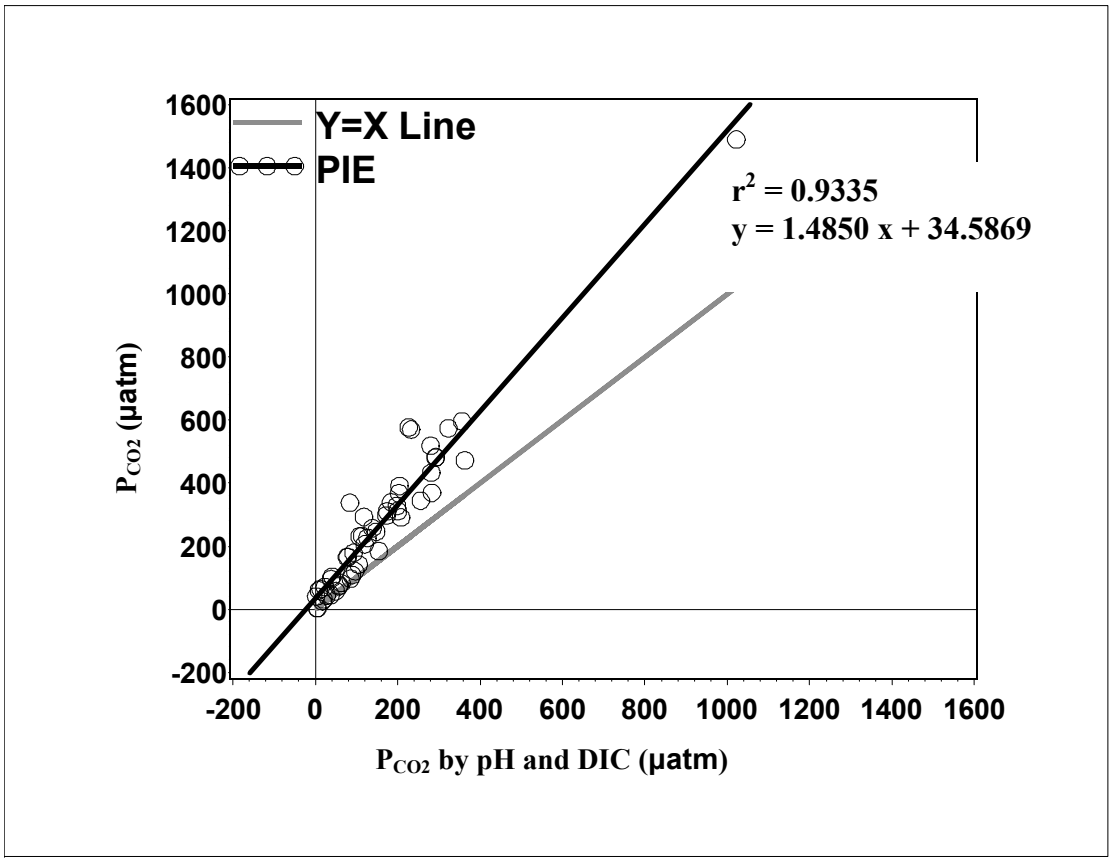

Figure 16. PIE in a fifty-two lake surface water survey (N = 52), PIE based P_{CO2} versus P_{CO2} by pH and laboratory DIC.

In Figure 17, PIE based P_{CO2} were regressed against the P_{CO2} by pH and ANC (Gran titration) measurements. Similar to the other indirect measurements, there was a strong correlation between PIE based P_{CO2} (Figure 17) and P_{CO2} by pH and ANC (r^2 = 0.9521, Table 6). However, the slope (1.3953 ± 0.0443, Table 6) was significantly different from one (p = 0.0002).

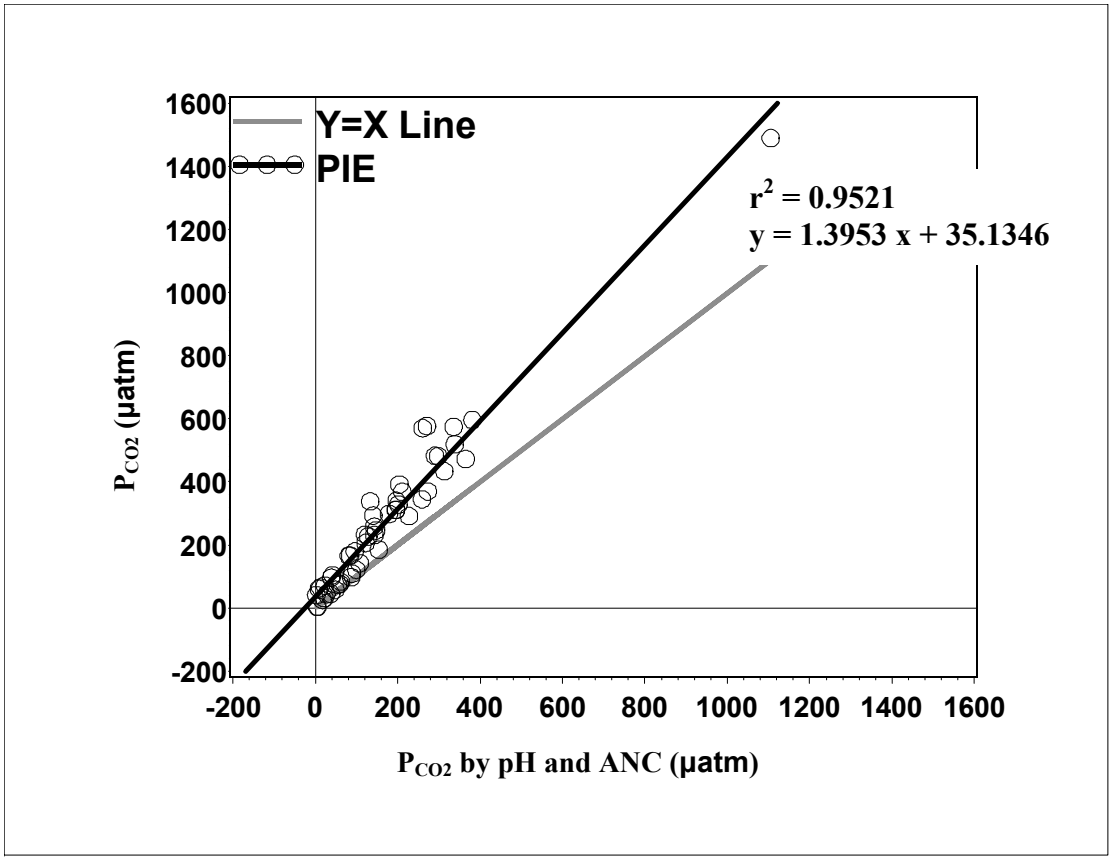

Figure 17. PIE in a fifty-two lake surface water survey (N = 52), PIE based P_{CO2} versus P_{CO2} by pH and ANC (Gran titration).

In Figure 18, PIE based P_{CO2} were also regressed against the P_{CO2} by pH and ANC (C_B and C_A) measurements. Similar to the other indirect measurements, there was a strong correlation between PIE based P_{CO2} (Figure 18) and P_{CO2} by pH and ANC ($r^2 = 0.9241$, Table 6). However, the slope (1.5620 ± 0.0633, Table 6) was significantly different from one ($p = 0.0002$).

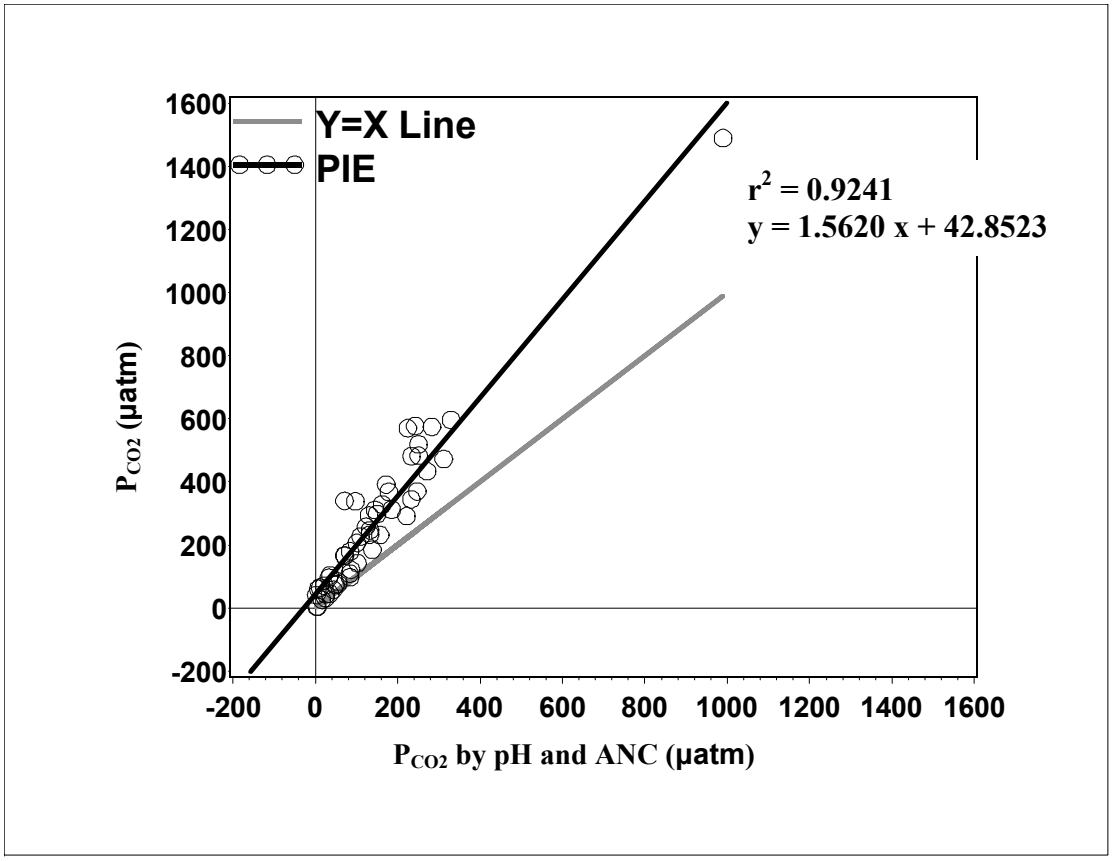

Figure 18. PIE in a fifty-two lake surface water survey (N = 52), PIE based P_{CO2} versus P_{CO2} by pH and ANC (C_B and C_A).

The results from the fifty-two lakes were also used to evaluate the importance of lake trophic state on the correlation between PIE and more traditional methods. Here are the method to method comparisons under different trophic conditions. Figure 19 shows a comparison between PIE based and headspace based P_{CO2} measurements for eutrophic lakes. There was a strong correlation between PIE based P_{CO2} (Figure 19) and headspace based P_{CO2} ($r^2 = 0.9878$, slope = 1.0527 ± 0.0302, Table 6).

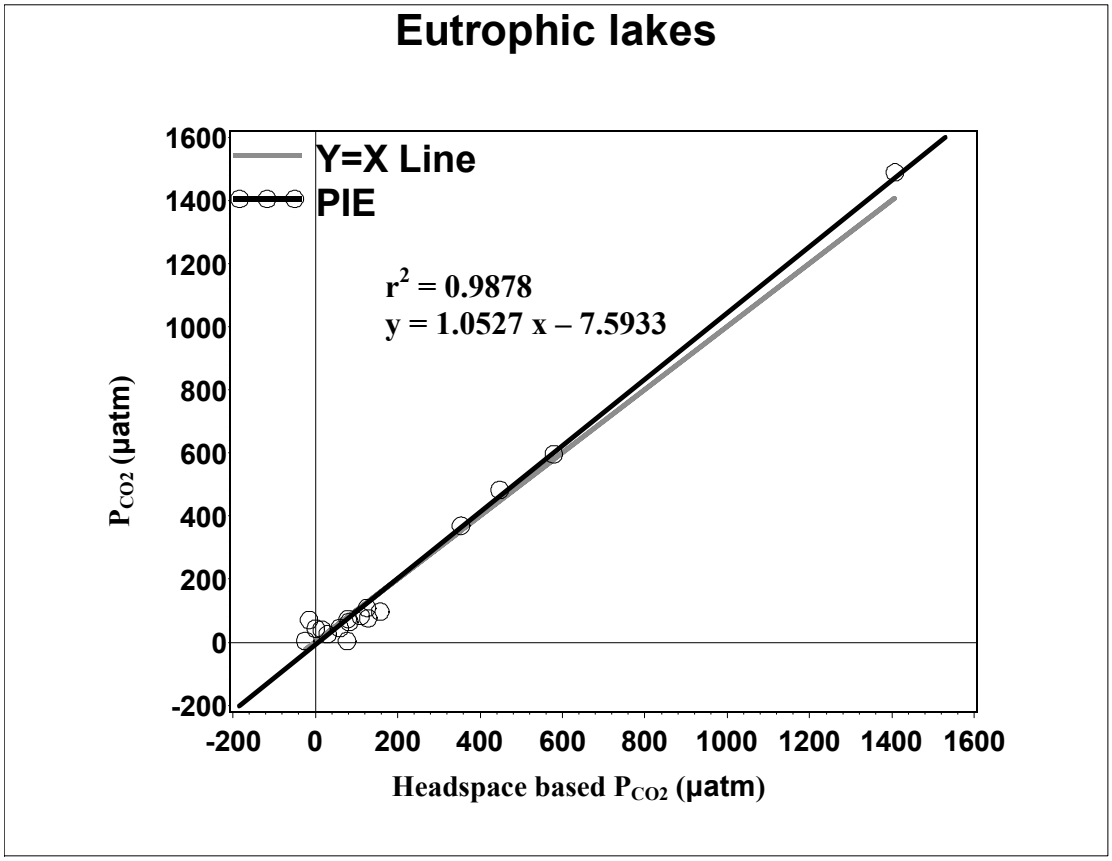

Figure 19. PIE in a fifty-two lake surface water survey (eutrophic lakes; N = 17), PIE based P_{CO2} versus headspace based P_{CO2}.

Figure 20 shows a comparison between PIE based and headspace based P_{CO2} measurements for mesotrophic lakes. There was a strong correlation between PIE based P_{CO2} (Figure 20) and headspace based P_{CO2} ($r^2 = 0.7989$, Table 6). However, the slope (0.6005 ± 0.0753, Table 6) was significantly different from one ($p = 0.0002$). Additionally, these mesotrophic lake results are more scattered than the eutrophic lakes above.

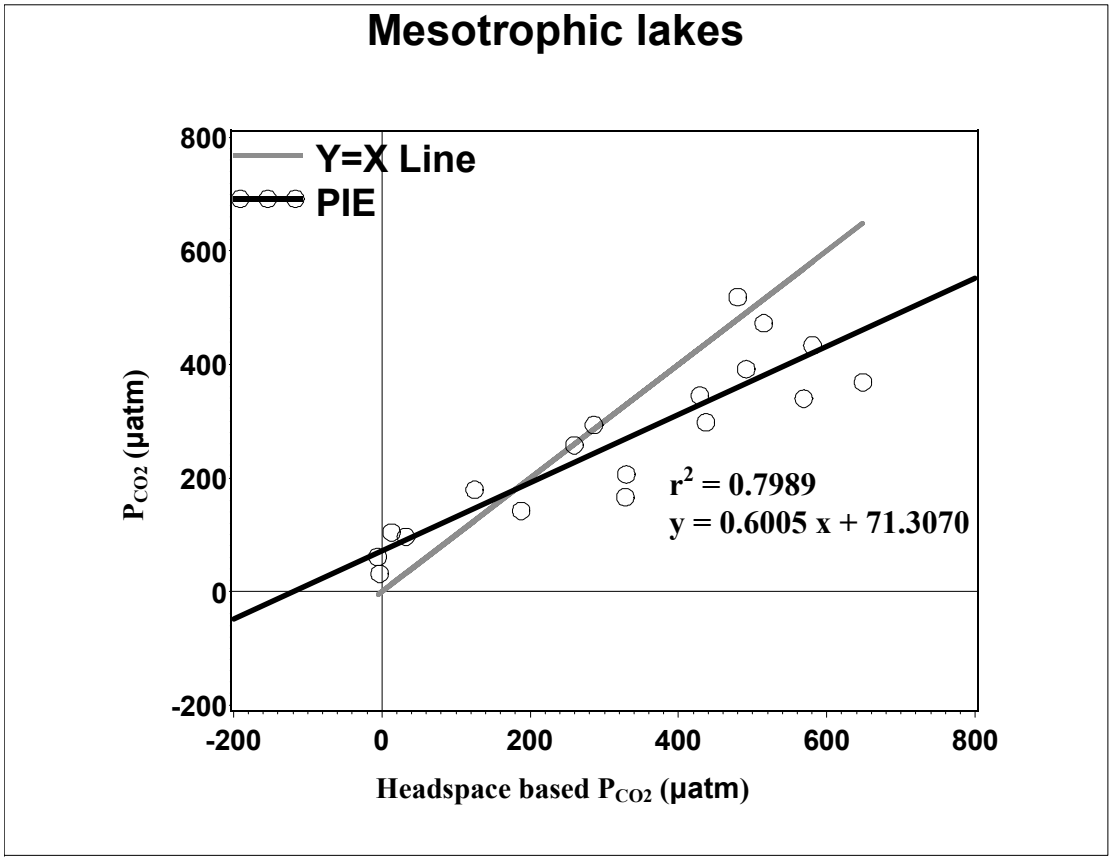

Figure 20. PIE in a fifty-two lake surface water survey (mesotrophic lakes; N = 18), PIE based P_{CO2} versus headspace based P_{CO2}.

Figure 21 shows a comparison between PIE based and headspace based P_{CO2} measurements for oligotrophic lakes. There was a strong correlation between PIE based P_{CO2} (Figure 21) and headspace based P_{CO2} ($r^2 = 0.8514$, slope = 0.9007 ± 0.0972, Table 6). However, these oligotrophic lake results are more scattered than the eutrophic lakes above.

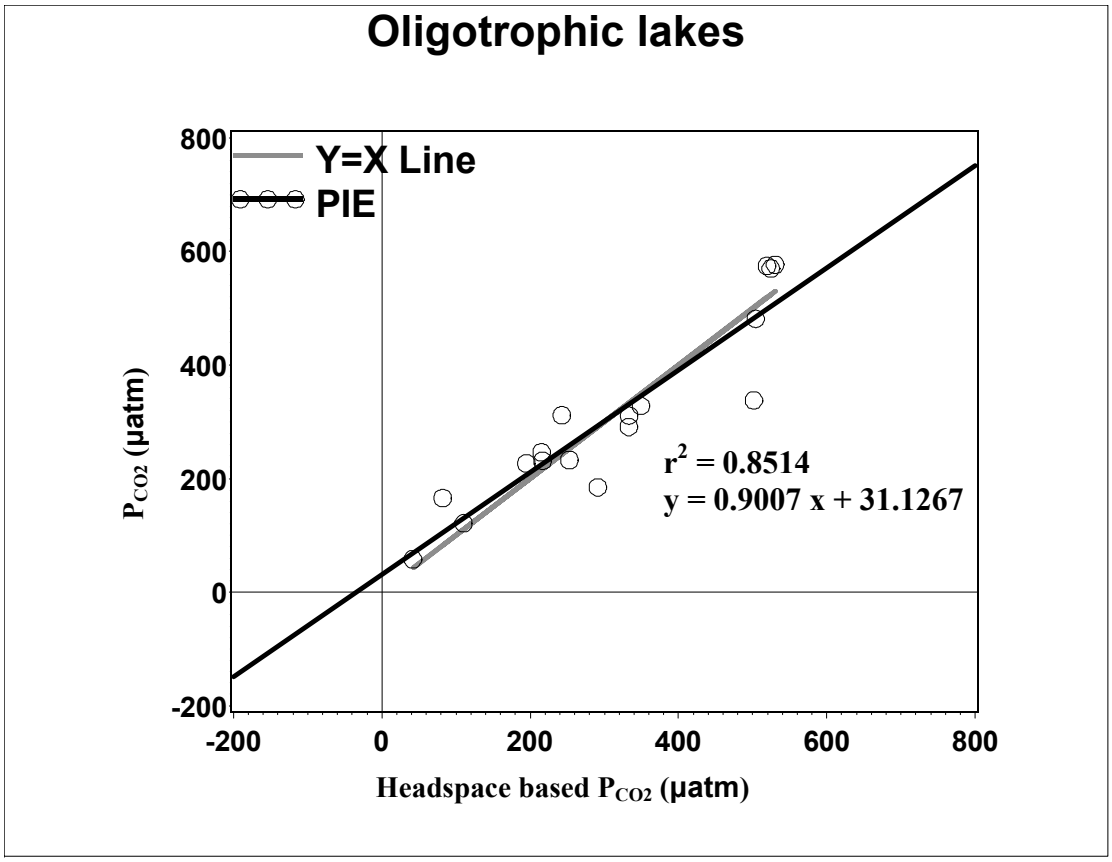

Figure 21. PIE in a fifty-two lake surface water survey (oligotrophic lakes; N = 17), PIE based P_{CO2} versus headspace based P_{CO2}.

As described in the *Introduction*, recent studies of lake metabolism have shown that most of the world's lakes surface waters are supersaturated with dissolved carbon dioxide (Sobek et al., 2005), suggesting that lakes may be a net source of carbon dioxide emission into the atmosphere (Sobek et al., 2005). However, most of the lakes in the *PIE in a fifty-two lake surface water survey* were not supersaturated with dissolved carbon dioxide. According to PIE based dissolved carbon dioxide measurements in Figure 22, thirteen lake samples were oversaturated and thirty-nine lake samples were undersaturated with respect to the July 2007 ambient atmospheric global average of 362 μatm P_{CO2} (381 ppmv P_{CO2}; Tans, 2008). Therefore, most of these lakes are a sink for atmospheric carbon dioxide.

These findings do not necessarily refute the supersaturation findings in Sobek et al. (2005). Considering that only 150 of the worlds lakes had direct measurements of carbon dioxide and 4582 of the worlds lakes have been indirectly measured (Table 1), more research is needed and many more lakes will have to be directly measured with PIE to build a better picture of why these particular lakes in this study were undersaturated with respect to atmospheric carbon dioxide.

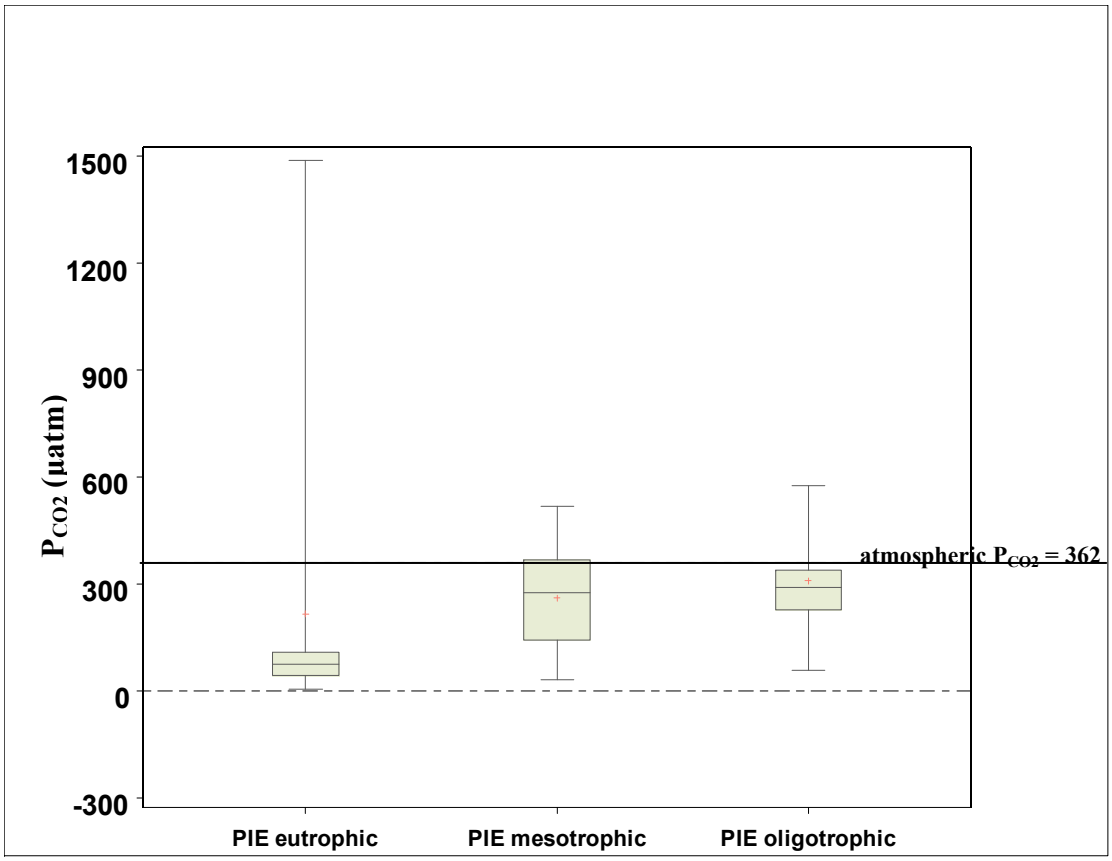

Figure 22. PIE in a fifty-two lake surface water survey (eutrophic, N = 17; mesotrophic, N= 18; oligotrophic, N = 17), measured PIE based P_{CO2} across trophic state.

Table 6. Pie in a fifty-two lake surface water survey.

Experiment	Figure	Dependent variable (y)	Indep. variable (x)	N	RMSE	dep. mean	coeff. of variation (CV, %)	r^2	Adj. r^2	slope	std error slope	y-int.	std error y-int.	p-value
52 Lakes	15	PIE P_{CO2}	headspace P_{CO2}	52	78.5658	262.4942	29.9305	0.8984	0.8964	0.9093	0.0432	7.6128	16.2971	< 0.0001
52 Lakes		PIE $[H_2CO_3^*]$	headspace $[H_2CO_3^*]$	52	2.57	8.75	29.36	0.90	0.90	0.92	0.04	0.22	0.53	< 0.0001
52 Lakes		headspace $[H_2CO_3^*]$	PIE $[H_2CO_3^*]$	52	2.66	9.32	28.59	0.90	0.90	0.99	0.05	0.70	0.55	< 0.0001
52 Lakes	16	PIE P_{CO2}	P_{CO2} by pH and laboratory DIC	52	63.5859	262.4942	24.2237	0.9335	0.9321	1.4850	0.0561	34.5869	12.3205	< 0.0001
52 Lakes	17	PIE P_{CO2}	P_{CO2} by pH and ANC (Gran tit.)	52	53.9699	262.4942	20.5604	0.9521	0.9511	1.3953	0.0443	35.1346	10.3953	< 0.0001
52 Lakes	18	PIE P_{CO2}	P_{CO2} by pH and ANC (C_B and C_A)	52	67.9007	262.4942	25.8675	0.9241	0.9226	1.5620	0.0633	42.8523	12.9566	< 0.0001
52 Lakes	19	PIE P_{CO2}	headspace P_{CO2}	17	42.3405	216.6604	19.5424	0.9878	0.9870	1.0527	0.0302	-7.5933	12.1183	< 0.0001
52 Lakes	20	PIE P_{CO2}	headspace P_{CO2}	18	67.5190	261.7323	25.7970	0.7989	0.7863	0.6005	0.0753	71.3070	28.7008	< 0.0001
52 Lakes	21	PIE P_{CO2}	headspace P_{CO2}	17	62.8400	309.1348	20.3277	0.8514	0.8415	0.9007	0.0972	31.1267	33.6432	< 0.0001

Depth profile lake measurements. To evaluate how PIE and traditional direct and indirect measurements compared within lakes, experiments were designed to explore the spatial resolution of PIE based measurements with depth for a mesotrophic lake (Allequash Lake) and an oligotrophic lake (Long Lake). These lakes were selected from the fifty-two study lakes and chosen because of easy accessibility.

Figure 23 shows the ten P_{CO2} depth profile measurements made for Allequash Lake's first depth profile on 09/15/2007 with PIE compared against the headspace measured P_{CO2}. There was a strong correlation between PIE based P_{CO2} (Figure 23) and headspace based P_{CO2} ($r^2 = 0.9279$, slope = 0.9527 ± 0.0939, Table 7). (The measurements made on this mesotrophic lake ranged from 15.18 to 15.80 °C in temperature.)

In Figures 24, 25, 26, and 27, the carbon dioxide measurement results from these methods and the oxygen results were graphed by depth for Allequash Lake. Figure 24 displays the high spatial resolution of the PIE based P_{CO2} measurements with depth. The O_2 and PIE based P_{CO2} fluctuations seemed to be a different magnitude, but opposite in direction. The profile (Figure 24) shows the dissolved oxygen (O_2) level had peak maximums (8.65 and 8.67 mg L^{-1}) and minimums (7.82 and 7.99 mg L^{-1}) at the same times that the PIE based P_{CO2} had at its minimums and maximums, respectively. Similar relationships were also found in diurnal studies of dissolved carbon dioxide and dissolved oxygen in Hanson et al., (2006). Among all the methods used, headspace based P_{CO2} (Figure 24) measurements more closely

mirrored the PIE based P_{CO2} values. Overall, the methods used had only small differences with depth for this shallow mesotrophic lake.

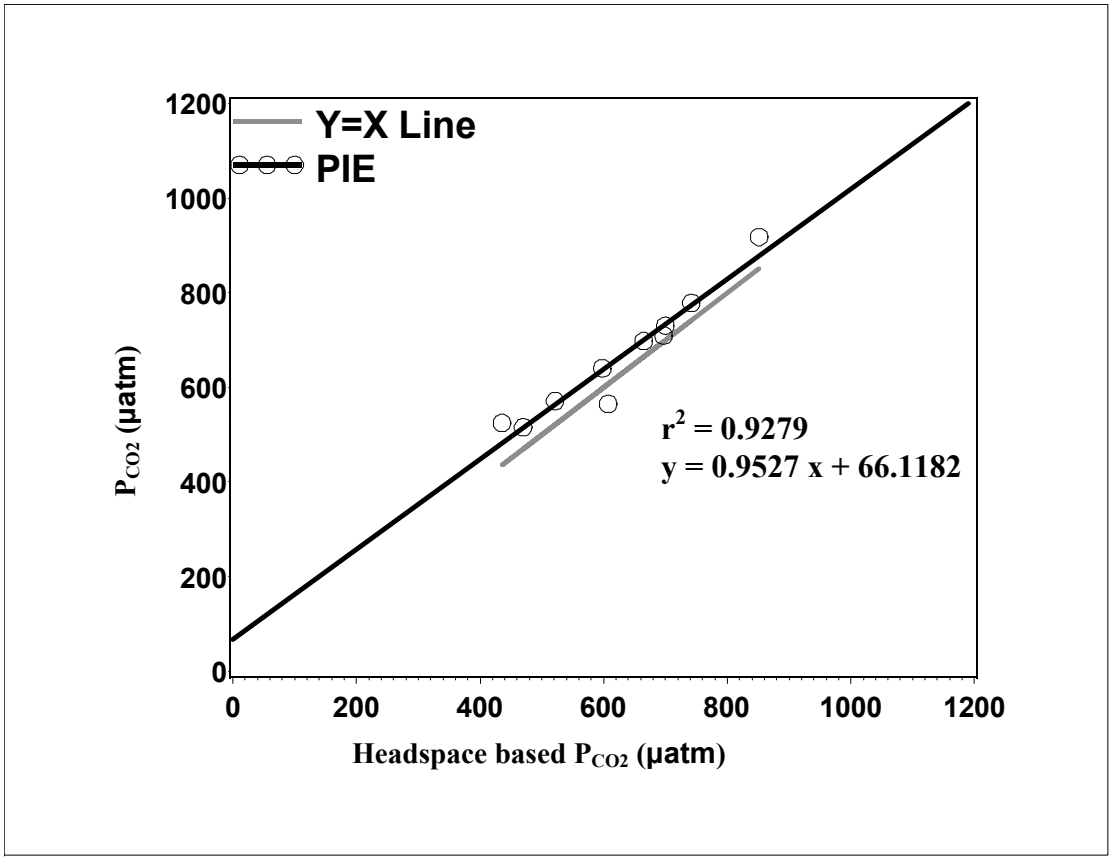

Figure 23. Allequash Lake's first depth profile measurements (N = 10), PIE based P_{CO2} versus headspace based P_{CO2}.

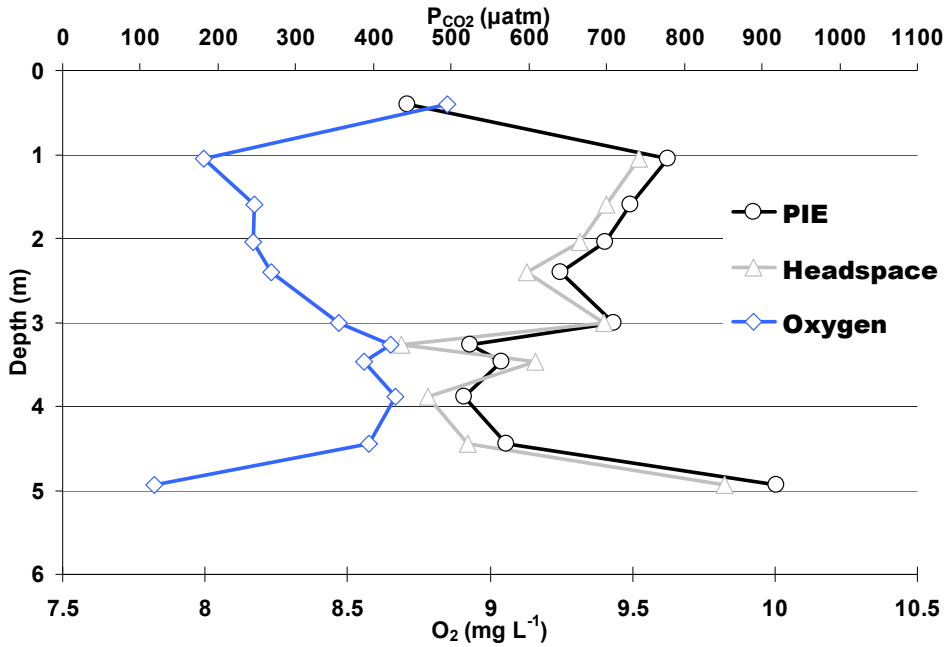

Figure 24. Allequash Lake's first depth profile measurements, PIE based P_{CO2} (N = 11), headspace based P_{CO2} (N = 10), and oxygen (N = 11) by depth.

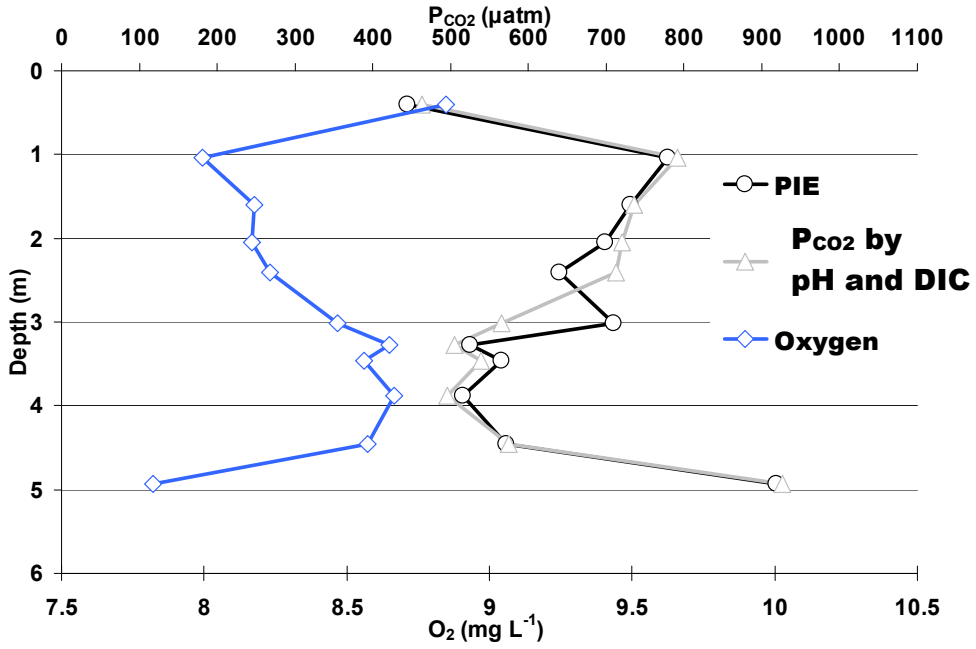

Figure 25. Allequash Lake's first depth profile measurements (N = 11), PIE based P_{CO2}, P_{CO2} by pH and laboratory DIC, and oxygen by depth.

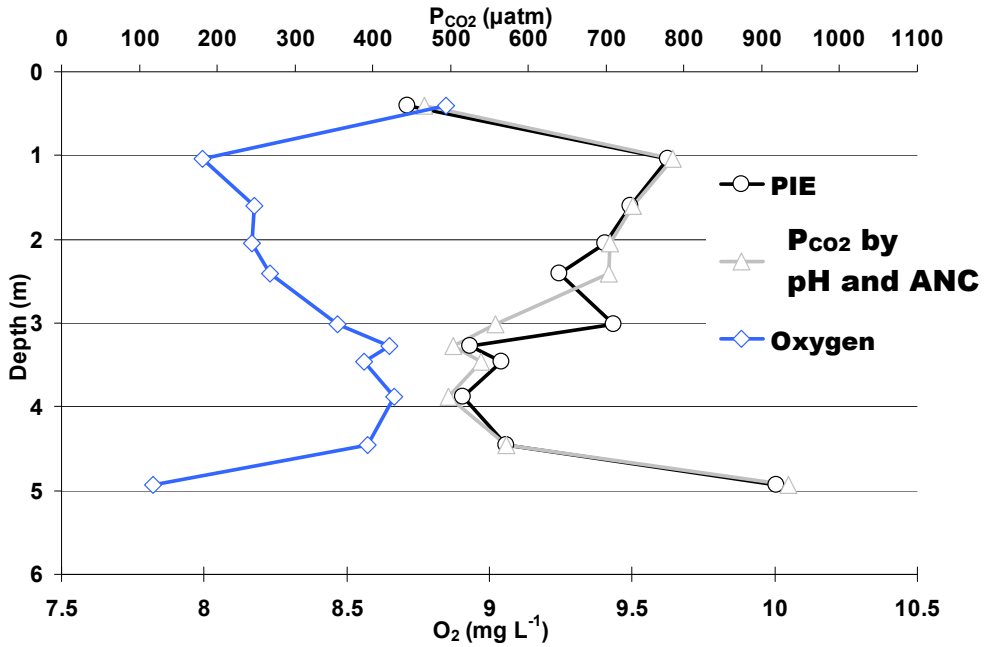

Figure 26. Allequash Lake's first depth profile measurements (N = 11), PIE based P_{CO2}, P_{CO2} by pH and ANC (Gran titration), and oxygen by depth.

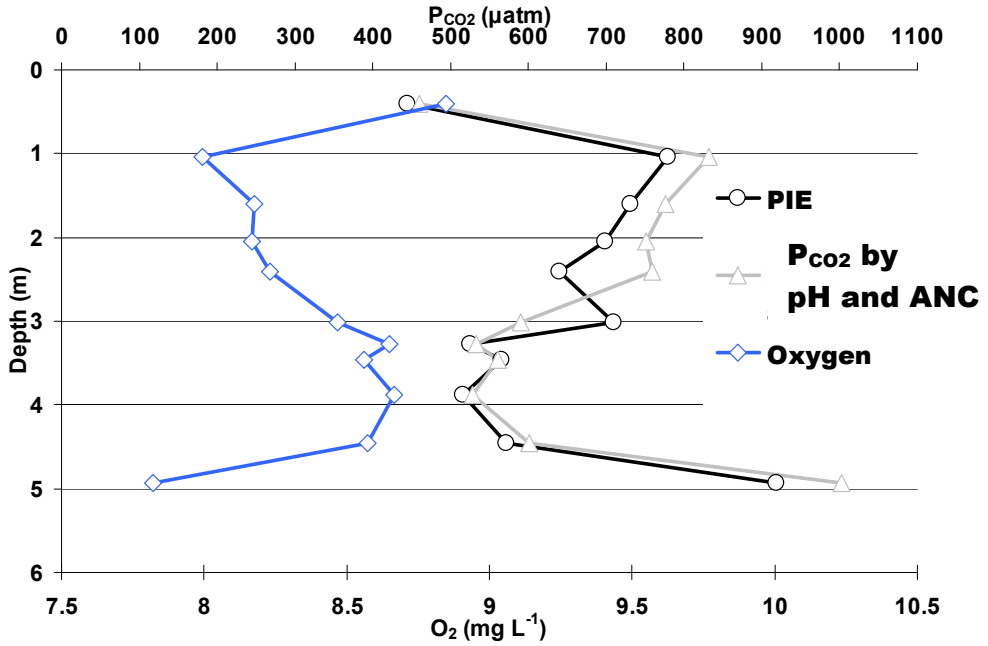

Figure 27. Allequash Lake's first depth profile measurements (N = 11), PIE based P_{CO2}, P_{CO2} by pH and ANC (C_B and C_A), and oxygen by depth.

Table 7, Allequash Lake's first depth profile.

Experiment	Figure	Dependent variable (y)	Indep. variable (x)	N	RMSE	dep. mean	coeff. of variation (CV, %)	r^2	Adj. r^2	slope	std error slope	y-int.	std error y-int.	p-value
Allequash depth	23	PIE P_{CO2}	headspace P_{CO2}	10	36.2553	665.3020	5.4495	0.9279	0.9189	0.9527	0.0939	66.1182	60.1632	< 0.0001
Allequash depth		PIE P_{CO2}	P_{CO2} by pH and laboratory DIC	10	52.2366	665.3020	7.8516	0.8503	0.8316	0.8249	0.1224	123.3614	82.0796	0.0001
Allequash depth		PIE P_{CO2}	P_{CO2} by pH and ANC (Gran tit.)	10	52.2223	665.3020	7.8494	0.8504	0.8317	0.8212	0.1218	129.0584	81.2258	0.0001
Allequash depth		PIE P_{CO2}	P_{CO2} by pH and ANC (C_B and C_A)	10	53.0947	665.3020	7.9805	0.8453	0.8260	0.7489	0.1133	146.0255	80.3075	0.0002

Allequash Lake was sampled again the next year in the middle of summer stratification. Even though the second depth profile was measured at a different time during the year and the carbon dioxide concentrations and temperatures were over a broader range, the PIE based measurements showed similar results as in the first depth profile.

Figure 28 shows the twelve P_{CO2} depth profile measurements made for Allequash Lake's second depth profile on 06/09/2008 with PIE compared against the headspace measured P_{CO2}. There was a strong correlation between PIE based P_{CO2} (Figure 28) and headspace based P_{CO2} ($r^2 = 0.9880$, slope = 1.1277 ± 0.0393, Table 8). However, the slope and the y-intercept of -180.9898 ± 64.4389 both seem to be influenced heavily by the one measurement above 4000 μatm P_{CO2}. (The measurements made on this mesotrophic lake ranged from 15.47 to 18.31 °C in temperature.)

The carbon dioxide measurement results from these methods and the oxygen results were also graphed by depth for Allequash Lake. Figure 29 also displays the same high spatial resolution of the PIE based P_{CO2} measurements with depth as in the first depth profile. The O_2 and PIE based P_{CO2} fluctuations also seem to be a different magnitude, but opposite in direction. Among all the methods used, headspace based P_{CO2} (Figure 29) measurements more closely mirrored the PIE based P_{CO2} values.

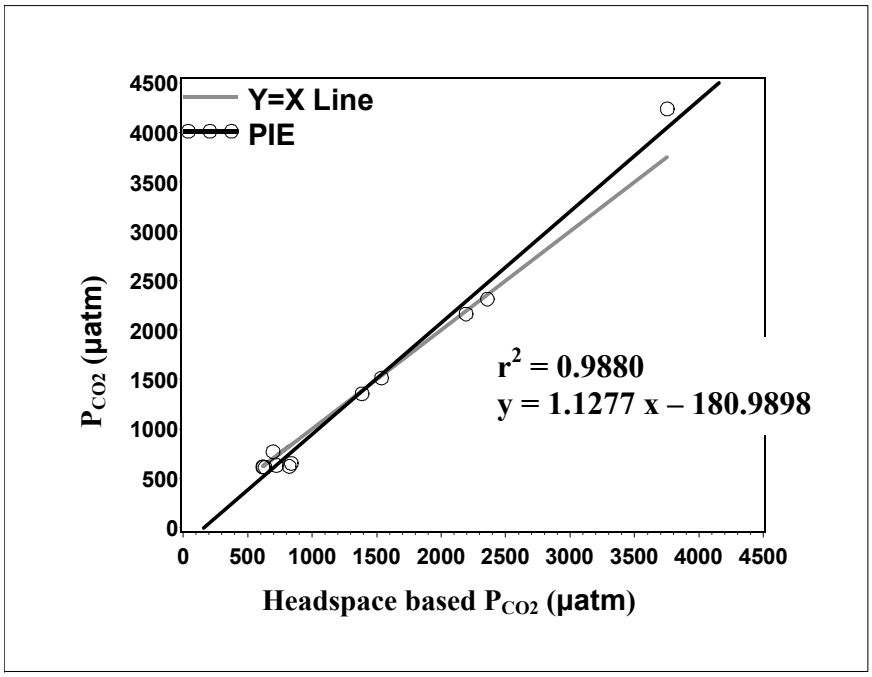

Figure 28. Allequash Lake's second depth profile measurements (N = 12), PIE based P_{CO2} versus headspace based P_{CO2}.

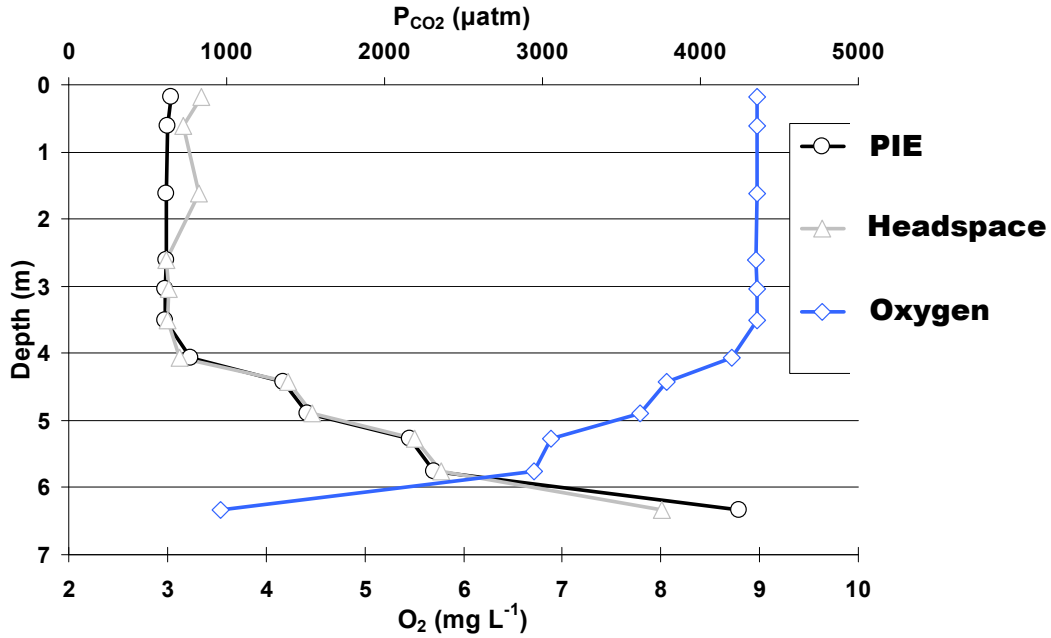

Figure 29. Allequash Lake's second depth profile measurements (N = 12), PIE based P_{CO2}, headspace based P_{CO2}, and oxygen by depth.

There were some problems verifying the accuracy and precision of PIE based DIC measurements. Figure 30 shows a comparison of PIE based DIC measurements to an estimated DIC (Eq. [43]) that was based on $[H_2CO_3^*]$ and ANC measurements:

[42] estimated DIC $\approx [H_2CO_3^*] + ANC$

[43] estimated DIC $\approx [H_2CO_3^*] + [HCO_3^-] + 2[CO_3^{2-}] + [OH^-] - [H^+]$

where $[H_2CO_3^*]$ was the PIE based $[H_2CO_3^*]$ (Eq. [14]) and ANC was the ANC by Gran titration (Eq. [34]). Note that when the carbonate, hydroxyl, and hydrogen ion concentrations are low, the estimated DIC (Eq. [43]) approximates the PIE based DIC (Eq. [23]).

However, the estimated DIC in Figure 30 does not closely mirror the PIE based DIC measurement. This is most likely a phenomenon associated with the nonlinear portion of the PIE based DIC calibration curve and shifts in the atmospheric pressure as described earlier in the *Methods* section. Ranging from 15,700 µatm to 17,600 µatm, the PIE based DIC measurements in Figure 30 are well into this nonlinear range.

To correct PIE based DIC measurements for this problem, an empirical response relationship (Eq. [27]) based on ANC, $[H_2CO_3^*]$, and Henry's law was used. Figure 31 shows a comparison of the corrected PIE based DIC measurements to an estimated DIC (Eq. [43]). There was a strong correlation between the corrected PIE based DIC (Figure 31) and the estimated DIC ($r^2 = 0.94$, slope = 1.04 ± 0.08, Table 8). Figure 32 also shows that the estimated DIC does closely mirror the corrected PIE

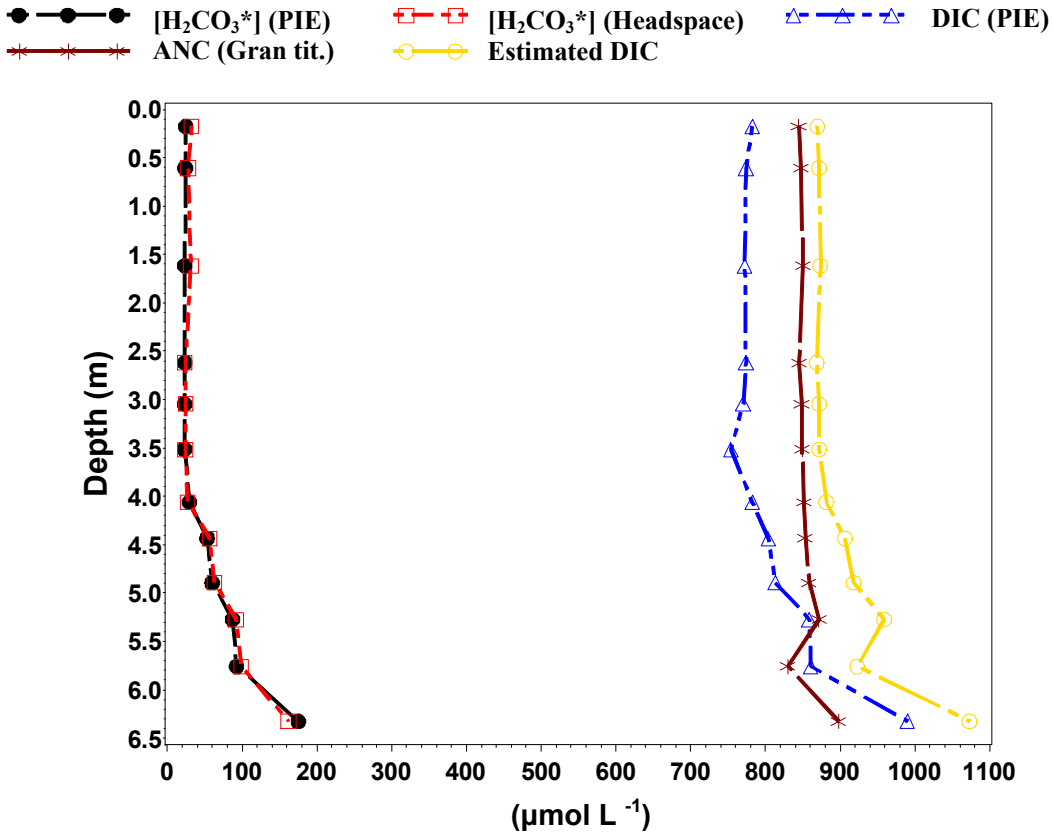

Figure 30. Allequash Lake's second depth profile measurements (N = 12), methods displayed by depth include PIE based [H_2CO_3*], headspace based [H_2CO_3*], PIE based DIC, ANC by Gran titration, and estimated DIC. The estimated DIC does not closely mirror the PIE based DIC.

based DIC measurements. The use of an empirical response relationship effectively improves the PIE based DIC measurements.

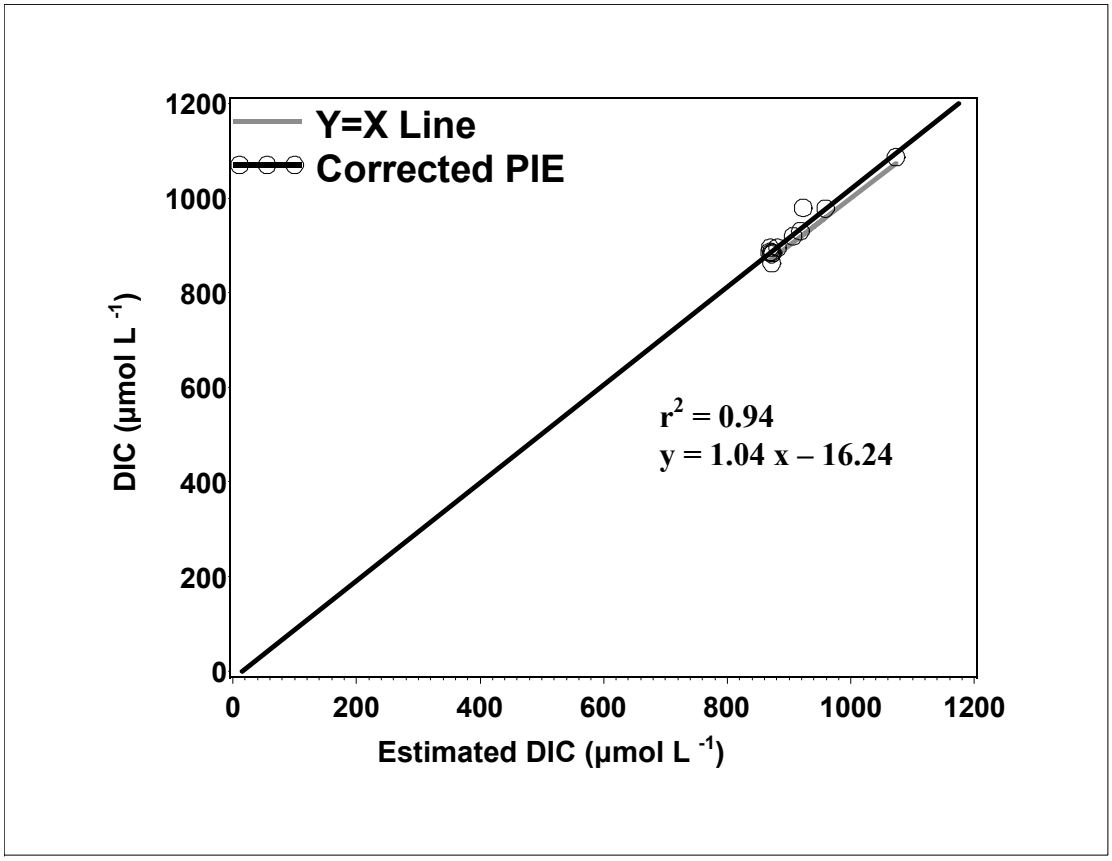

Figure 31. Allequash Lake's second depth profile measurements (N = 12), corrected PIE based DIC (Eq. [27]) versus estimated DIC (Eq. [43]).

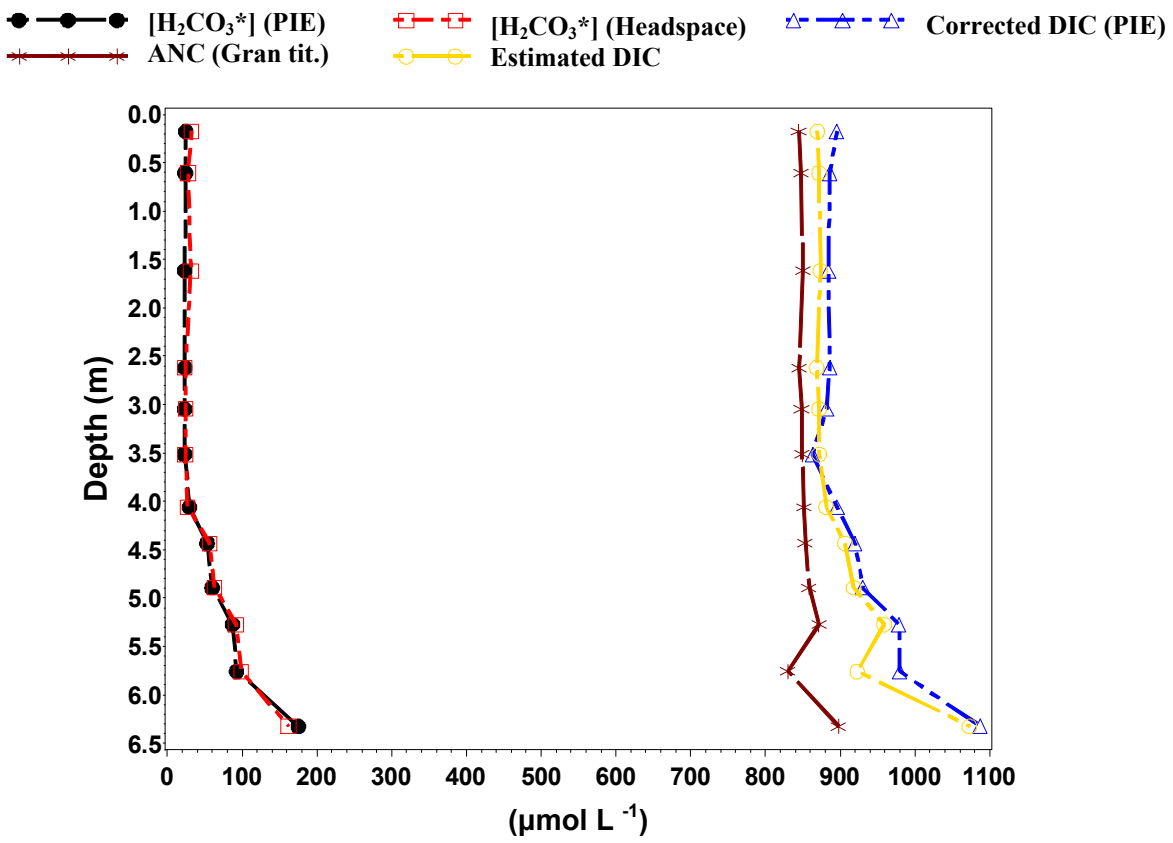

Figure 32. Allequash Lake's second depth profile measurements (N = 12), methods displayed by depth include PIE based [H_2CO_3*], headspace based [H_2CO_3*], corrected PIE based DIC, ANC by Gran titration, and estimated DIC. The estimated DIC mirrors the corrected PIE based DIC.

Table 8, Allequash Lake's second depth profile.

Experiment	Figure	Dependent variable (y)	Indep. variable (x)	N	RMSE	dep. mean	coeff. of variation (CV, %)	r^2	Adj. r^2	slope	std error slope	y-int.	std error y-int.	p-value
Allequash depth	28	PIE P_{CO2}	headspace P_{CO2}	12	127.0389	1341.4577	9.4702	0.9880	0.9868	1.1277	0.0393	-180.9898	64.4389	< 0.0001
Allequash depth		PIE P_{CO2}	P_{CO2} by pH and ANC (Gran tit.)	12	34.0233	1341.4577	2.5363	0.9991	0.9991	1.1892	0.0110	-28.1076	16.0503	< 0.0001
Allequash depth	31	Corr. PIE DIC	Estimated DIC	12	15.69	924.06	1.70	0.94	0.94	1.04	0.08	-16.24	72.23	< 0.0001

The depth profile made on Long Lake differed from those on Allequash Lake. Figure 33 shows the twelve P_{CO2} depth profile measurements made for Long Lake's depth profile on 09/16/2007 with PIE compared against the headspace measured P_{CO2}. There was a strong correlation between PIE based P_{CO2} (Figure 33) and headspace based P_{CO2} ($r^2 = 0.9954$, Table 9). However, the slope (1.8436 ± 0.0398, Table 9) was significantly different from one ($p = 0.0002$). (The measurements made on this oligotrophic lake ranged from 6.38 to 17.02 °C in temperature.)

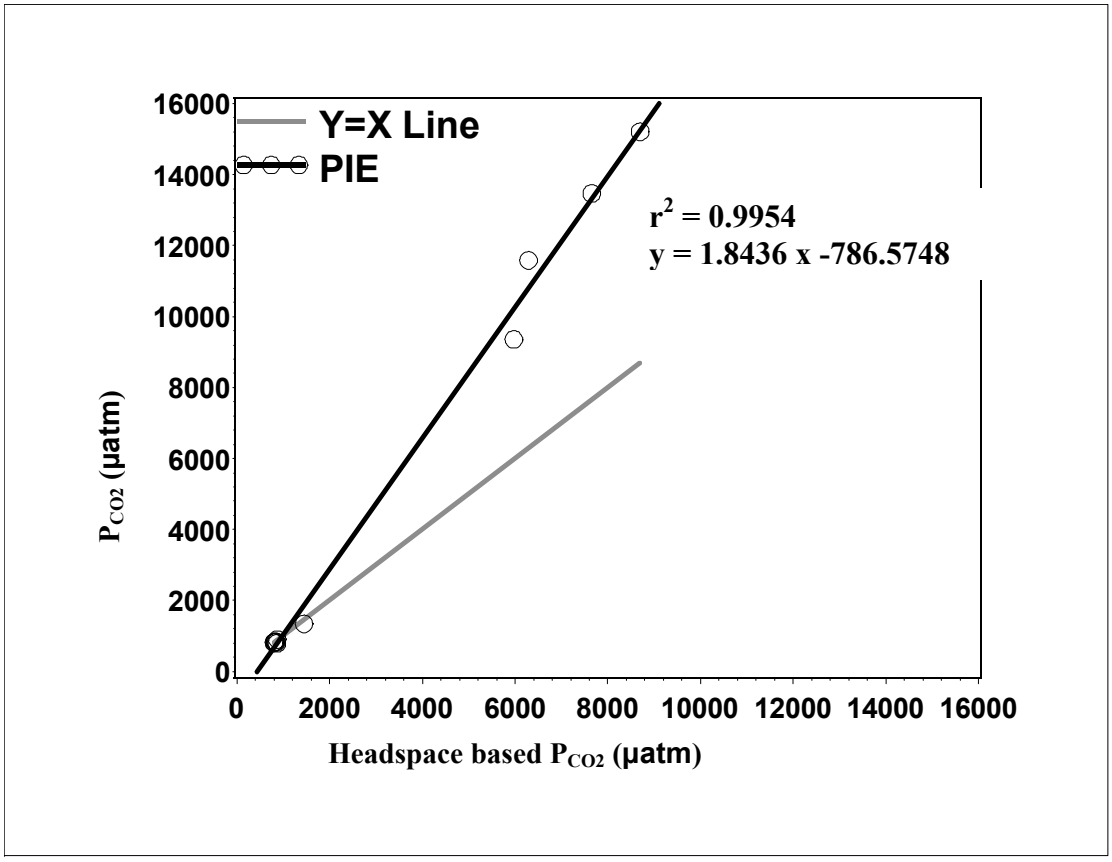

Figure 33. Long Lake's depth profile measurements (N = 12), PIE based P_{CO2} versus headspace based P_{CO2}.

In Figures 34, 35, 36, and 37, the carbon dioxide measurement results from these methods and the oxygen results were also graphed by depth for Long Lake. At ten meters depth and above, Figure 34 also displays the same high spatial resolution of the PIE based P_{CO2} measurements with depth as in the Allequash Lake depth profiles. These O_2 and PIE based P_{CO2} fluctuations also seem to be a different magnitude, but opposite in direction.

Among all the methods used at nine meters depth and above, headspace based P_{CO2} (Figure 34) measurements more closely mirrored the PIE based P_{CO2} values. However, at depths greater than nine meters, none of the methods had a close relationship with the PIE based P_{CO2} values. The PIE based measurements at depths greater than nine meters likely reflect a phenomenon associated with the nonlinear portion of the PIE based P_{CO2} calibration curves and shifts in the atmospheric pressure as described earlier in the *Methods* section. Ranging from 790 to 15,200 μatm, some of the PIE based P_{CO2} measurements are well into this nonlinear range.

To correct PIE based P_{CO2} measurements for this problem, an empirical response relationship (Eq. [25]) based on ANC by Gran titration, laboratory DIC, and Henry's law was used. Figure 38 shows a comparison of the corrected PIE based P_{CO2} measurements to the headspace based P_{CO2} measurements. There was a strong correlation between the corrected PIE based P_{CO2} (Figure 38) and the headspace based P_{CO2} ($r^2 = 0.9299$, slope = 0.8368 ± 0.0727, Table 9). However, the slope and the y-intercept of 39.7045 ± 308.8456 continue to be influenced heavily by the P_{CO2}

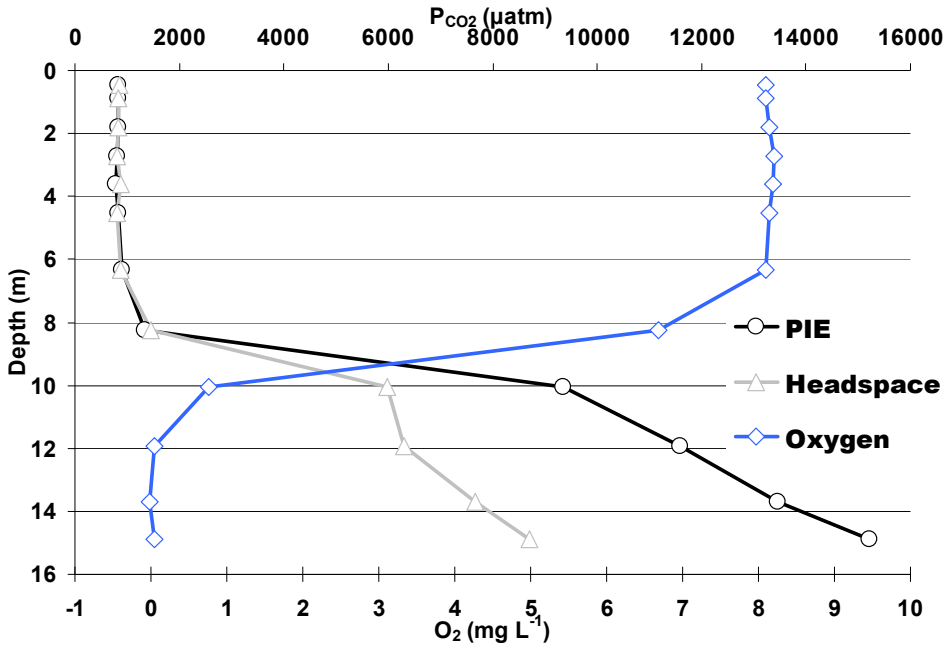

Figure 34. Long Lake's depth profile measurements (N = 12), PIE based P_{CO2}, headspace based P_{CO2}, and oxygen by depth.

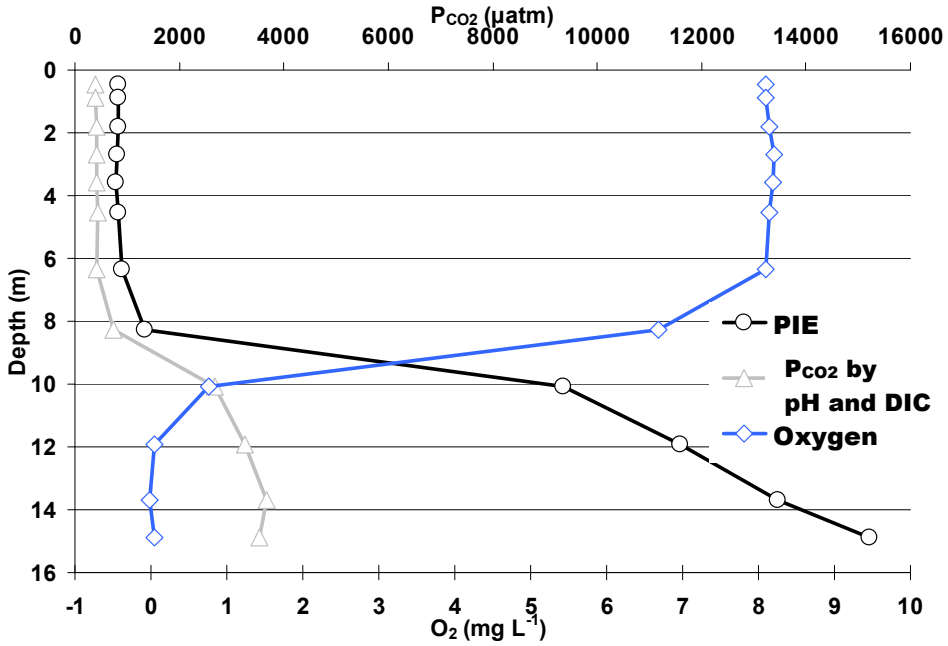

Figure 35. Long Lake's depth profile measurements (N = 12), PIE based P_{CO2}, P_{CO2} by pH and laboratory DIC, and oxygen by depth.

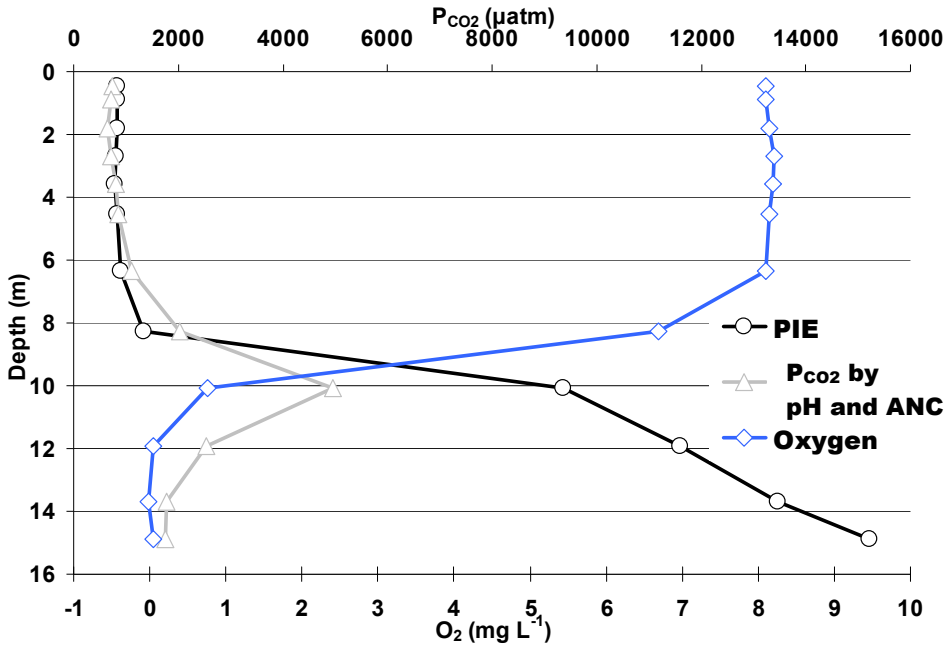

Figure 36. Long Lake's depth profile measurements (N = 12), PIE based P_{CO2}, P_{CO2} by pH and ANC (Gran titration), and oxygen by depth.

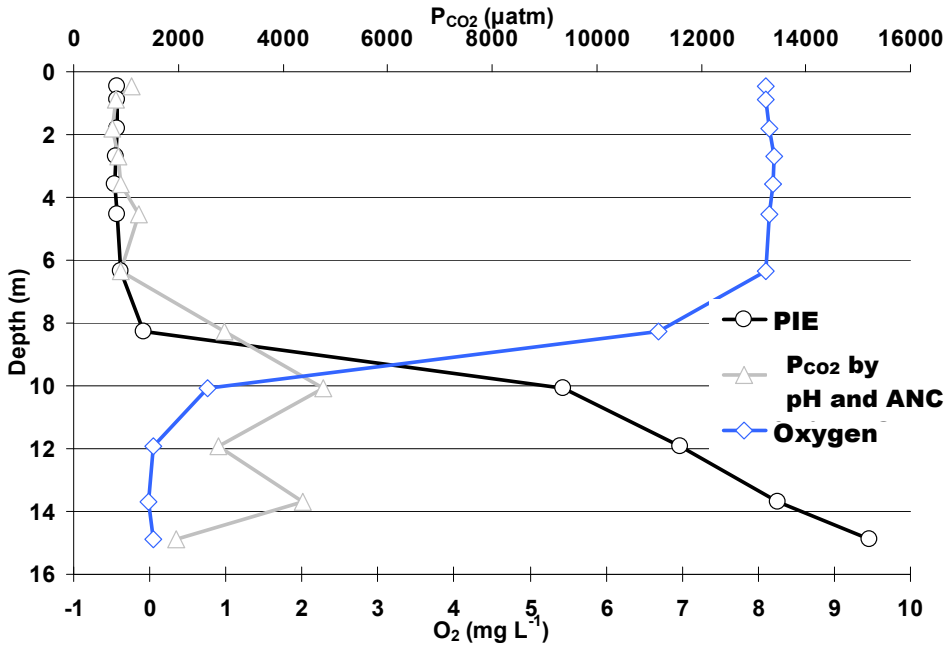

Figure 37. Long Lake's depth profile measurements (N = 12), PIE based P_{CO2}, P_{CO2} by pH and ANC (C_B and C_A), and oxygen by depth.

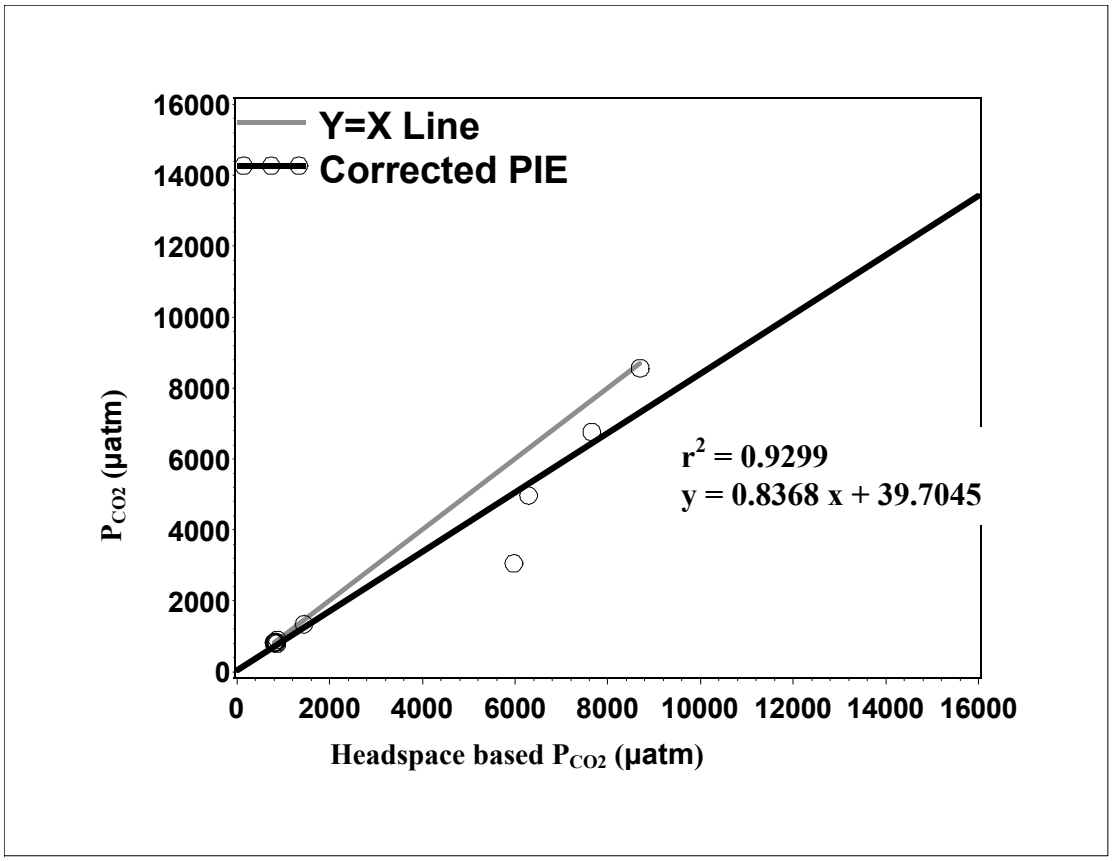

Figure 38. Long Lake's depth profile measurements (N = 12), corrected PIE based P_{CO2} versus headspace based P_{CO2}.

measurements above 4000 µatm. Further, Figure 39 shows that the headspace based P_{CO2} measurements do not closely mirror the corrected PIE based P_{CO2} values. In this case, the use of an empirical response relationship for PIE based P_{CO2} is in need of more study.

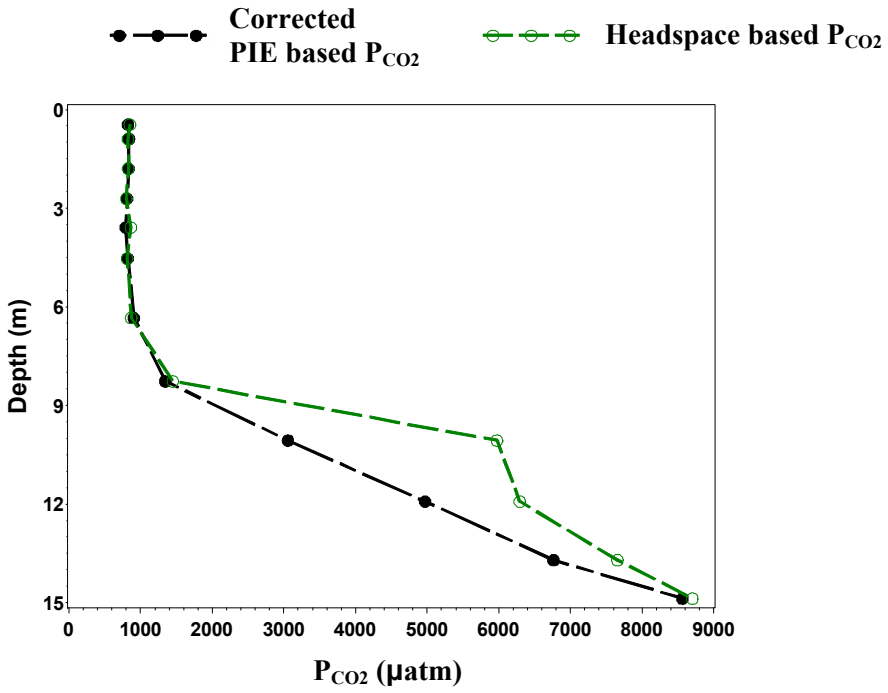

Figure 39. Long Lake's depth profile measurements (N = 12), corrected PIE based P_{CO2} (Eq. [25]) and headspace based P_{CO2} by depth.

Several observations do stand out for this depth profile analysis. Figure 34 shows differences as large as 6500 µatm P_{CO2} between PIE based and headspace based P_{CO2} measurements. Further, Figure 38 shows that the comparison of the corrected PIE based P_{CO2} to the headspace based P_{CO2} yields a y-intercept of 39.7045 ± 308.8456. The error term of this y-intercept is huge in comparison to the intercept itself, which gives question of whether to use a corrected PIE based P_{CO2} in this instance. Additionally, previous experiments have shown only small differences between PIE based P_{CO2} and headspace based P_{CO2} measurements. Therefore, it is

likely that the influence of the phenomenon associated with the nonlinear portion of the PIE based P_{CO2} calibration curves and shifts in the atmospheric pressure may be small for this depth profile. Further, it could be concluded that there may be other factors influencing these measurements.

PIE based P_{CO2} measurements could have other issues that are in need of further study. An improvement of the internal pressure compensation function of the LI-COR model LI-840, that has failed as a reliable algorithm for mole fraction (X_{CO2}) estimates, may be very helpful in correcting some of these issues. It is also unknown if low oxygen concentrations, high hydrogen sulfide concentrations, high methane concentrations, low temperatures, or other characteristics in the hypolimnion (Figure 40) of this deep oligotrophic lake have an influence on these PIE based P_{CO2} measurements.

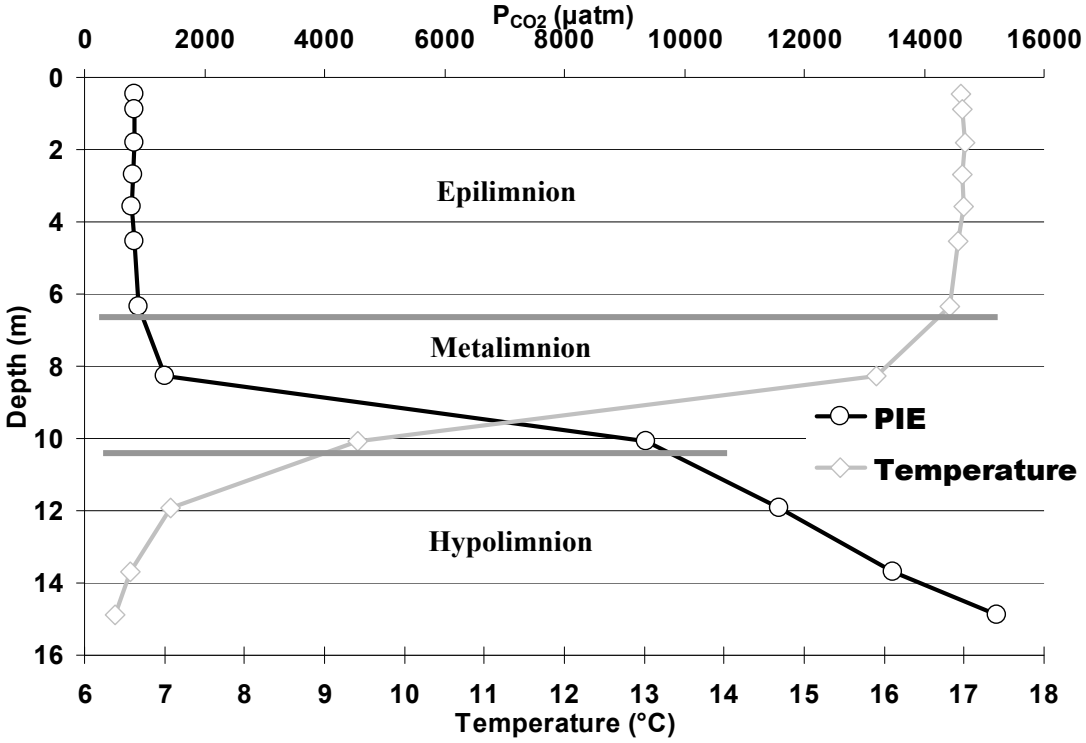

Figure 40. Long Lake's depth profile measurements (N = 12), PIE based P_{CO2} and temperature by depth. Epilimnion, metalimnion, and hypolimnion zones are also included for reference.

Table 9, Long Lake's depth profile.

Experiment	Figure	Dependent variable (y)	Indep. variable (x)	N	RMSE	dep. mean	coeff. of variation (CV, %)	r^2	Adj. r^2	slope	std error slope	y-int.	std error y-int.	p-value
Long depth	33	PIE P_{CO2}	headspace P_{CO2}	12	415.2946	4735.2592	8.7703	0.9954	0.9949	1.8436	0.0398	-786.5748	168.9851	< 0.0001
Long depth		PIE P_{CO2}	P_{CO2} by pH and laboratory DIC	12	700.2916	4735.2592	14.7889	0.9868	0.9855	4.0867	0.1493	-977.4601	290.5294	< 0.0001
Long depth		PIE P_{CO2}	P_{CO2} by pH and ANC (Gran tit.)	12	5002.7290	4735.2592	105.6485	0.3281	0.2609	2.6863	1.2156	565.6784	2376.0954	0.0516
Long depth		PIE P_{CO2}	P_{CO2} by pH and ANC (C_B and C_A)	12	4360.9561	4735.2592	92.0954	0.4894	0.4384	2.8321	0.9147	-762.1580	2176.5746	0.0113
Long depth	38	Corr. PIE P_{CO2}	headspace P_{CO2}	12	759.0130	2545.8555	29.8137	0.9299	0.9228	0.8368	0.0727	39.7045	308.8456	< 0.0001

Conclusion – Traditional Lake Studies with PIE

For the traditional lake studies, the PIE based measurements also had high accuracy and precision. For one particular lake study (*PIE based replicate measurements on Allequash Lake)*, PIE based measurements had the lowest coefficient of variation (3.0239 %) amongst direct and indirect methods used (Table 5). This CV falls within the CV range of the laboratory experiments. However, a comparison of PIE based [$H_2CO_3^*$] versus headspace based [$H_2CO_3^*$] for Experiment 4 (Figure 8) and a lake study (Figure 12; *Comparison of PIE to traditional methods on Allequash Lake*) showed lower precision and accuracy ($r^2 = 0.99$, slope = 1.00 ± 0.03 (Table 3) and $r^2 = 0.98$, slope = 0.87 ± 0.02 (Table 4), respectively) for this lake study.

The *fifty-two lake surface water survey* also showed high precision and accuracy of the PIE based measurements. However, a comparison of PIE based [$H_2CO_3^*$] versus headspace based [$H_2CO_3^*$] for Experiment 4 (Figure 8) and this lake study (Table 6) showed a decrease in the precision and accuracy ($r^2 = 0.99$, slope = 1.00 ± 0.03 (Table 3) and $r^2 = 0.90$, slope = 0.92 ± 0.04 (Table 6), respectively) for this lake study.

PIE based P_{CO2} measurements were highly correlated with the headspace based P_{CO2} measurements for eutrophic and oligotrophic lakes, except not for mesotrophic lakes. Eutrophic lakes show the tightest correlation, where the majority of lakes interestingly have P_{CO2} concentrations below 200 μatm.

As described in the *Introduction*, recent studies of lake metabolism have shown that most of the world's lakes surface waters are supersaturated with dissolved

carbon dioxide (Sobek et al., 2005), suggesting that lakes may be a net source of carbon dioxide emission into the atmosphere (Sobek et al., 2005). However, most of the lakes in the *PIE in a fifty-two lake surface water survey* were not supersaturated with dissolved carbon dioxide. According to PIE based dissolved carbon dioxide measurements in Figure 22, most of the fifty-two lakes were undersaturated with respect to ambient atmospheric P_{CO2}. Therefore, these lakes are a sink for atmospheric carbon dioxide. More lakes will have to be directly measured with PIE to build a better picture of why these particular lakes in this study were undersaturated with respect to atmospheric carbon dioxide. These findings were based on the traditional collection of one surface-water sample from each lake, which will be further examined in the next chapter with diurnal patterns from one surface-water point and whole lake surface-water mapping.

There was also high precision and accuracy of the PIE based measurements in the depth-profile lake studies. For the Allequash and Long Lake depth profiles, the PIE based P_{CO2} measurements were highly correlated with the headspace based P_{CO2} measurements. The r^2 values ranged from 0.9279 to 0.9954 and the mean r^2 value was 0.9704. However, the coefficients of variation (CV) were high and ranged from 5.4495 to 9.4702 % and the mean CV was 7.8966 %. The accuracy of the PIE based measurement was also high for both Allequash Lake depth profiles. The PIE based P_{CO2} measurements trend with the headspace based P_{CO2} measurements was close to the one-to-one line. These slope values ranged from 0.9527 to 1.1277. In contrast, the accuracy of the PIE based measurement was low for the Long Lake depth profile. The

PIE based P_{CO2} measurements trend with the headspace based P_{CO2} measurements was biased high with a slope of 1.8436. However, the corrected PIE based P_{CO2} measurements improved the relationship with the headspace based P_{CO2} measurements with a slope of 0.8368.

For the Allequash and Long Lake depth profiles, PIE based P_{CO2} and oxygen measurements were graphed by depth along side headspace based P_{CO2}, P_{CO2} by pH and laboratory DIC, P_{CO2} by pH and ANC (Gran titration), and P_{CO2} by pH and ANC (C_B and C_A) measurements. At ten meters depth and above, the PIE based measurements had high spatial resolution with the dissolved oxygen levels. The dissolved oxygen (O_2) level had a peak maximum at or near the same time and a minimum at the same time that the PIE based P_{CO2} had at its minimum and maximum, respectively. Our O_2 and PIE based P_{CO2} fluctuations seemed to be a different magnitude, but opposite in direction. Similar relationships were also found in diurnal studies of dissolved carbon dioxide and dissolved oxygen in Hanson et al., (2006). Among all the methods used at depths of nine meters and above, headspace based P_{CO2} measurements more closely mirrored the PIE based P_{CO2} values.

However, at depths greater than nine meters on Long Lake, none of the methods has a close relationship to the PIE based P_{CO2} values. It is unknown if low oxygen concentrations, high hydrogen sulfide concentrations, high methane concentrations, low temperatures, or other characteristics in the hypolimnion (Figure 40) of this deep oligotrophic lake have an influence on the PIE based P_{CO2}

measurements or other direct and indirect measurements. This is an area in need of further research.

In summary, this chapter has shown how PIE based direct carbon dioxide measurements in a limited study of lakes across three trophic classes (eutrophic, mesotrophic, oligotrophic) compare to traditional direct and indirect carbon dioxide measurements. PIE based P_{CO2} have proved to be a precise, accurate, and reliable measurement for surface analyses of lake bodies ranging from zero to 2314 μatm P_{CO2} and for depth analyses of lake bodies ranging from 450 to 4250 μatm P_{CO2}. Researchers now have a PIE based direct measurement with known precision and accuracy that can be applied to natural systems and traditional lake studies.

TEMPORAL and SPATIAL RESOLUTION of PIE

This chapter contains the methods, and results for the temporal and spatial lake experiments. This is where the PIE method was shown to substantially increase the ability to measure carbon dioxide variations in time and space. In a continuous twenty-four hour diurnal pattern, PIE based partial pressure of carbon dioxide (P_{CO2}) and DIC measurements showed the actual respiration and photosynthesis of the lake from day to night and back to day at temporal resolutions inaccessible via traditional indirect and other direct sampling methods. PIE based P_{CO2} and DIC whole lake maps also showed spatial variation of dynamic lake systems at spatial resolution inaccessible via traditional indirect and other direct sampling methods. Several locations on these maps indicated possible ground and/or surface water entry of dissolved carbon dioxide into the lake. These maps were also used to show the spatial variation of dissolved carbon dioxide over time.

Methods - Temporal and Spatial Resolution of PIE

PIE based diurnal carbon dioxide measurements were used to develop graphs of temporal variation within Allequash Lake. To accomplish this, one continuous twenty-four hour diurnal pattern of PIE based P_{CO2} and DIC measurements were taken from one point and 0.5m depth on Allequash Lake. The boat was secured with two anchors at this sampling point. Note that this is the same sampling point coordinate (Appendices B and C) as for the fifty-two lake study, carbon dioxide replicate study, and depth profile studies. Water temperature measurements for the PIE based

measurements were made with a Fluke® temperature probe (resolution = 0.0001 °C) in the gas collection chamber.

PIE based measurements of carbon dioxide were also used to develop whole lake maps for Allequash Lake. Development focused on surface-water lake maps of carbon dioxide concentration, more specifically PIE based P_{CO2} and DIC. This was an exploratory use of this PIE device for literature searches had provided no known existing sources of accurate carbon dioxide lake maps.

Surface water carbon dioxide measurements for these whole lake maps were made at multiple discrete points collected over the daylight hours (from dawn to dusk) in as few days as possible (two to three days). Note that these experiments were extended for a day or two in order to collect traditional direct and indirect measurements of dissolved carbon dioxide at some of these sampling points. Samples were collected while the sampling boat was slowly moving under power, adrift, or anchored. Selection of which technique used depended on location, wave action, and wind condition.

Allequash Lake's PIE based P_{CO2} mapping measurements (07/01/2007 to 07/03/2007) were used to develop lake maps with P_{CO2} concentration. These maps were used to show spatial variation of P_{CO2} concentration in a mesotrophic lake. The sampling boat was secured with two anchors at each randomly selected sampling point. A combined ninety-six near-shore and deep-water surface water samples were taken at a one-half meter depth or at least 30 cm above the sediment throughout Allequash Lake. A Trimble GeoExplorer Geo (CE) XT Global Positioning System (GPS) was

used to record the location of each sampling point. After the PIE device stabilization, a two-minute average from these PIE records was used to estimate PIE based P_{CO2} for each mapped sampling point. Allequash Lake's PIE based P_{CO2} maps were developed using ESRI ArcGIS ArcMAP. These images and points were geo-referenced to the Wisconsin Transverse Mercator (WTM83/91) geographic coordinate system (meters) and North American 1983 HARN geographic projection system.

Allequash Lake's PIE based P_{CO2} and DIC mapping measurements (06/06/2008 to 06/08/2008) were used to develop lake maps with P_{CO2} or DIC concentration. These maps were used to illustrate spatial variation of P_{CO2} and DIC concentration in a mesotrophic lake. PIE based P_{CO2} and DIC surface water samples were measured simultaneously on different PIE devices. The sampling boat was secured with two anchors for each near-shore surface water sampling point. Deep-water surface water samples were obtained while the boat drifted on the calm lake. Near-shore and deep-water surface water samples were taken at a one-half meter depth or at least 30 cm above the sediment throughout Allequash Lake. After the PIE device stabilization, a two-minute average from these PIE records was used to estimate PIE based P_{CO2} and PIE based DIC for each mapped sampling point. A continuous record of surface water samples were also taken at a one-half meter depth or at least 30 cm above the sediment throughout the perimeter of Allequash Lake. The continuous record perimeter measurements were taken as the boat moved at minimum trolling speed about 70 meters from shore. After the PIE device stabilization, a one-minute average from these PIE records was used to estimate PIE based P_{CO2} and PIE based

DIC for each mapped perimeter sampling point. A Trimble GeoExplorer Geo (CE) XT Global Positioning System (GPS) was used to record the location of each sampling point. A total of four hundred fifty-eight near-shore, deep-water, and perimeter surface water sampling points were recorded for each PIE based P_{CO2} and DIC measurement. Allequash Lake's PIE based P_{CO2} and DIC maps were developed using ESRI ArcGIS ArcMAP. These images and points were geo-referenced to the Wisconsin Transverse Mercator (WTM83/91) geographic coordinate system (meters) and North American 1983 HARN geographic projection system.

Results and Discussion – Temporal and Spatial Resolution of PIE

The PIE based dissolved carbon dioxide method allows for measurements to be made efficiently and repeatedly in time and space. This method was used to explore carbon dioxide variations in detail for Allequash Lake. Allequash Lake's continuous twenty-four hour diurnal pattern of PIE based P_{CO2} measurements are shown in Figures 41 and 42. These measurements show the actual respiration of a mesotrophic lake from day to night and back to day at temporal resolutions inaccessible via traditional indirect and direct carbon dioxide sampling methods.

These diurnal PIE based P_{CO2} measurement results might show a repeatable pattern on a daily scale. The PIE based P_{CO2} concentration (Figure 41) decreased steadily throughout the daylight hours. At the midway between sunset and last twilight, the P_{CO2} (Figure 41) abruptly dropped to a minimum value of 125 μatm. The P_{CO2} then increased steadily throughout the night until it reached its peak of 230 μatm at 7:00 a.m. about two hours after sunrise on the second day (Figures 41 and 42).

Figure 41, Allequash Lake Diurnal O_2 and PIE based P_{CO2} 06/30/2008, noon to midnight.

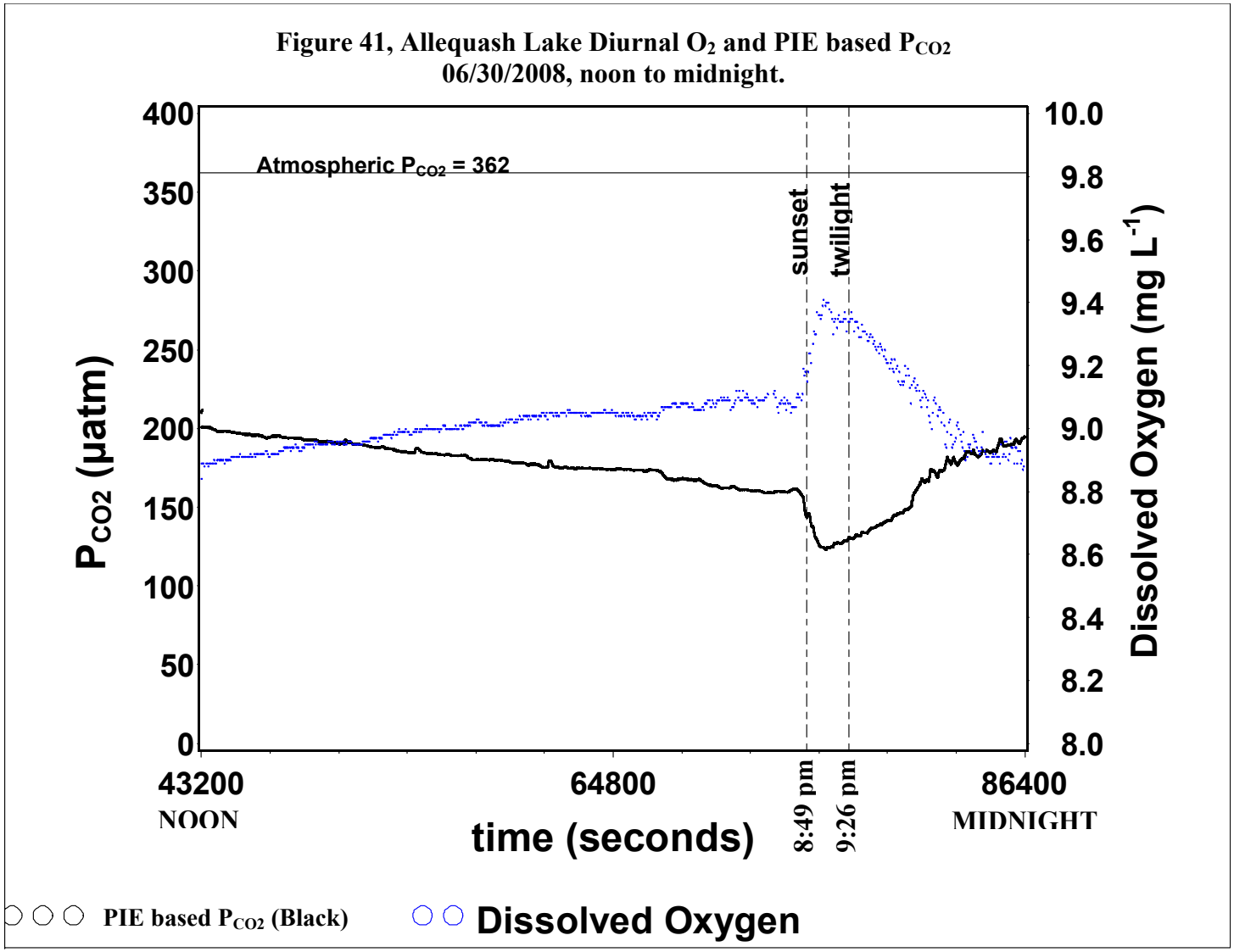

Figure 42, Allequash Lake Diurnal O_2 and PIE based P_{CO2}
06/30/2008 midnight to 07/01/2008 noon.

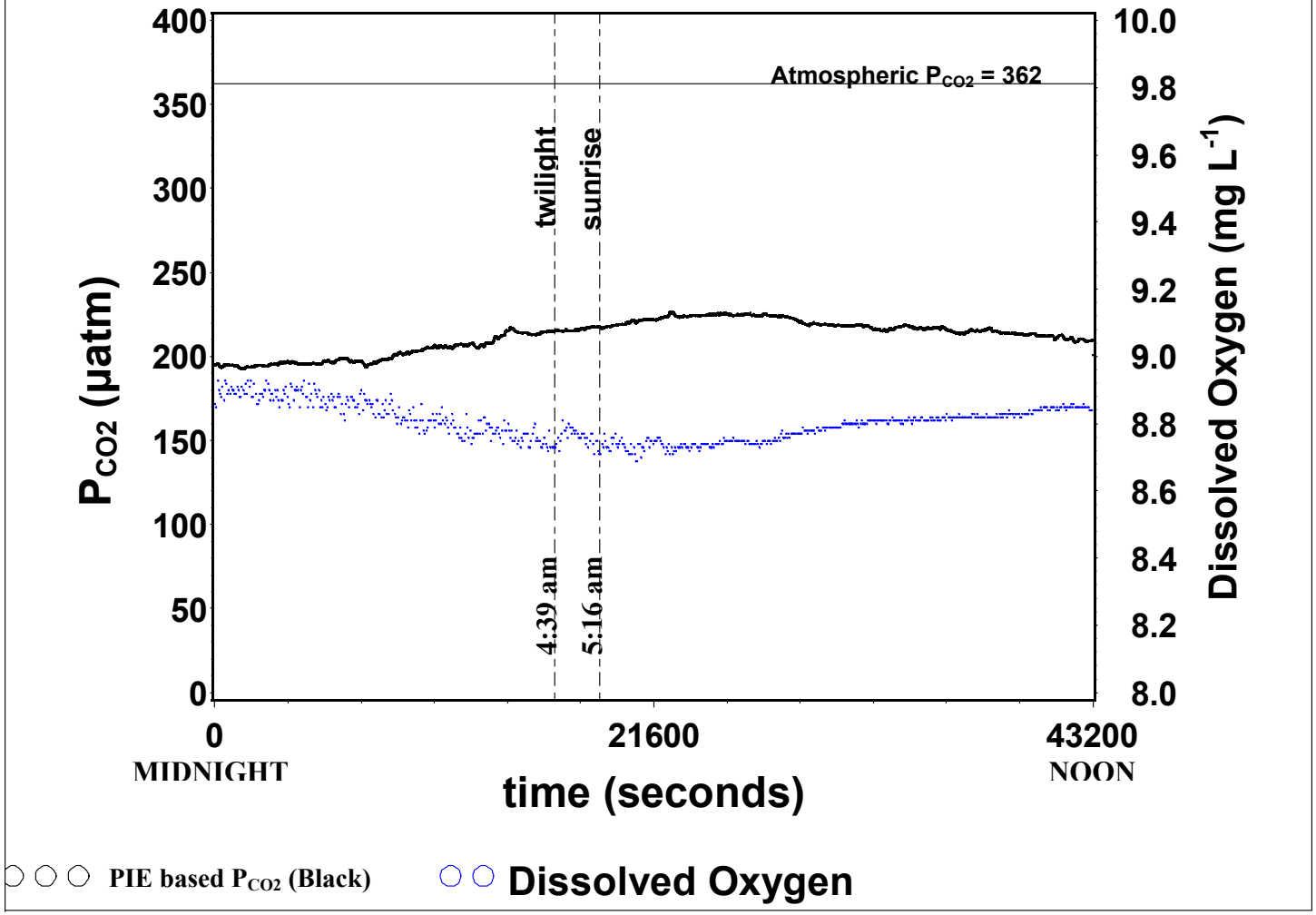

After which, the P_{CO2} steadily decreased to a value at noon on the second day that was within 20 μatm of the value of the previous noon.

The PIE based P_{CO2} pattern during the day is consistent with CO_2 consumption and oxygen production during plant photosynthesis. The pattern of CO_2 increase throughout the night time hours is also consistent with plant respiration, where the energy or sugar stored during the day during photosynthesis is consumed along with oxygen to produce carbon dioxide and water during the night.

The minimum value, maximum value, and general shape of the diurnal O_2 and PIE based P_{CO2} fluctuations seemed to be a different magnitude, but opposite in direction. The dissolved oxygen (DO, O_2) level also had a peak 9.4 mg L^{-1} maximum (Figure 41) and about an 8.7 mg L^{-1} minimum (Figure 42) at the same time that the PIE based P_{CO2} had at its minimum and maximum, respectively. Similar relationships were also found in the depth profile experiments discussed earlier and in diurnal studies of dissolved carbon dioxide and dissolved oxygen in Hanson et al. (2006).

These PIE based P_{CO2} diurnal measurements were also reported and graphed at temporal resolutions inaccessible via traditional indirect and direct carbon dioxide sampling methods. These diurnal patterns closely matched what was found by Hanson et al. (2006) and Carignan (1998), where both Hanson's and Carignan's CO_2 and O_2 data sets were reported as a one record per half-hour time series. In contrast, these PIE based data sets were recorded at a temporal resolution of one record per second P_{CO2}. However, limitations on the oxygen data logger led to a one record per minute O_2 time series. Therefore, a one-minute average was produced from the P_{CO2} record

and then both CO_2 and O_2 were graphed as a one record per minute time series (one open circle per record; Figures 41 and 42).

Similar temporal resolution as found above was shown with the PIE based DIC measurements. Figures 43 and 44 show Allequash Lake's continuous twenty-four hour diurnal pattern of PIE based DIC measurements, which were also taken at the same sampling times and locations as the PIE based P_{CO2} diurnal measurements. These PIE based DIC diurnal measurements were also recorded and reported at temporal resolutions (one record per minute time series with one open circle per record) inaccessible via traditional indirect and direct carbon dioxide sampling methods, as described in the PIE based P_{CO2} diurnal measurements above.

These PIE based DIC measurement results also might show a repeatable pattern on a daily scale. After measurement had started at noon on the first day, the PIE based DIC concentration (Figure 43) remained steady at its maximum level around 870 μmol L^{-1} throughout the daylight hours until it proceeded to decrease about one hour after last twilight. The DIC (Figures 43 and 44) fluctuated quite rapidly after this until it decreased to its minimum value of 670 μmol L^{-1} on the second day at 1:00, 2:00, and finally at 5:15 a.m. sunrise. The DIC (Figure 44) then proceeded to fluctuate again quite erratically as it increased to a value at noon on the second day that was within 50 μmol L^{-1} of the value of the previous noon (Figure 43).

The drop and fluctuations of PIE based DIC concentrations at night are also consistent with rising carbon dioxide levels from plant respiration, where the lake becomes more acidic and the pH drops. A decrease in pH could dissolve base cation

Figure 43, Allequash Lake Diurnal O_2 and PIE based DIC 06/30/2008, noon to midnight.

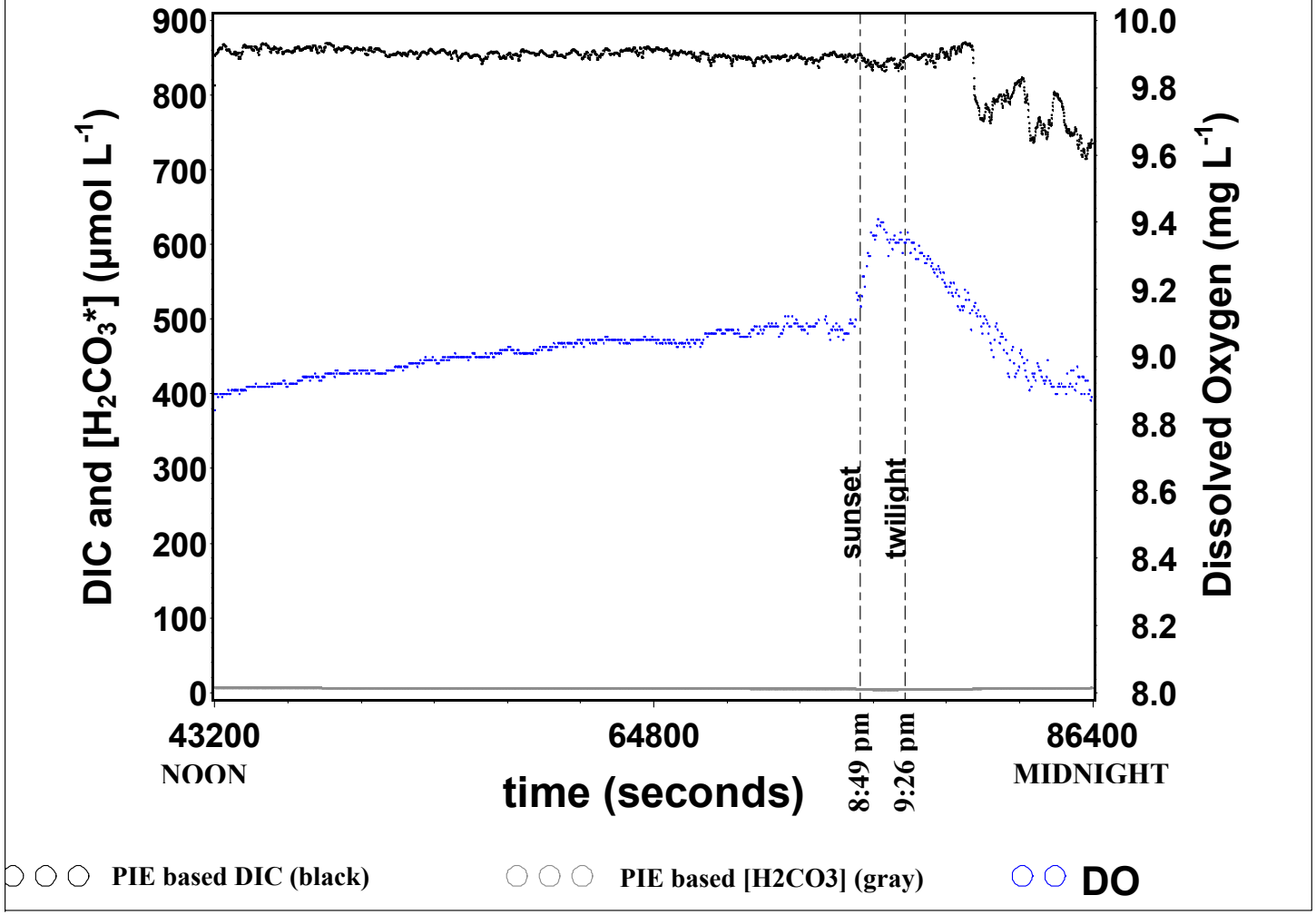

Figure 44, Allequash Lake Diurnal O_2 and PIE based DIC 06/30/2008 midnight to 07/01/2008 noon.

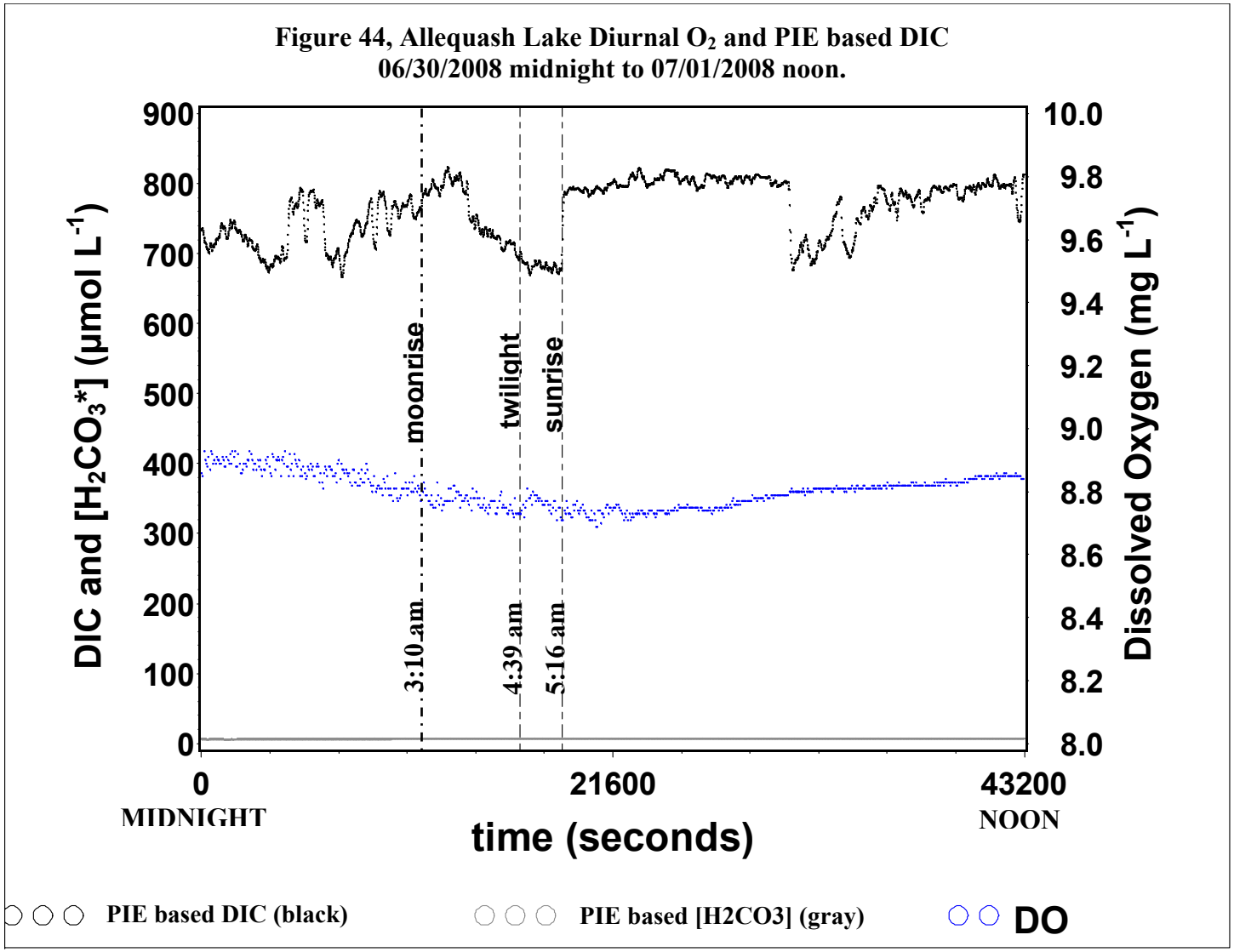

or mineral acid anion into solution, which could drive increases or decreases in ANC. Figures 43 and 44 also show that the carbon dioxide concentration is only a small portion of the total DIC concentration. The DIC concentration consists mainly of bicarbonate. With a decrease in pH, this bicarbonate could transform into carbonic acid, which could also decrease the ANC concentration. As ANC concentration decreases or increases rapidly, DIC concentration would have decreased or increased, respectively.

Allequash Lake's PIE based P_{CO2} measurements (07/01/2007 to 07/03/2007) were used to develop lake maps (Figures 45, 46, and 47) with P_{CO2} concentration. These maps show the variation of P_{CO2} concentration in the northern bay of Allequash Lake, a mesotrophic lake, at spatial resolutions inaccessible via traditional indirect and direct carbon dioxide sampling methods. Lake bathymetry are indicated in shades of gray and labeled in black. The open circles represent the ninety-six sampling point locations and are color coded with the P_{CO2} levels in μatm. Figure 45 shows that some of the near shore sampling locations overshot the lakeshore edge (1621 feet above mean sea level) as indicated by the bathymetry. At the time of these carbon dioxide measurements, the water levels were higher than the lakeshore edge datum. In Figures 46 and 47, the color shading for the P_{CO2} between open circles were done in ESRI ArcGIS ArcMAP with a triangulated irregular network (TIN) model and displayed as shaded triangles. Note that some of the TIN model has overshot the outside the lakeshore edge (1621 feet above mean sea level). This resulted from the rough edging

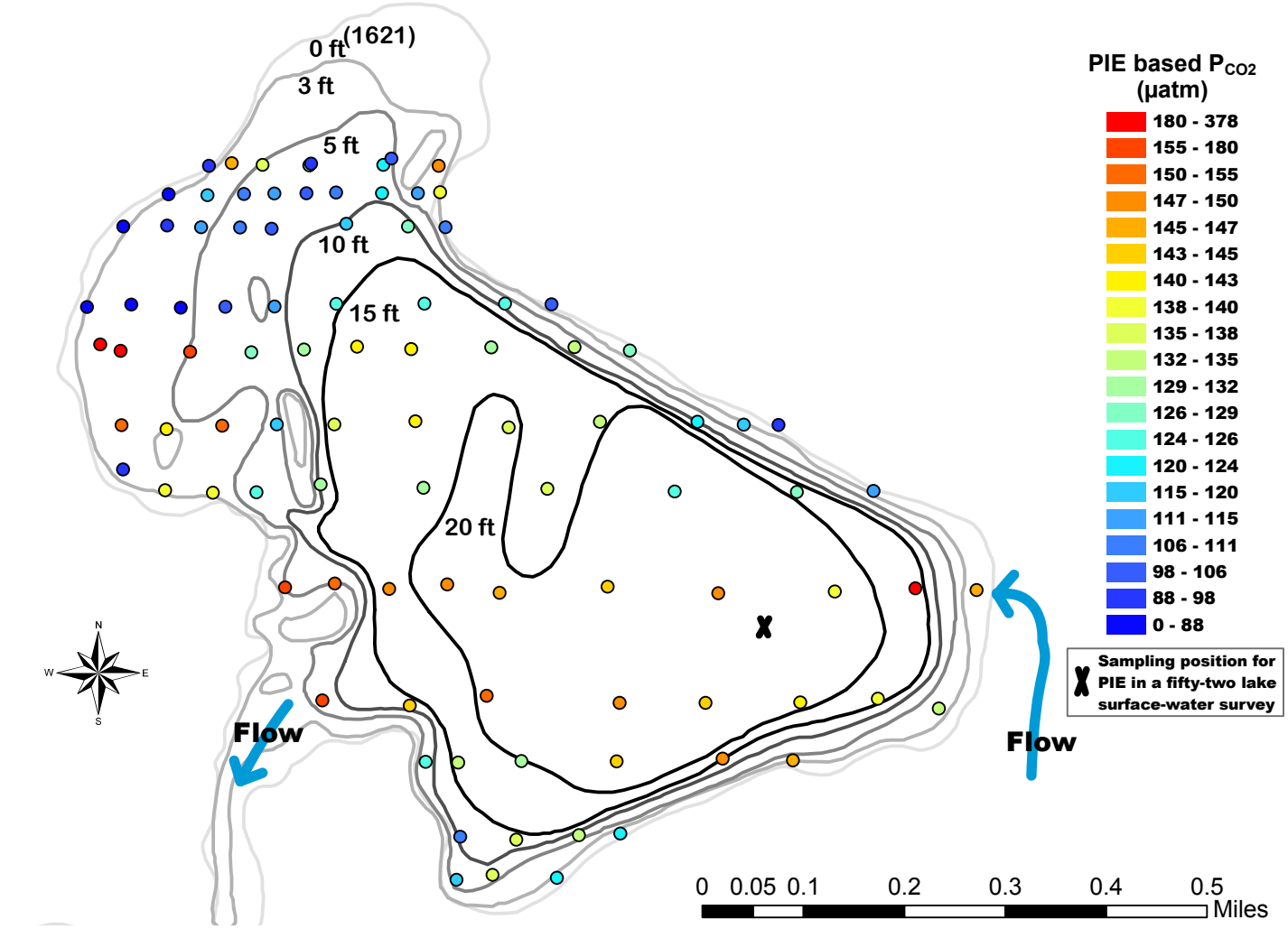

Figure 45. PIE based P_{CO2} for Allequash Lake, Vilas County, WI, July 1 – 3, 2007.

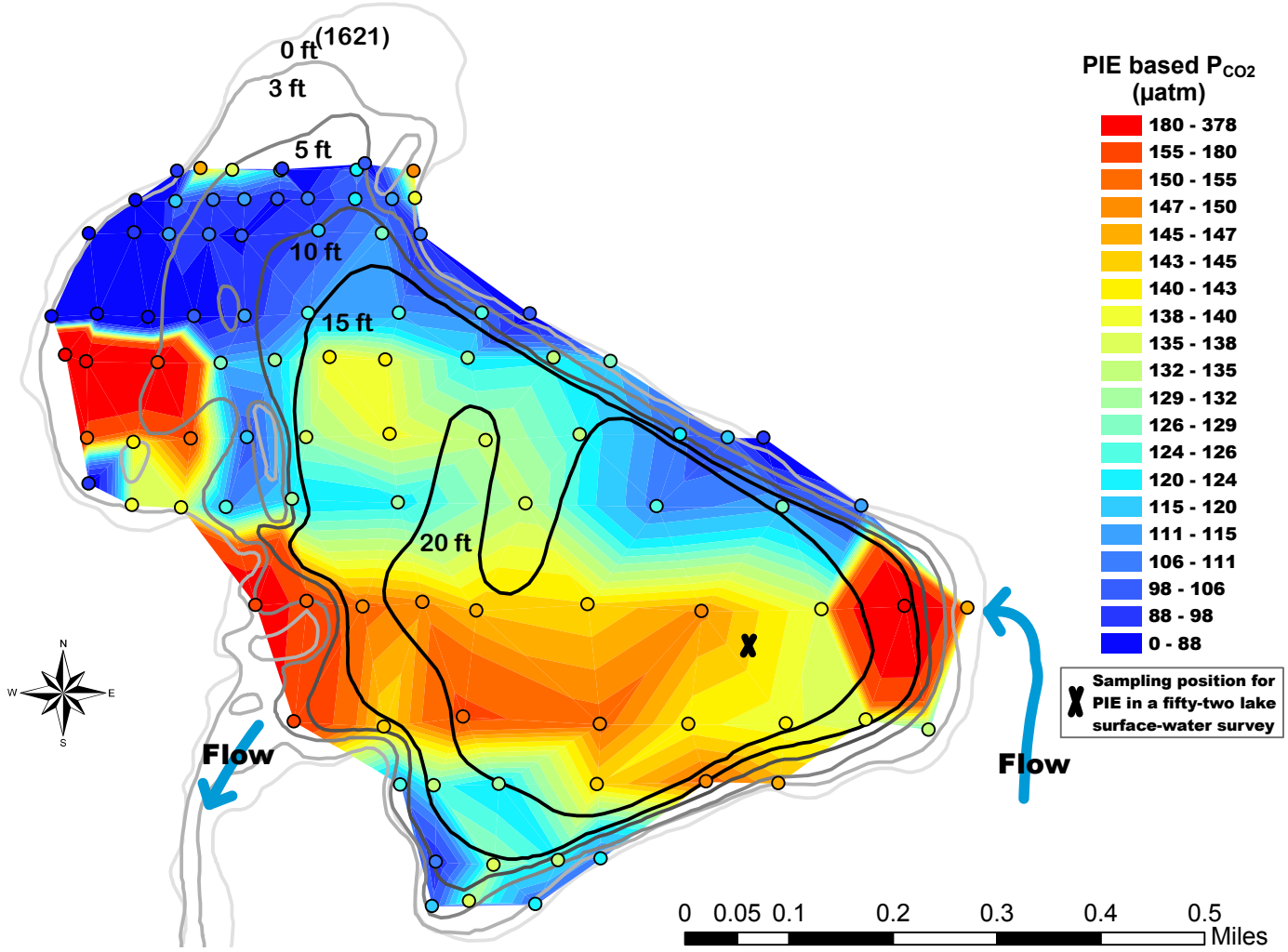

Figure 46. PIE based P_{CO2} (TIN model) for Allequash Lake, Vilas County, WI, July 1 – 3, 2007.

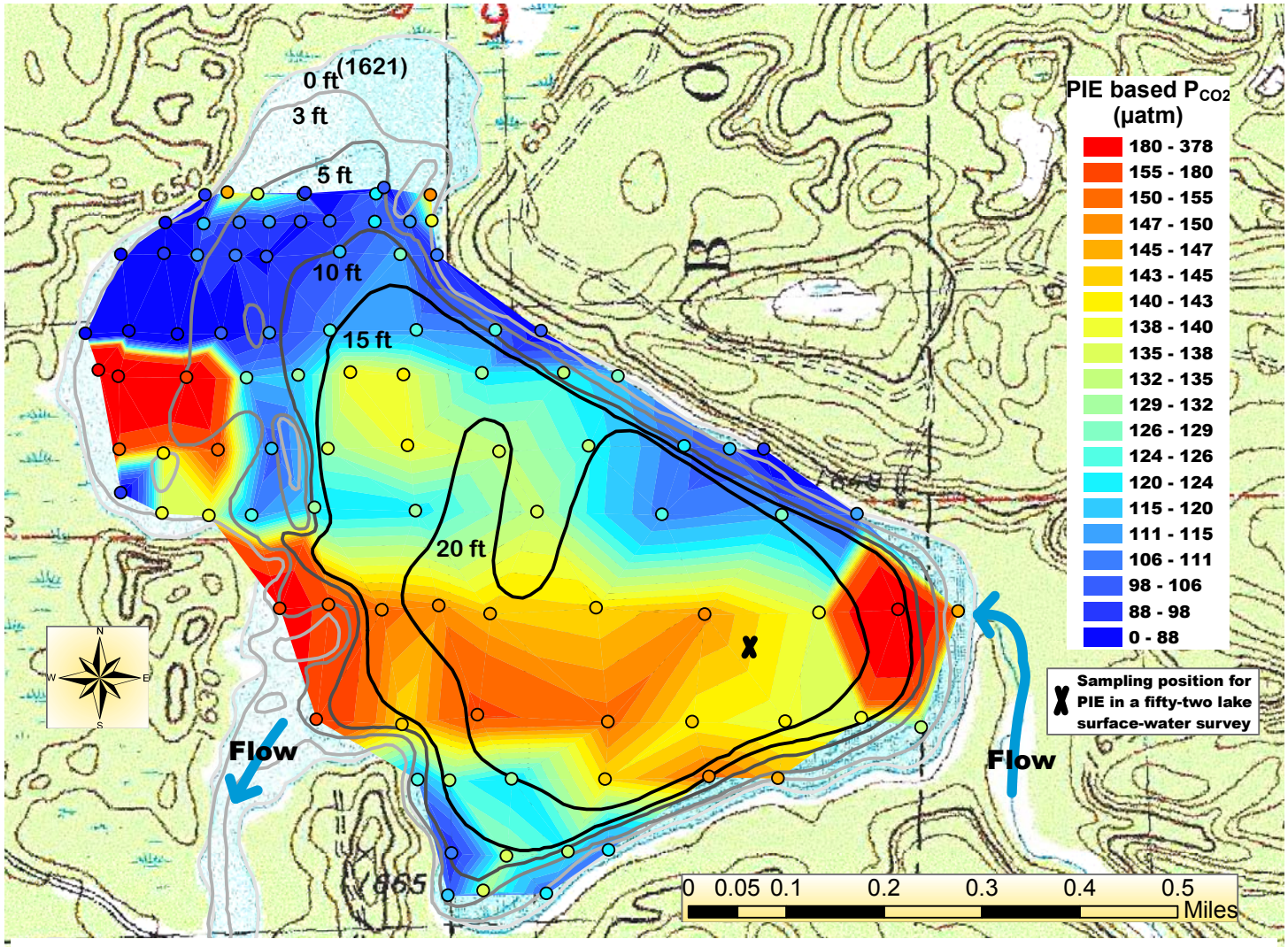

Figure 47. PIE based P_{CO2} (TIN model) and a topographic map for Allequash Lake, July 1 – 3, 2007.

function of the TIN model (i.e convex hull boundary). Map legends were created using quantile classification with twenty classes (min = 39 μatm P_{CO2}; max = 378 μatm P_{CO2}; mean = 131 μatm P_{CO2}; and standard deviation = 30 μatm P_{CO2}). Figure 47 was created by overlaying the map of the PIE based P_{CO2} measurements onto a digital raster graphic (DRG) map. The DRG is a scanned image of a U.S. Geological Survey (USGS) standard series 1:24,000 topographic map.

These maps show that most of the ninety-six measured near-shore and deep-water surface-water carbon dioxide sample values were undersaturated with respect to the July 2007 ambient atmospheric global average of 362 μatm P_{CO2} (381 ppmv; Tans, 2008). At this time, Allequash Lake would have been a sink for atmospheric carbon dioxide. Carbon dioxide would have been moving from the atmosphere into the lake.

Several locations displayed in red (Figures 45, 46, and 47) in the northern bay of Allequash Lake indicate possible ground and/or surface water entry of dissolved carbon dioxide. Figures 46 and 47 show a red plume on the eastern edge of Allequash Lake indicating possible surface water entry of carbon dioxide from Allequash Creek. This red plume starts at the Allequash Creek surface water entry into the northern bay and extends all the way to the surface water exit (channel) into the southern bay of Allequash Lake (see the blue arrows labeled as flow). (Note that Allequash Creek then proceeds to a surface water exit at the southern end of the southern bay of Allequash Lake, which is not shown.) Figure 47 shows wetland areas in the northern and western end of the northern bay of Allequash Lake. The plume on the western end of the lake shows a possible surface water entry of carbon dioxide into the lake.

There are two sampling points near the wetland on the northern end of the bay that show possible surface water or ground water entry of carbon dioxide into the lake.

These 96 samples in Figures 45, 46, and 47 are more representative of the whole lake than the traditional single surface water sampling location used in the fifty-two lake surface water survey (black X on map). Traditional lake studies involving collecting one sample from a lake only offer a very small glimpse of that sampling point in time and space.

PIE based carbon dioxide measurements offer a method of measuring multiple samples over a lake surface in a short time. PIE based carbon dioxide measurements also offer spatial resolution unavailable with traditional methods (e.g. bottle samples of headspace, ANC, DIC) of measuring carbon dioxide.

Allequash Lake's PIE based P_{CO2} and DIC measurements (06/06/2008 to 06/08/2008) were used to develop lake maps with P_{CO2} (Figures 48, 49, and 50) and DIC (Figure 51, 52, and 53) concentration. These maps show the variation of P_{CO2} and DIC concentration in the northern bay of Allequash Lake at spatial resolutions inaccessible via traditional indirect and direct carbon dioxide sampling methods. The open circles represent the four hundred fifty-eight sampling point locations and are color coded with P_{CO2} or DIC concentration. Note that some of the near shore sampling locations, like the previous year, also overshot the lakeshore edge (1621 feet above mean sea level) as indicated by the bathymetry. At the time of these carbon dioxide and DIC measurements, the water levels were also higher than the lakeshore edge datum. The TIN models, as described earlier, also had similar issues with

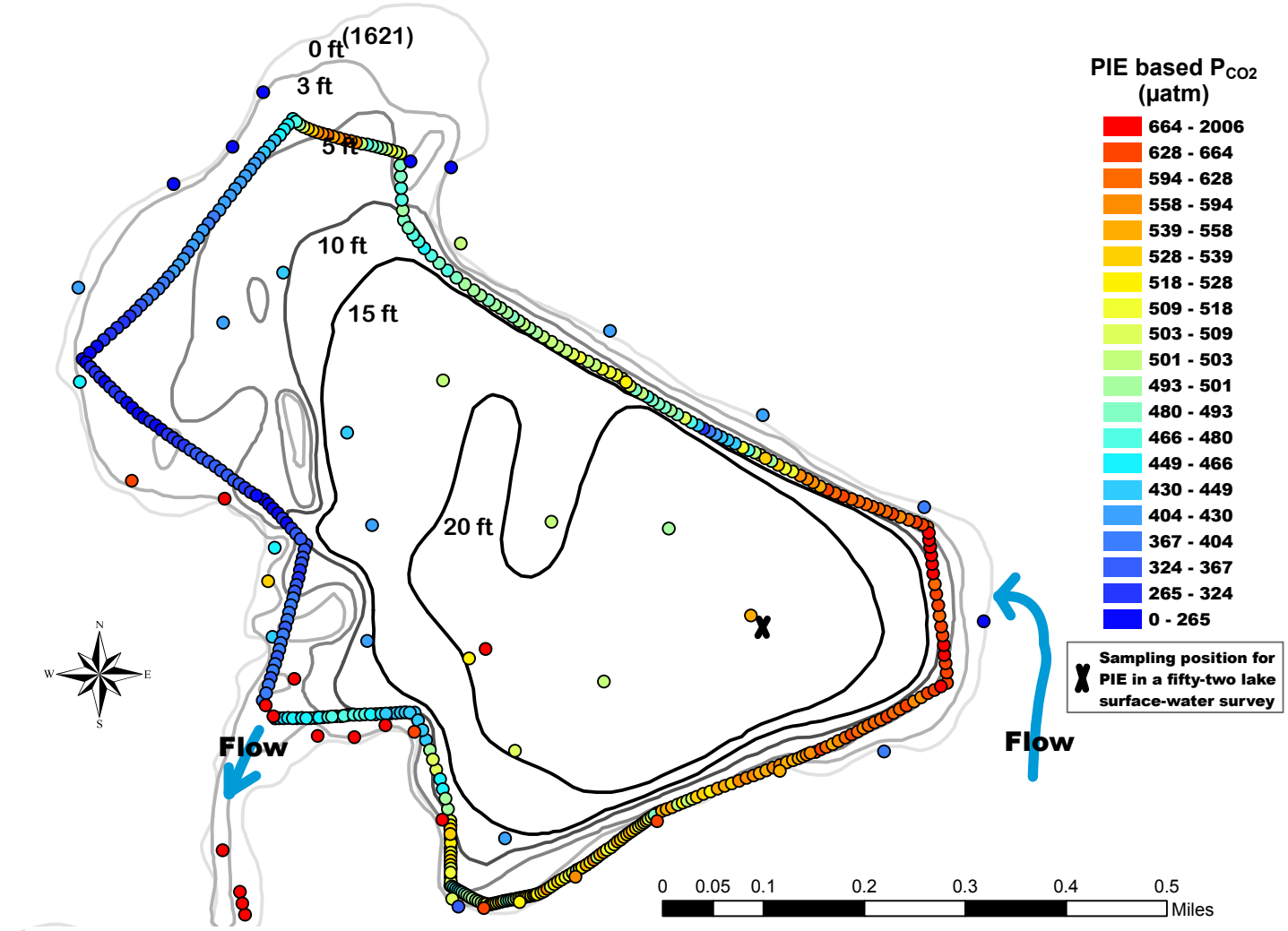

Figure 48. PIE based P_{CO2} for Allequash Lake, Vilas County, WI, June 6 - 8, 2008.

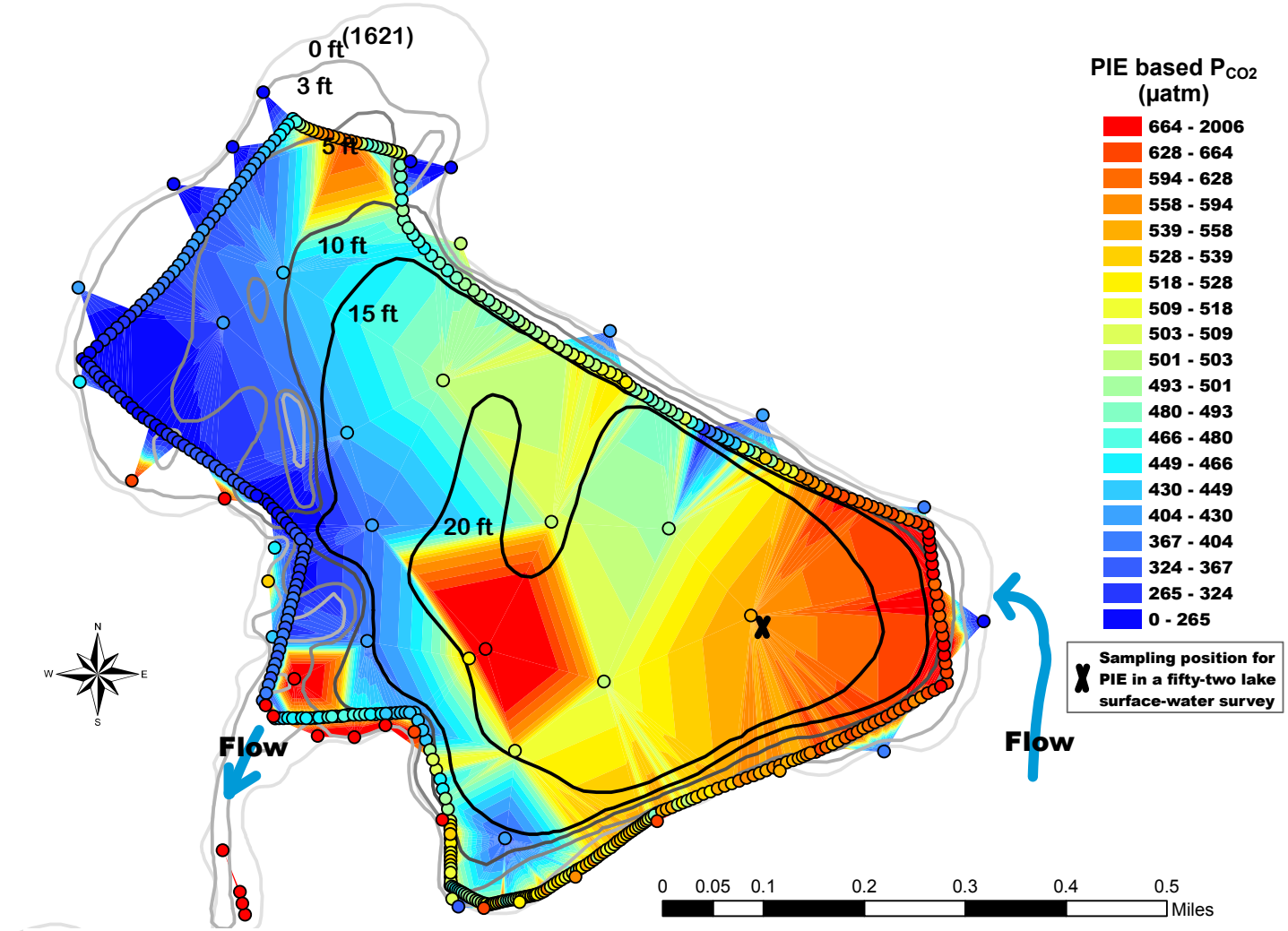

Figure 49. PIE based P_{CO2} (TIN model) for Allequash Lake, Vilas County, WI, June 6 - 8, 2008.

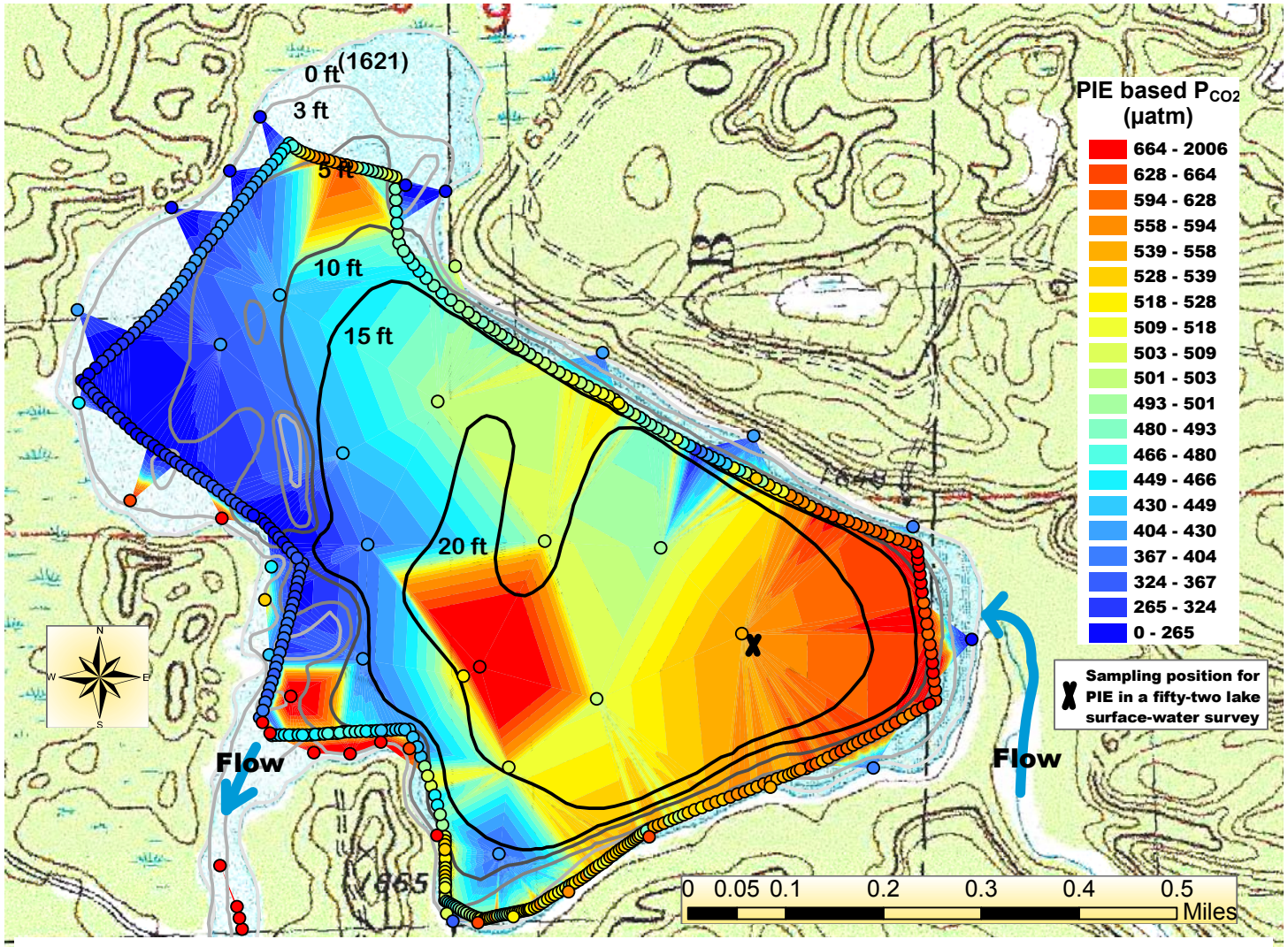

Figure 50. PIE based P_{CO2} (TIN model) and a topographic map for Allequash Lake, June 6 - 8, 2008.

overshooting the lakeshore edge. Map legends for Figures 48, 49, and 50 were created using quantile classification with twenty classes (min = 83 μatm P_{CO2}; max = 2006 μatm P_{CO2}; mean = 486 μatm P_{CO2}; and standard deviation = 120 μatm P_{CO2}). Map legends for Figure 51, 52, and 53 were created using quantile classification with twenty classes (min = 567 μmol L^{-1} DIC; max = 943 μmol L^{-1} DIC; mean = 899 μmol L^{-1} DIC; and standard deviation = 16 μmol L^{-1} DIC).

Unlike the previous year, Figures 48, 49, and 50 show that three-fourths of the four hundred fifty-eight measured surface water carbon dioxide sample values were oversaturated with respect to the June 2008 ambient atmospheric global average of 362 μatm P_{CO2} (385 ppmv; Tans, 2008). Three-fourths of Allequash Lake would likely have been a source for atmospheric carbon dioxide. Carbon dioxide would have been releasing from the lake surface into the atmosphere.

Even though the P_{CO2} levels are higher than the previous year, some of the same locations had higher P_{CO2} levels. As in the previous year, a red plume (Figures 49 and 50) on the eastern edge of Allequash Lake indicates possible surface water entry of carbon dioxide from Allequash Creek. A red plume starts at the Allequash Creek surface water entry into the northern bay and extend in patches all the way to the surface water exit (channel) into the southern bay of Allequash Lake (see the blue arrows labeled as flow). Several point locations (Figure 50) in the channel between bays display possible flow of carbon dioxide from the northern bay through the channel to the southern bay. The wetland on the western end shows two sampling points (Figure 50) of possible surface water entry of carbon dioxide into the lake.

There is also a plume (Figure 50) near the wetland on the northern end of the bay that shows possible surface water and/or ground water entry of carbon dioxide into the lake. The entire northeastern shoreline (Figure 50) shows possible ground water entry of carbon dioxide into the lake, conforming to the known flow paths for the groundwater hydrology of this watershed (Kratz et al., 1997).

These PIE based P_{CO2} measurements continue to offer spatial resolution unavailable with traditional methods (e.g. bottle samples of headspace, ANC, DIC) of measuring carbon dioxide.

The dissolved inorganic carbon (DIC) concentrations in Figures 51, 52, and 53 show some interesting patterns. Several locations in the northern bay of Allequash Lake (Figure 53) indicate possible consumption and creation of DIC. Areas of red (Figure 53) could indicate these areas of DIC creation. The spatial pattern of DIC suggests a very dynamic system with high DIC concentrations next to low DIC concentrations. There are higher DIC concentrations for the deep-water surface water samples, than for the near-shore surface water samples. Some of the DIC concentrations are 100 μmol L^{-1} higher than in the diurnal DIC study (Figures 43 and 44). Similar to the dissolved carbon dioxide maps, the traditional method of collecting one DIC sample is obviously not representative of the whole lake system. This lake has an intriguing dynamic pattern of dissolved inorganic carbon in definite need of further study.

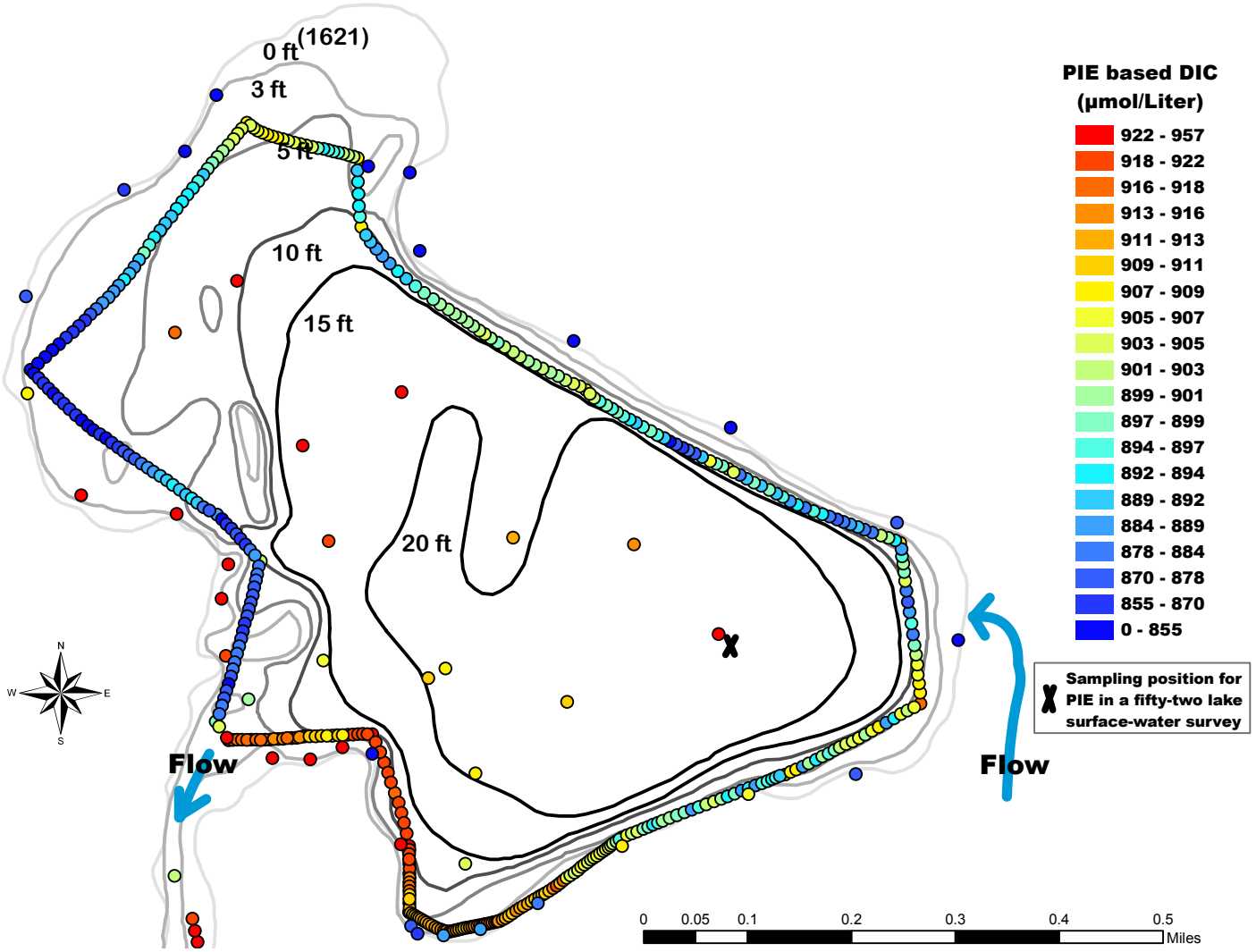

Figure 51. PIE based DIC for Allequash Lake, Vilas County, WI, June 6 - 8, 2008.

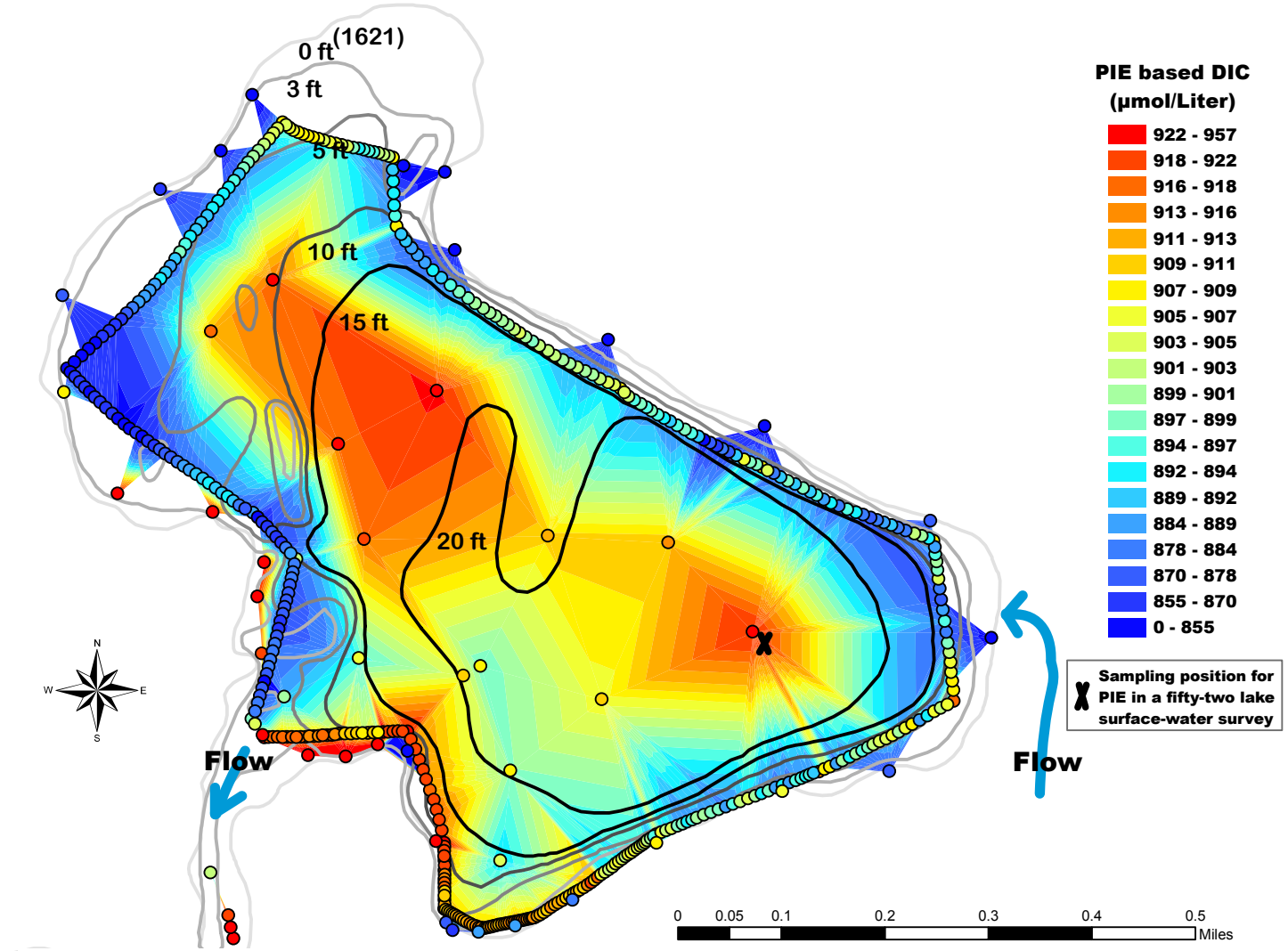

Figure 52. PIE based DIC (TIN model) for Allequash Lake, Vilas County, WI, June 6 - 8, 2008.

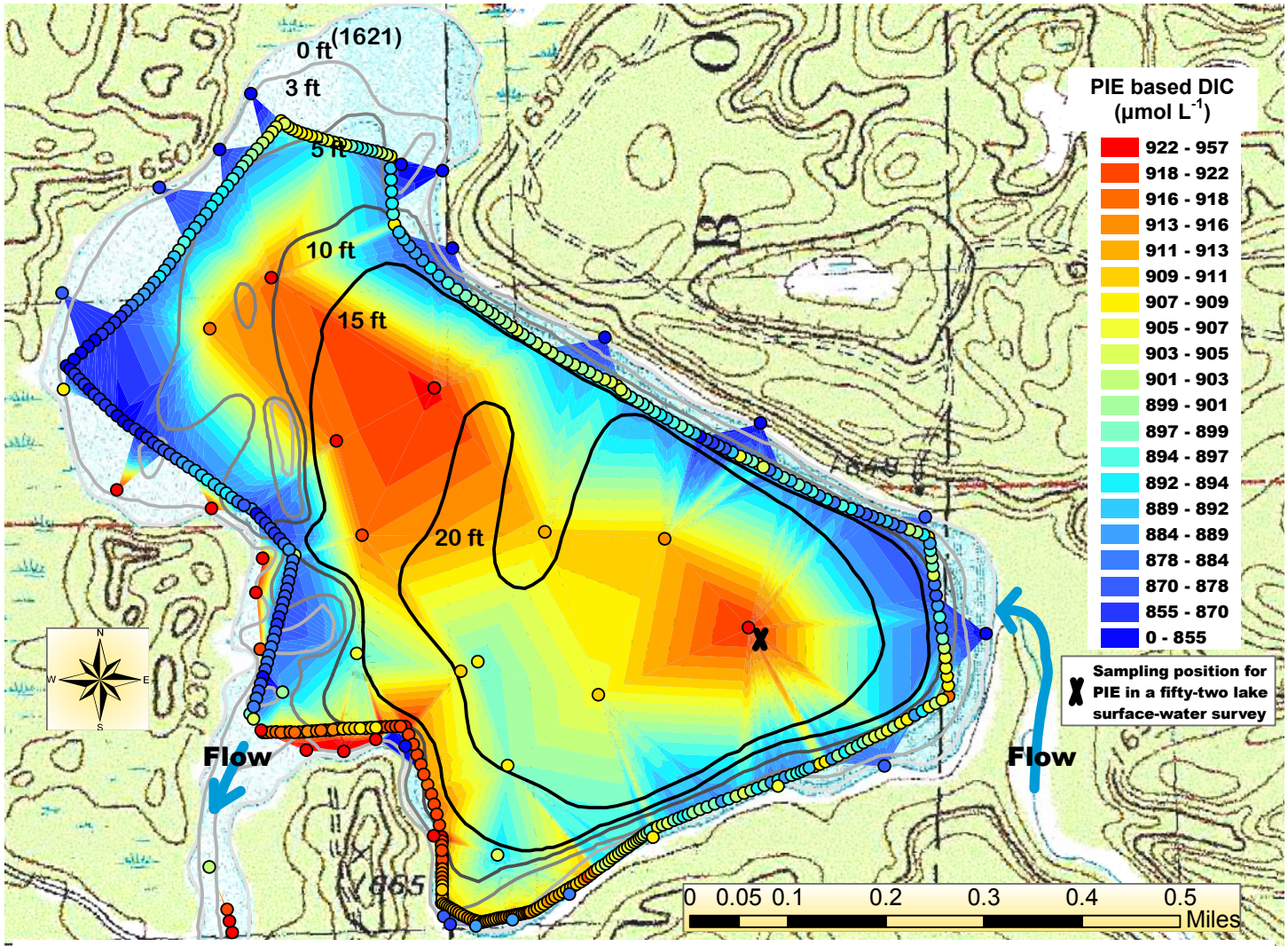

Figure 53. PIE based DIC (TIN model) and a topographic map for Allequash Lake, June 6 - 8, 2008.

Comparing maps of DIC (Figure 53) and P_{CO2} (Figure 50) can also give clues to the carbonate chemistry of this lake. Areas of high DIC and low P_{CO2} concentrations will have high levels of bicarbonate concentration. These high bicarbonate concentrations may give detail on the acid neutralizing capacity available in each part of the lake.

PIE based DIC measurements offer a method of measuring multiple samples over a lake surface in a short time. PIE based DIC measurements also offer spatial resolution unavailable with traditional methods (e.g. bottle samples of DIC) of measuring dissolved inorganic carbon.

PIE based measurements were also used for change detection in the environment, specifically the spatial variation of dissolved carbon dioxide concentration over time. Allequash Lake's PIE based P_{CO2} measurements taken from 07/01/2007 to 07/03/2007 and from 06/06/2008 to 06/08/2008 were used to develop lake maps (Figures 54 and 55) with P_{CO2} concentration. These maps were used to show the spatial variation of PIE based P_{CO2} measurements between these two years. The map legend for Figure 54 was created using manual classification with six classes and intervals of sixty-seven (min = 39 μatm P_{CO2}; max = 378 μatm P_{CO2}; mean = 131 μatm P_{CO2}; and standard deviation = 30 μatm P_{CO2}). The map legend for Figure 55 was created using manual classification with thirty-one classes and intervals of sixty-seven (min = 83 μatm P_{CO2}; max = 2006 μatm P_{CO2}; mean = 486 μatm P_{CO2}; and standard deviation = 120 μatm P_{CO2}). These maps were developed using the same

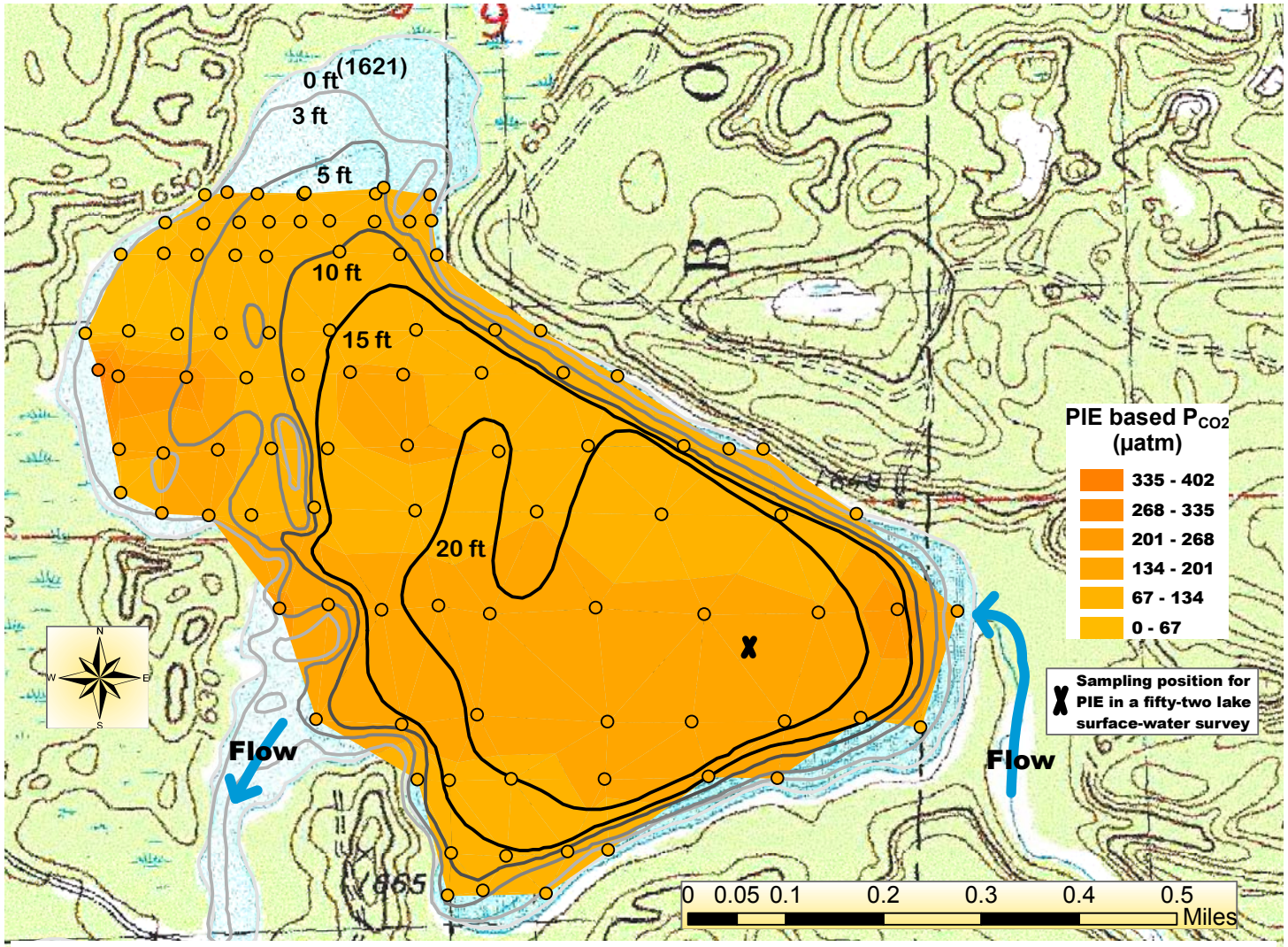

Figure 54. PIE based P_{CO2} (TIN model) and a topographic map for Allequash Lake, July 1 – 3, 2007.

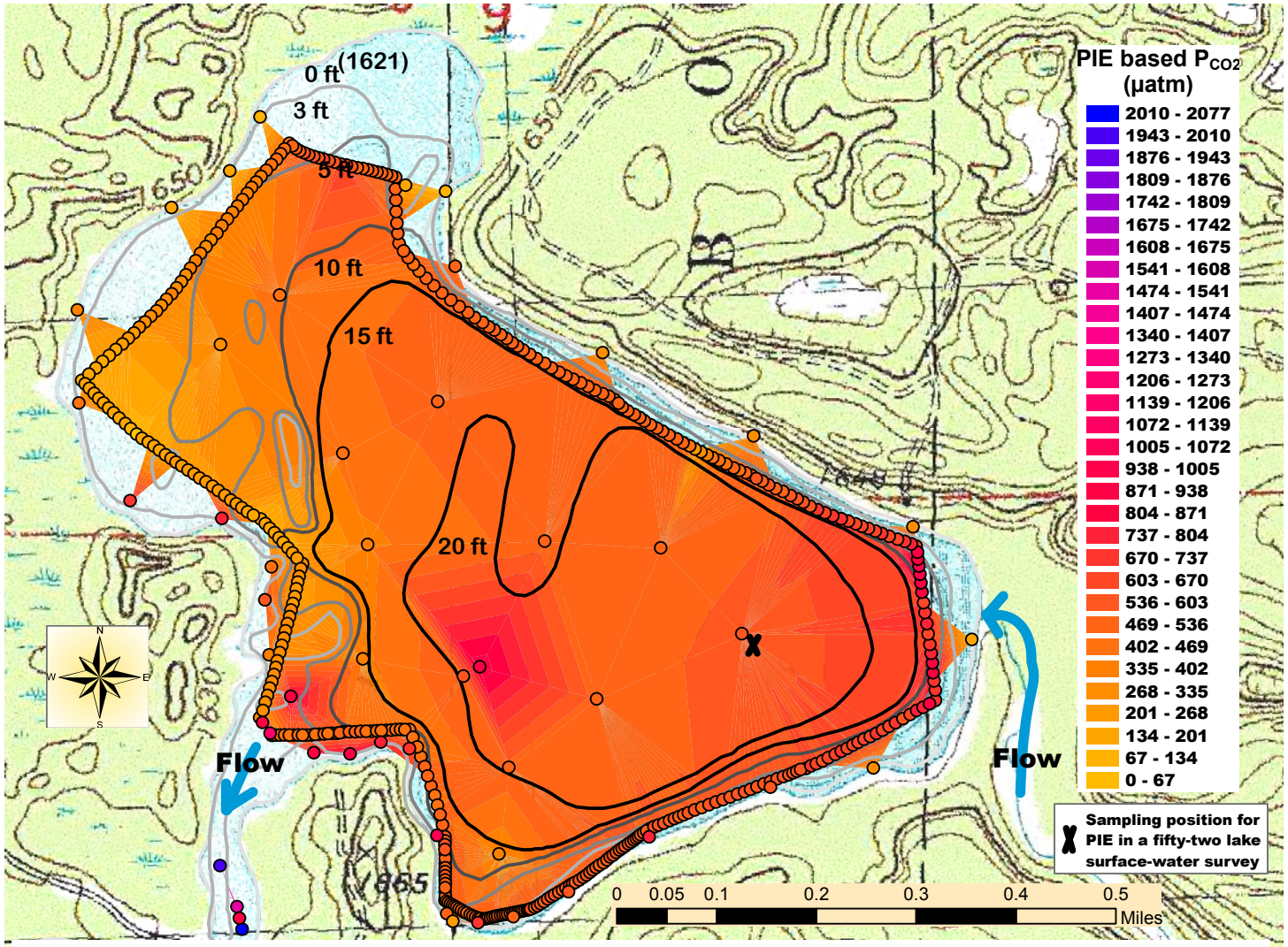

Figure 55. PIE based P_{CO2} (TIN model) and a topographic map for Allequash Lake, June 6 - 8, 2008.

legend interval, in order to show how much higher the carbon dioxide concentrations are from year 2007 to year 2008. The carbon dioxide concentrations in June 2008 (Figure 55) are many times higher than in July 2007 (Figure 54). The mean value for the June 2008 carbon dioxide concentrations is nearly four times that of the July 2007 mean value. The change in carbon dioxide concentration from year 2007 to year 2008 could be from external or internal sources. What percentage of the carbon input came from runoff, ground water, surface water, or internal processes is unknown. This lake has carbon dioxide spatial variations in definite need of further study.

The PIE method substantially increases the ability to measure the spatial variation of dissolved carbon dioxide concentration over time. PIE based measurements show the variation of P_{CO2} concentration in the northern bay of Allequash Lake at spatial and temporal resolutions inaccessible via traditional indirect and direct carbon dioxide sampling methods.

Conclusion – Temporal and Spatial Resolution of PIE

The PIE method substantially increases the ability to measure carbon dioxide variations in time and space. The PIE method allows for rapid measurement of carbon dioxide and improved understanding of carbon dioxide dynamics.

In a continuous twenty-four hour diurnal pattern of one surface water point on Allequash Lake, PIE based P_{CO2} and DIC measurements showed the actual respiration and photosynthesis of a mesotrophic lake from day to night and back to day at temporal resolutions inaccessible via traditional indirect and other direct sampling methods. These diurnal PIE based P_{CO2} measurement results also might have shown a repeatable pattern on a daily scale. The PIE based P_{CO2} pattern during the day is consistent with CO_2 consumption and oxygen production during plant photosynthesis. The pattern of CO_2 increase throughout the night time hours is also consistent with plant respiration, where the energy or sugar stored during the day during photosynthesis is consumed along with oxygen to produce carbon dioxide and water during the night.

The minimum value, maximum value, and general shape of the diurnal O_2 and PIE based P_{CO2} fluctuations seemed to be a different magnitude, but opposite in direction. Similar relationships were also found in the depth profile experiments discussed earlier and in diurnal studies of dissolved carbon dioxide and dissolved oxygen in Hanson et al., (2006).

These PIE based P_{CO2} diurnal measurements were also recorded and reported at temporal resolutions inaccessible via traditional indirect and direct carbon dioxide

sampling methods. The PIE based data sets were recorded at a temporal resolution of one record per second P_{CO2} and both CO_2 and O_2 were graphed as a one record per minute time series. Similar temporal resolution was also found with the PIE based DIC measurements.

PIE based P_{CO2} and DIC measurements showed lake maps with P_{CO2} and DIC concentration at spatial and temporal resolutions inaccessible via traditional laboratory DIC and traditional indirect (P_{CO2} by pH and ANC, P_{CO2} by pH and DIC) and direct (headspace) dissolved carbon dioxide measurement methods. PIE based P_{CO2} and DIC whole lake maps showed spatial variation of dynamic lake systems at rarely documented spatial resolution. PIE based P_{CO2} whole lake maps displayed possible ground and/or surface water entry of dissolved carbon dioxide to a lake. PIE based P_{CO2} maps also showed spatial variation of dissolved carbon dioxide concentration over time. PIE based DIC whole lake maps showed an intriguing dynamic pattern of DIC in definite need of further study. PIE based carbon dioxide measurements offer a method of measuring multiple samples (P_{CO2}, [H_2CO_3*], and DIC) over a lake surface in a short time. The PIE method offers one sample measured per second, which can add up to thousands (86400) of samples measured for a whole lake in just one day.

PIE gives researchers direct measurement methods of known quality (accuracy and precision), spatial resolution, and temporal resolution for studying dissolved carbon dioxide, which were inaccessible via traditional sampling methods (indirect and other direct carbon dioxide measurement methods).

APPENDIX A

Bibliography

Anderson, D., D. Stannard, R. Striegl, and T. McConnaughey. 1997. Exchange of Carbon Dioxide and Water Vapor between Williams Lake and the Atmosphere. Hydrological and biogeochemical research in the Shingobee River headwaters area. Water-reources investigation report 96-4215. U. S. Geological Survey: pp. 31-40

Baehr, M.M., and M.D. DeGrandpre. 2004. In situ pCO_2 and O_2 measurements in a lake during turnover and stratification: Observations and modeling. *Limnology and Oceanography* 49: pp. 330-340.

Baehr, M.M., and M.D. DeGrandpre. 2002. Under-Ice CO2 and O2 Variability in a Freshwater Lake. *Biogeochemistry* 61: pp. 95-113.

Baker, J.P., Gherini, S.A., Christensen, S.W., Driscoll, C.T., Gallagher, J., Munson, R.K., Newton, R.M., Reckhow, K.H., and Schofield, C.L. 1990. Adirondack lakes survey: An interpretive analysis of fish communities and water chemistry, 1984-87. Adirondack Lakes Survey Corporation, Ray Brook, NY.

Browne, B. 2004a. Pumping-Induced Ebullition: A Unified and Simplified Method for Measuring Multiple Dissolved Gases. *Environmental Science & Technology* 38: pp. 5729-5736.

Browne, B. 2004b. Supporting Information for Pumping-Induced Ebullition: A Unified and Simplified Method for Measuring Multiple Dissolved Gases. *Environmental Science & Technology* 38: pp. S1-S21

Carignan, Richard. 1998. Automated determination of carbon dioxide, oxygen, and nitrogen partial pressures in surface waters. *Limnology and Oceanography*. 43(5): pp. 969-975.

Carlson, R.E. 1977. A trophic state index for lakes. *Limnology and Oceanography*. 22(2): pp. 361-369.

Chipman, J. W., T. M. Lillisand, J. E. Schmaltz, J. E. Leale and M. J. Nordheim, 2004. Mapping lake water clarity with Landsat images in Wisconsin, USA. *Canadian Journal of Remote Sensing* 30(1): pp. 1-7.

Cole, J.J., and N.F. Caraco. 1998. Atmospheric exchange of carbon dioxide in a low-wind oligotrophic lake measured by the addition of SF_6. *Limnology and Oceanography* 43: pp. 647-656.

Cole, J.J., N.F. Caraco, G.W. Kling, and T.K. Kratz. 1994. Carbon-dioxide supersaturation in the surface waters of lakes. *Science* 265: pp. 1568-1570.

DeGrandpre, M.D., and M.M. Baehr. 1999. Calibration-free optical chemical sensors. *Analytical Chemistry* 71(6): pp. 1152-1159.

DeGrandpre, M.D., T. R. Hammar, S. P. Smith, and F. L. Sayles. 1995. In situ measurements of seawater pCO_2. *Limnology and Oceanography* 40(5): pp 969-975.

Hanson, Paul C., Stephen R. Carpenter, David E. Armstrong, Emily H. Stanley, and Timothy K. Kratz. 2006. Lake Dissolved Inorganic Carbon and Dissolved Oxygen: Changing Drivers from Days to Decades. *Ecological Monographs*. Ecological Society of America. 76(3), pp. 343–363.

Harned, H. S., F. T. Bonner. 1945. The first ionization of carbonic acid in aqueous solutions of sodium chloride. *Journal of the American Chemical Society*. 67: pp. 1026-1031.

Herczeg, A.L., W.S. Broecker, R.F. Anderson, and S.L. Schiff. 1985. A new method for monitoring temporal trends in the acidity of fresh waters. *Nature* 315: pp. 133-135.

Hope, D., T.K. Kratz, and J.L. Riera. 1996. Relationship between pCO_2 and dissolved organic carbon in northern Wisconsin lakes. *Journal of Environmental Quality* 25: pp. 1442-1445.

Jonsson, A., J. Karlsson, and M. Jansson. 2003. Sources of carbon dioxide supersaturation in clearwater and humic lakes in northern Sweden. *Ecosystems* 6: pp. 224-235.

Kling, G., G. Kipphut, and M. Miller. 1992. The Flux of CO2 and CH4 from Lakes and Rivers in Arctic Alaska. *Hydrobiologia* 240: pp. 23-36.

Kratz, T.K., K.E. Webster, C.J. Bowser, J.J. Magnuson, B.J. Benson. 1997.The influence of landscape position on lakes in northern Wisconsin. *Freshwater Biology* 37: pp. 209-217.

Lahav, O., B. Morgan, and R. Loewenthal. 2001. Measurement of pH, alkalinity and acidity in ultra-soft waters. *Water SA* 27(4): pp. 423-432.

Lillie, R. A., S. Graham, and P. Rasmussen. 1993. Trophic State Index Equations and Regional Predictive Equations For Wisconsin Lakes. *Wisconsin Department of Natural Resources Research Management Findings*. May, 1993. No. 35.

Loftfield, N., H. Flessa, J. Augustin, and F. Beese. 1997. Automated Gas Chromatographic System for Rapid Analysis of the Trace Gases Methane, Carbon Dioxide, and Nitrous Oxide. *Journal of Environmental Quality* 26: pp. 560-564.

McDermitt, D.K., J.M. Welles, and R.D. Eckles. 1993a. Effects of Temperature, Pressure and Water Vapor on Gas Phase Infrared Absorption by CO_2. LI-COR, inc., Lincoln, NE.

McDermitt, D.K., R.D. Eckles, G.L. Biggs, and J.M. Welles. 1993b. Effects of temperature and pressure on CO_2 infrared absorption with special emphasis on problems resulting from operation at high flow rates. LI-COR, inc., Lincoln, NE.

McMurry, John, and Robert C. Fay. 2001. *Chemistry, Third Edition*. Prentice Hall, Inc., Upper Saddle River, New Jersey, USA.

Mook, Willem G, and J.J. de Vries. 1999. Environmental Isotopes in the Hydrological Cycle Principles and Applications. International Atomic Energy Agency (IAEA), Vienna, Austria. Centre for Isotope Research, Groningen. Volume I: Introduction - Theory, Methods, Review. Ch.9, CHEMISTRY OF CARBONIC ACID IN WATER: pp. 143-165.

Neumann, K., W.B. Lyons, J.C. Priscu, and R.J. Donahoe. 2001. CO_2 concentrations in perennially ice-covered lakes of Taylor Valley, Antarctica. *Biogeochemistry* 56: pp. 27-50.

Portielje, R., and L. Lijklema. 1995. Carbon dioxide fluxes across the air-water interface and its impact on carbon availability in aquatic aystems. *Limnology and Oceanography* 40: pp. 690-699.

Raymond, P.A., N.F. Caraco, and J.J. Cole. 1997. Carbon Dioxide Concentration and Atmospheric Flux in the Hudson River. *Estuaries* 20: pp. 381-390.

Rosich, R.S. 2002. Comments on Measurement of pH, alkalinity and acidity in ultra-soft waters by Lahav, O., Morgan, BE., and Loewenthal, RE. *Water SA* 28(3): pp. 346-348.

Rounds, S.A. 2006. Alkalinity and Acid Nuetralizing Capacity, pp. 1-50, *In* U. S. G. Survey TWRI National Field Manual for the Collection of Water Quality Data, Book 9, Chapter A6 Field Measurements, Section 6.6.

Sellers, P., R.H. Hesslein, and C.A. Kelly. 1995. Continuous measurement of CO_2 for estimation of air-water fluxes in lakes - An in-situ technique. *Limnology and Oceanography* 40: pp. 575-581.

Shimadzu Corporation and p.a.e.i. division. 1994. Instruction manual total organic carbon analyzer model toc-5000a.

SLU. 2000. Swedish National Lake Monitoring. Swedish University of Agricultural Sciences.

Sobek, S., L.J. Tranvik, and J.J. Cole. 2005. Temperature independence of carbon dioxide supersaturation in global lakes. *Global Biogeochemical Cycles* 19:Art. No. GB2003 2005.

Striegl, R.G., and C.M. Michmerhuizen. 1998. Hydrologic influence on methane and carbon dioxide dynamics at two north-central Minnesota lakes. *Limnology and Oceanography* 43: pp. 1519-1529.

Stumm, W., and J.J. Morgan. 1981. *Aquatic Chemistry*. 2nd ed. John Wiley and Sons, New York.

Tans, Dr. Pieter. 2008. NOAA/ESRL, Internet data source *(www.esrl.noaa.gov/gmd/ccgg/trends)*10/22/2008.

Tyler, John E. 1968. The Secchi Disc. *Limnology and Oceanography*. 13(1): pp. 1-6.

Wetzel, R.G. 2001. *Limnology: Lake and River Ecosystems*. Academic Press, San Diego, California, USA.

Wilde, F.D., E. Busenberg, and D.B. Radtke. 2006. pH, pp. 1-29, *In* U. S. G. Survey TWRI National Field Manual for the Collection of Water Quality Data, Book 9, Chapter A6 Field Measurements, Section 6.4.

APPENDIX B

Table B-1. ***PIE in a fifty-two lake surface water survey (07/09/2007 to 07/22/2007). These GPS sampling points were geo-referenced to the Wisconsin Transverse Mercator (WTM83/91) projection system (meters) and North American 1983 HARN geographic coordinate system.***

Lake Name	WDNR Lake ID	Lake Number (Figure 11)	GPS Easting (m)	GPS Northing (m)	Sampling Depth (m)	Landsat Average SDT (m) (Chipman et al., 2004)	WTSI (SDT) (Lillie et al., 1993)	Sample Site Lake depth (m)	Lake Area (m^2)	Lake Perimeter (m)	Specific Conductivity (µS)	Air Temp (F)	Atmospheric Barometric Pressure (atm)	Sampling Date
Allequash Lake	2332400	1	549494.6	618382.5	0.245	2.95	44.43	6.71	1641117.50	9422.64	108.7	71.0	0.9309	7/10/2007
Arrowhead Lake	1541500	2	544093.9	603652.6	0.374	4.50	38.34	12.19	389962.80	3357.96	108.1	68.0	0.9445	7/19/2007
Ballard Lake	2340700	3	558370.1	621061.7	0.149	3.43	42.26	4.27	2033907.16	8994.41	75.0	66.0	0.9376	7/11/2007
Bearskin Lake	1523600	4	545314.9	584518.7	0.443	1.57	53.52	3.20	1629661.24	9803.85	125.5	60.0	0.9535	7/21/2007
Big Arbor Vitae Lake	1545600	5	547307.1	606335.0	0.343	1.69	52.43	11.28	4331578.05	13494.89	126.2	58.0	0.9445	7/16/2007
Big Carr Lake	971600	6	548514.5	590800.7	0.392	5.77	34.76	21.31	845287.44	6065.32	30.0	68.0	0.9474	7/19/2007
Big Lake	2334700	7	537465.3	630373.4	0.320	3.34	42.62	11.28	3347132.87	15215.55	145.0	79.0	0.9472	7/9/2007
Big Muskellunge Lake	1835300	8	550015.2	616433.9	0.328	4.56	38.15	16.76	3631625.99	16140.98	60.0	59.0	0.9397	7/15/2007
Big Saint Germain Lake	1591100	9	556603.9	606103.5	0.312	1.82	51.37	10.97	6563022.92	12994.03	112.0	69.0	0.9432	7/18/2007
Bolger Lake	973000	10	541790.9	596483.5	0.424	4.62	37.96	9.75	465530.51	4728.60	27.3	57.0	0.9547	7/20/2007
Buffalo Lake	974200	11	553600.1	600694.9	0.338	4.54	38.20	6.25	423780.25	3337.79	28.3	65.0	0.9437	7/17/2007

Table B-1. ***(continued).***

Lake Name	WDNR Lake ID	Lake Number (Figure 11)	GPS Easting (m)	GPS Northing (m)	Sampling Depth (m)	Landsat Average SDT (m) (Chipman et al., 2004)	WTSI (SDT) (Lillie et al., 1993)	Sample Site Lake depth (m)	Lake Area (m^2)	Lake Perimeter (m)	Specific Conductivity (µS)	Air Temp (F)	Atmospheric Barometric Pressure (atm)	Sampling Date
Carrol Lake	1544800	12	549278.7	602135.5	0.338	1.96	50.32	8.23	1336783.23	8306.32	127.6	58.0	0.9436	7/16/2007
Clear Lake	2329000	13	534431.1	630062.0	0.329	3.69	41.21	7.92	2084726.06	7869.41	103.9	79.0	0.9445	7/9/2007
Clear Lake	977500	14	549123.2	601096.3	0.346	6.37	33.33	7.92	3534737.42	23624.62	37.5	58.0	0.9453	7/16/2007
Crab Lake	2953500	15	541223.1	635646.1	0.385	4.09	39.71	4.88	3678157.12	27509.40	60.0	68.0	0.9445	7/22/2007
Escanaba Lake	2339900	16	552043.3	620990.0	0.317	3.24	43.06	7.92	1225683.83	8134.69	57.0	59.0	0.9404	7/15/2007
Fawn Lake	2328900	17	533524.9	629137.2	0.327	2.73	45.51	2.74	282795.99	4514.20	96.0	79.0	0.9461	7/9/2007
Flannery Lake	985300	18	559107.3	576822.6	0.418	5.46	35.57	8.23	432582.98	5626.35	24.0	60.0	0.9517	7/21/2007
Found Lake	1593800	19	562935.2	608715.2	0.305	1.58	53.46	5.79	1361192.06	6362.03	66.5	69.0	0.9440	7/18/2007
Gilmore Lake	1589300	20	554047.5	597522.1	0.326	1.50	54.19	7.32	1268804.12	7326.94	102.1	65.0	0.9420	7/17/2007
Hasbrook Lake	1589100	21	552839.5	596371.3	0.381	5.58	35.25	14.33	1243841.75	7491.66	53.0	68.0	0.9465	7/19/2007
Hodstradt Lake	990700	22	553967.0	592496.7	0.393	5.44	35.60	4.08	483373.98	4075.40	30.4	68.0	0.9465	7/19/2007
Horsehead Lake	1588000	23	552199.5	589704.0	0.411	1.69	52.47	2.74	1526450.07	9722.90	117.3	57.0	0.9522	7/20/2007

Table B-1. ***(continued).***

Lake Name	WDNR Lake ID	Lake Number (Figure 11)	GPS Easting (m)	GPS Northing (m)	Sampling Depth (m)	Landsat Average SDT (m) (Chipman et al., 2004)	WTSI (SDT) (Lillie et al., 1993)	Sample Site Lake depth (m)	Lake Area (m^2)	Lake Perimeter (m)	Specific Conductivity (µS)	Air Temp (F)	Atmospheric Barometric Pressure (atm)	Sampling Date
Irving Lake	2340900	24	560167.8	620930.8	0.313	1.79	51.62	0.76	1694270.01	6622.03	78.0	66.0	0.9363	7/11/2007
Island Lake	2334400	25	535193.0	627494.0	0.306	2.78	45.30	9.75	3501526.95	19988.48	107.0	79.0	0.9397	7/9/2007
Katherine Lake	1543300	26	542040.5	592718.4	0.451	4.61	37.98	7.32	2121475.06	17127.94	52.2	57.0	0.9532	7/20/2007
Little Arbor Vitae Lake	1545300	27	549714.1	604578.0	0.349	1.23	57.06	8.23	2186544.75	10326.89	135.2	58.0	0.9452	7/16/2007
Little John Lake	2332300	28	547493.3	616065.0	0.329	1.46	54.55	5.18	611225.63	5369.32	120.3	61.0	0.9372	7/12/2007
Little Saint Germain Lake	1596300	29	560937.2	604004.1	0.311	2.32	47.86	14.33	2948206.52	17856.42	90.0	69.0	0.9409	7/18/2007
Little Star Lake	2334300	30	530894.9	626738.0	0.300	4.74	37.60	19.17	1052179.08	6288.73	105.2	79.0	0.9390	7/9/2007
Long Lake	1001300	31	550610.6	583315.7	0.438	4.24	39.20	16.15	456901.10	4592.95	23.9	60.0	0.9540	7/21/2007
Lost Lake	1593400	32	560202.4	610158.7	0.326	1.28	56.39	5.49	2179519.38	7537.18	100.9	69.0	0.9424	7/18/2007
Madeline Lake	1544700	33	547876.0	602424.7	0.335	1.17	57.68	3.35	694128.88	6338.16	120.8	58.0	0.9431	7/16/2007
Manitowish Lake	2329400	34	532299.6	625926.9	0.317	3.49	41.98	1.68	2006569.76	13565.50	109.0	79.0	0.9404	7/9/2007

Table B-1. ***(continued).***

Lake Name	WDNR Lake ID	Lake Number (Figure 11)	GPS Easting (m)	GPS Northing (m)	Sampling Depth (m)	Landsat Average SDT (m) (Chipman et al., 2004)	WTSI (SDT) (Lillie et al., 1993)	Sample Site Lake depth (m)	Lake Area (m^2)	Lake Perimeter (m)	Specific Conductivity (µS)	Air Temp (F)	Atmospheric Barometric Pressure (atm)	Sampling Date
Mann Lake	2332000	35	546627.4	613047.1	0.282	1.48	54.38	4.88	1022686.54	7673.59	110.1	59.0	0.9395	7/15/2007
McNaughton Lake	1587600	36	552276.3	586321.5	0.411	1.30	56.19	1.68	487937.51	4552.82	98.0	57.0	0.9506	7/20/2007
Minocqua Lake	1542400	37	543842.1	599843.5	0.349	3.28	42.88	16.46	5420605.86	33756.11	137.0	65.0	0.9438	7/17/2007
Pickerel Lake	1590400	38	555894.1	601336.9	0.330	1.52	53.99	3.66	2358921.03	16245.06	100.0	65.0	0.9434	7/17/2007
Plum Lake	1592400	39	556494.5	614116.6	0.290	3.35	42.60	17.37	4279474.54	21548.20	104.4	59.0	0.9411	7/15/2007
Presque Isle Lake	2956500	40	536873.6	638921.8	0.409	4.20	39.35	20.73	4715123.55	15998.46	152.0	68.0	0.9518	7/22/2007
Razorback Lake	1013800	41	556773.5	616673.2	0.335	3.88	40.47	3.44	1543634.26	9666.67	53.7	59.0	0.9363	7/15/2007
Snipe Lake	1018500	42	569286.6	607543.6	0.288	3.32	42.70	3.66	872113.38	5826.30	36.3	69.0	0.9401	7/18/2007
Spider Lake	2329300	43	533909.4	627596.1	0.325	3.37	42.49	11.95	1125548.66	9574.07	108.0	79.0	0.9440	7/9/2007
Star Lake	1593100	44	560676.7	616992.9	0.309	4.13	39.58	8.63	4934021.21	19124.09	89.3	66.0	0.9378	7/11/2007

Table B-1. ***(continued).***

Lake Name	WDNR Lake ID	Lake Number (Figure 11)	GPS Easting (m)	GPS Northing (m)	Sampling Depth (m)	Landsat Average SDT (m) (Chipman et al., 2004)	WTSI (SDT) (Lillie et al., 1993)	Sample Site Lake depth (m)	Lake Area (m^2)	Lake Perimeter (m)	Specific Conductivity (µS)	Air Temp (F)	Atmospheric Barometric Pressure (atm)	Sampling Date
Stone Lake	2328800	45	533224.9	628049.3	0.332	3.39	42.41	8.99	557276.76	5896.13	106.3	79.0	0.9441	7/9/2007
Sweeny Lake	1589600	46	551810.1	598608.5	0.341	1.20	57.32	3.66	773463.68	5264.03	106.3	65.0	0.9445	7/17/2007
Towanda Lake	1022900	47	542313.0	607448.2	0.355	3.39	42.42	6.71	563082.64	6119.11	31.1	58.0	0.9450	7/16/2007
Trout Lake	2331600	48	546038.5	617603.0	0.336	4.62	37.96	32.92	15638240.93	32448.09	107.0	59.0	0.9384	7/15/2007
Upper Gresham Lake	2330800	49	540397.0	621673.9	0.312	3.04	43.97	8.53	1465496.21	9480.09	132.8	79.0	0.9416	7/9/2007
Van Vliet Lake	2956800	50	538864.3	636021.3	0.394	1.32	56.02	4.18	930841.05	8522.39	117.7	68.0	0.9487	7/22/2007
White Birch Lake	2340500	51	557114.6	621094.5	0.322	3.42	42.31	3.96	456967.14	3944.32	73.2	66.0	0.9386	7/11/2007
White Sand Lake	2339100	52	551891.4	623946.9	0.362	5.12	36.49	20.42	3020698.29	9881.23	82.1	66.0	0.9379	7/11/2007

APPENDIX C

Table C-1. ***PIE in a fifty-two lake surface water survey (07/09/2007 to 07/22/2007).***

Lake Name	WDNR Lake ID	Lillie WTSI (SDT) Trophic Class	Lake Temp. (F)	YSI sonde Lake pH	PIE based P_{CO2} (µatm)	Headspace based P_{CO2} (µatm)	P_{CO2} by pH and laboratory DIC (µatm)	P_{CO2} by pH and ANC (Gran titration) (µatm)	P_{CO2} by pH and ANC (C_B and C_A) (µatm)	ANC by Gran titration (µmol L^{-1})	ANC by C_B and C_A (µmol L^{-1})	Laboratory DIC (µmol L^{-1})
Allequash Lake	2332400	mesotrophic	76.8659	8.6494	206.5385	329.8705	120.1782	122.7059	101.1649	907.5190	748.2044	871.7735
Arrowhead Lake	1541500	oligotrophic	72.8768	8.8463	58.2858	42.0226	50.3813	49.1761	44.7526	604.3725	550.0072	599.4172
Ballard Lake	2340700	mesotrophic	73.6025	8.9315	96.7503	32.7111	38.6693	39.6958	33.8137	593.8007	505.8122	556.0921
Bearskin Lake	1523600	eutrophic	77.4975	9.5725	64.8085	82.8089	12.9563	12.8620	12.0374	1080.8585	1011.5583	926.4779
Big Arbor Vitae Lake	1545600	eutrophic	72.7144	8.3818	370.0988	354.2127	283.3957	273.3083	247.8069	1105.3241	1002.1905	1141.8263
Big Carr Lake	971600	oligotrophic	73.0344	7.2717	231.6575	216.9013	107.6226	143.8198	157.8417	42.9064	47.0896	35.9450
Big Lake	2334700	mesotrophic	76.0464	8.5868	392.0199	491.5259	205.1814	204.6216	172.2633	1319.7097	1111.0147	1302.5257
Big Muskellunge Lake	1835300	oligotrophic	70.7165	8.3998	121.6279	110.4203	96.8277	100.1006	86.8647	421.7912	366.0195	406.6334
Big Saint Germain Lake	1591100	eutrophic	76.2302	8.7287	109.3267	126.1022	89.6045	89.5117	84.1095	806.4860	757.8130	787.6769
Bolger Lake	973000	oligotrophic	73.0534	7.4535	311.4928	333.5170	174.9212	195.8007	145.6704	88.7596	66.0347	85.4677
Buffalo Lake	974200	oligotrophic	74.9402	7.7775	233.1469	253.0921	113.9195	121.4142	133.0805	114.7840	125.8132	111.3517
Carrol Lake	1544800	eutrophic	75.0223	8.9795	83.4049	110.4472	63.9288	62.4333	55.8904	1059.0434	948.0581	1034.6933

Table C-1. (continued)

Lake Name	WDNR Lake ID	Lillie WTSI (SDT) Trophic Class	Lake Temp. (F)	YSI sonde Lake pH	PIE based P_{CO2} (µatm)	Headspace based P_{CO2} (µatm)	P_{CO2} by pH and laboratory DIC (µatm)	P_{CO2} by pH and ANC (Gran titration) (µatm)	P_{CO2} by pH and ANC (C_B and C_A) (µatm)	ANC by Gran titration (µmol L^{-1})	ANC by C_B and C_A (µmol L^{-1})	Laboratory DIC (µmol L^{-1})
Clear Lake	2329000	mesotrophic	76.5229	8.7600	166.5031	328.5905	79.7142	84.7513	71.1899	820.7240	689.3971	751.4849
Clear Lake	977500	oligotrophic	74.8095	7.6241	481.6983	504.1607	292.3020	298.3088	234.0104	198.6631	155.8427	204.4685
Crab Lake	2953500	oligotrophic	72.0758	8.0381	291.4159	333.1439	208.3345	228.2562	222.1165	408.2543	397.2729	378.1848
Escanaba Lake	2339900	mesotrophic	71.2150	7.9220	433.9354	580.8687	281.6710	313.8563	271.8435	431.0321	373.3341	395.6425
Fawn Lake	2328900	mesotrophic	78.8893	9.5428	61.2402	-5.3610	9.7752	9.6340	7.9819	727.1866	602.4832	633.6386
Flannery Lake	985300	oligotrophic	76.4207	6.8249	570.4209	524.8418	232.8551	261.1800	224.8870	27.0336	23.2771	32.0400
Found Lake	1593800	eutrophic	75.3227	8.5365	97.6091	157.8734	86.2023	87.5051	84.7604	493.8436	478.3536	480.9326
Gilmore Lake	1589300	eutrophic	74.4501	9.3295	25.9077	30.1979	17.3203	17.7182	16.7473	748.7253	707.6998	663.8079
Hasbrook Lake	1589100	oligotrophic	73.2955	8.4386	166.1321	82.3210	77.4782	81.6721	72.3152	369.3081	326.9976	348.3486
Hodstradt Lake	990700	oligotrophic	74.0298	6.9122	577.1774	530.6428	227.0161	271.0632	243.0303	35.0454	31.4211	37.3716
Horsehead Lake	1588000	eutrophic	75.2553	9.2641	71.3235	-14.5441	23.5941	23.4204	22.0655	829.2062	781.2351	765.6675
Irving Lake	2340900	eutrophic	69.9893	7.9796	596.6035	579.3357	356.8258	381.8088	329.9975	608.2915	525.7466	579.2395
Island Lake	2334400	mesotrophic	77.9224	8.4389	340.2447	569.0883	184.3946	197.5699	71.5343	876.1059	317.2126	811.5182
Katherine Lake	1543300	oligotrophic	73.9673	8.0906	246.7385	215.4876	148.6188	148.1047	133.1205	294.4485	264.6584	298.8898

Table C-1. (continued)

Lake Name	WDNR Lake ID	Lillie WTSI (SDT) Trophic Class	Lake Temp. (F)	YSI sonde Lake pH	PIE based P_{CO2} (µatm)	Headspace based P_{CO2} (µatm)	P_{CO2} by pH and laboratory DIC (µatm)	P_{CO2} by pH and ANC (Gran titration) (µatm)	P_{CO2} by pH and ANC (C_B and C_A) (µatm)	ANC by Gran titration (µmol L^{-1})	ANC by C_B and C_A (µmol L^{-1})	Laboratory DIC (µmol L^{-1})
Little Arbor Vitae Lake	1545300	eutrophic	73.6742	9.0496	74.1991	79.9017	57.8689	55.1161	49.3815	1128.9580	1011.4943	1122.3980
Little John Lake	2332300	eutrophic	72.8560	8.3438	483.1692	448.1634	293.3621	290.7401	251.6226	1072.5305	928.2274	1080.2109
Little Saint Germain Lake	1596300	mesotrophic	76.1275	8.5935	142.3913	188.1295	105.7467	108.2948	103.0008	700.7196	666.4647	673.7996
Little Star Lake	2334300	oligotrophic	77.1335	8.1723	575.0515	519.4868	323.3654	336.0808	283.3502	800.1500	674.6076	774.4935
Long Lake	1001300	oligotrophic	74.5285	7.0870	338.1908	501.7944	84.3126	133.9933	97.7604	25.7498	18.7869	19.1535
Lost Lake	1593400	eutrophic	73.8421	9.0638	45.3840	59.8358	38.0152	38.2748	36.2020	804.7101	761.1294	756.3974
Madeline Lake	1544700	eutrophic	74.4069	7.7233	1490.2035	1407.2597	1022.4178	1106.0089	990.0661	949.2092	849.7037	910.9076
Manitowish Lake	2329400	mesotrophic	77.8994	8.3943	369.0030	648.8963	203.5516	211.8266	178.6837	845.8073	713.4701	808.4652
Mann Lake	2332000	eutrophic	70.6375	9.8700	4.7536	-23.5330	4.8566	4.5054	4.0052	980.4638	871.5982	826.9775
McNaughton Lake	1587600	eutrophic	76.1151	9.9284	41.4487	15.5670	2.4979	2.5931	2.5591	673.6032	664.7857	492.3952

Table C-1. (continued)

Lake Name	WDNR Lake ID	Lillie WTSI (SDT) Trophic Class	Lake Temp. (F)	YSI sonde Lake pH	PIE based P_{CO2} (µatm)	Headspace based P_{CO2} (µatm)	P_{CO2} by pH and laboratory DIC (µatm)	P_{CO2} by pH and ANC (Gran titration) (µatm)	P_{CO2} by pH and ANC (C_B and C_A) (µatm)	ANC by Gran titration (µmol L^{-1})	ANC by C_B and C_A (µmol L^{-1})	Laboratory DIC (µmol L^{-1})
Minocqua Lake	1542400	mesotrophic	72.4831	8.3400	345.2782	429.0133	256.2258	259.6703	233.2852	955.1929	858.1360	940.8826
Pickerel Lake	1590400	eutrophic	72.1580	9.6655	4.3887	77.7292	6.2317	6.2794	5.9284	706.5353	667.0402	586.6223
Plum Lake	1592400	mesotrophic	70.9495	8.1506	472.8329	515.1459	363.2989	365.5495	312.3475	866.5329	740.4178	868.4430
Presque Isle Lake	2956500	oligotrophic	70.5474	8.5997	311.7635	242.9667	200.6272	196.9627	185.8387	1365.1889	1288.0859	1369.6919
Razorback Lake	1013800	mesotrophic	73.2746	8.6814	104.4677	13.3748	41.6947	41.8892	36.3158	338.1572	293.1652	330.2248
Snipe Lake	1018500	mesotrophic	76.6833	8.4113	31.4634	-2.7060	20.4814	22.4770	25.3062	92.3491	103.9729	83.7497
Spider Lake	2329300	mesotrophic	78.6632	8.2660	519.0460	480.0752	280.4192	338.8186	250.8067	993.5639	735.4747	823.0919
Star Lake	1593100	oligotrophic	73.2551	8.4841	227.0513	195.1956	127.3164	129.0694	110.8835	657.0187	564.4446	642.5479
Stone Lake	2328800	mesotrophic	79.4371	8.4712	298.2881	437.3496	173.1716	179.2998	150.5275	848.6872	712.4977	811.8512
Sweeny Lake	1589600	eutrophic	74.0852	8.9428	76.7684	128.5466	59.2171	59.6382	55.5280	923.0891	859.4700	878.9897
Towanda Lake	1022900	mesotrophic	70.9550	7.7407	293.6705	286.1859	118.4661	141.0014	131.3170	126.3446	117.6668	110.2692
Trout Lake	2331600	oligotrophic	68.8319	8.5101	184.9889	291.4401	154.5275	154.9100	138.7295	869.5676	778.7400	859.5615
Upper Gresham Lake	2330800	mesotrophic	76.4344	8.5750	258.0503	259.7699	139.3631	143.6662	123.8797	896.0678	772.6564	856.2309

Table C-1. (continued)

Lake Name	WDNR Lake ID	Lillie WTSI (SDT) Trophic Class	Lake Temp. (F)	YSI sonde Lake pH	PIE based P_{CO2} (µatm)	Headspace based P_{CO2} (µatm)	P_{CO2} by pH and laboratory DIC (µatm)	P_{CO2} by pH and ANC (Gran titration) (µatm)	P_{CO2} by pH and ANC (C_B and C_A) (µatm)	ANC by Gran titration (µmol L^{-1})	ANC by C_B and C_A (µmol L^{-1})	Laboratory DIC (µmol L^{-1})
Van Vliet Lake	2956800	eutrophic	72.7155	9.2882	43.8282	1.6036	28.1315	27.6311	26.4591	1059.1781	1014.2505	986.4002
White Birch Lake	2340500	mesotrophic	74.0677	8.5578	179.4578	125.5038	92.9991	96.5201	85.0302	579.6056	510.6088	551.5404
White Sand Lake	2339100	oligotrophic	71.7895	8.3200	328.4521	349.5053	198.7501	201.9104	162.5504	703.7939	566.5977	692.7560

APPENDIX D

Table D-1. A comparison of total sample analytical measurement time (N = 52) in the laboratory for the direct and indirect dissolved carbon dioxide measurement methods used in the *PIE in a fifty-two lake surface water survey*.

Methods to Measure P_{CO2}

(N= 52 lake samples)

Method	Collecting Sample for Laboratory Analytic Measurement	Sample Analytic Measurement Time in Laboratory
PIE based P_{CO2}	None! (Real Time Continuous; 1 record/ sec)	None!
Headspace based P_{CO2}	One bottle (gas) sample	6 Hours (automated)
P_{CO2} by pH and DIC	One bottle (liquid) grab sample	12 Hours (automated)
P_{CO2} by pH and ANC (Gran titration)	One bottle (liquid) grab sample	20 Hours (manual)

APPENDIX E

Accuracy and precision of PIE based measurements in estimating the pK_a of carbonic acid - Experiment 6.

This experiment was used to show the accuracy and precision of PIE based measurements in estimating the pK_a of an acid. The negative log of the first dissociation constant (pK_a) of an acid expresses the pH buffering characteristic of a particular acid and its base. This means that the acid-base system will resist change most effectively within a narrow pH range of 3.4 units wide that is centered on its pK_a value. When the concentrations of the acid and base forms are equal in solution, the value of the pH (Eq. [E1]) is equivalent to the negative log of the first dissociation constant of the acid (pK_a):

[E1] $$pH = pK_a .$$

For example, when the concentrations of the acid and base forms of carbonic acid are equal in solution, the value of the pH is equivalent to the negative log of the first dissociation constant of carbonic acid (pK_1).

PIE based measurements can be used to estimate the known pK_1 or pK_a of carbonic acid at a given temperature. A theoretical construct in carbonic chemistry is used to estimate this pK_a. The theoretical construct is completed by using a ratio of PIE based measurements (ratio, Eq. [E2]) to graph the fraction of total DIC (carbonic acid) in base form versus the pH to estimate the pK_1 or pK_a of the acid:

[E2] $$\text{ratio} = 1 - \frac{[H_2CO_3^*]}{DIC}.$$

By acidifying solutions of sodium bicarbonate with known additions of sulfuric acid, the amount of solution in the acid form can be measured. From this, the percent of solution in the base form can be estimated from Eq. [E2] and graphed against the pH (Figure E-1). A horizontal bisector line can then drawn through the 50 % acid and base point on the ratio s-curve. Next, a perpendicular bisector line can be dropped down at the point of intersection of the horizontal bisector line and the ratio s-curve, and the pH read. This pH (Eq. [E1]) constitutes the estimation for the pK_1 or pK_a of carbonic acid.

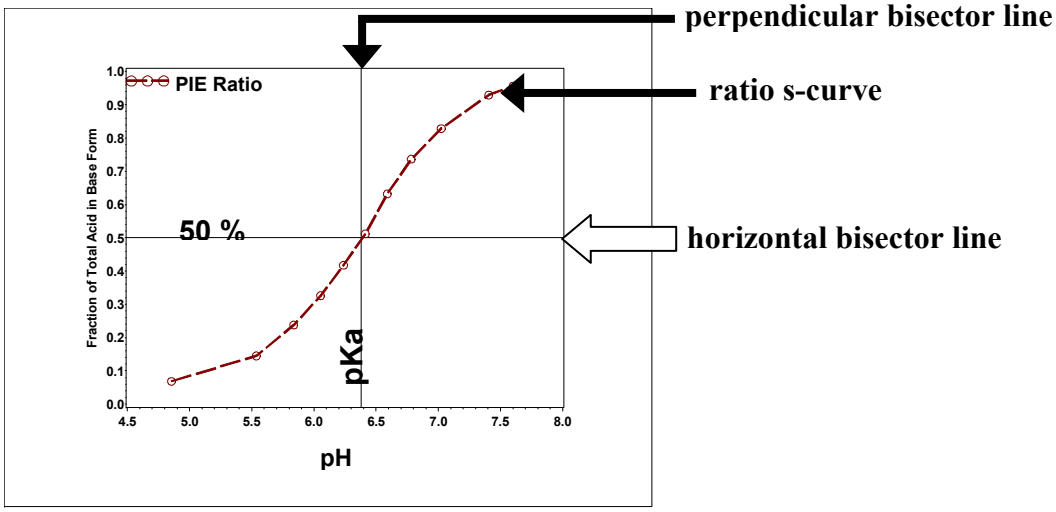

Figure E-1. Theoretical construct for estimating the pK_1 or pK_a of carbonic acid. The theoretical construct was completed by using a ratio of PIE based measurements (ratio, Eq. [E2]) to graph the fraction of total carbonic acid in base form versus pH to estimate the pK_1 or pK_a (Eq. [E1]) of the acid.

The theoretical construct (Figure E-2) was completed by using a ratio of PIE based measurements (ratio, Eq. [E2]) to graph the fraction of total DIC (carbonic acid)

in base form versus the pH to estimate the pH (Eq. [E1]). A pK_a of 6.38 pH was estimated for the carbonic acid, which matches the theoretical value at this temperature (@ 20°C, Harned and Bonner, 1945).

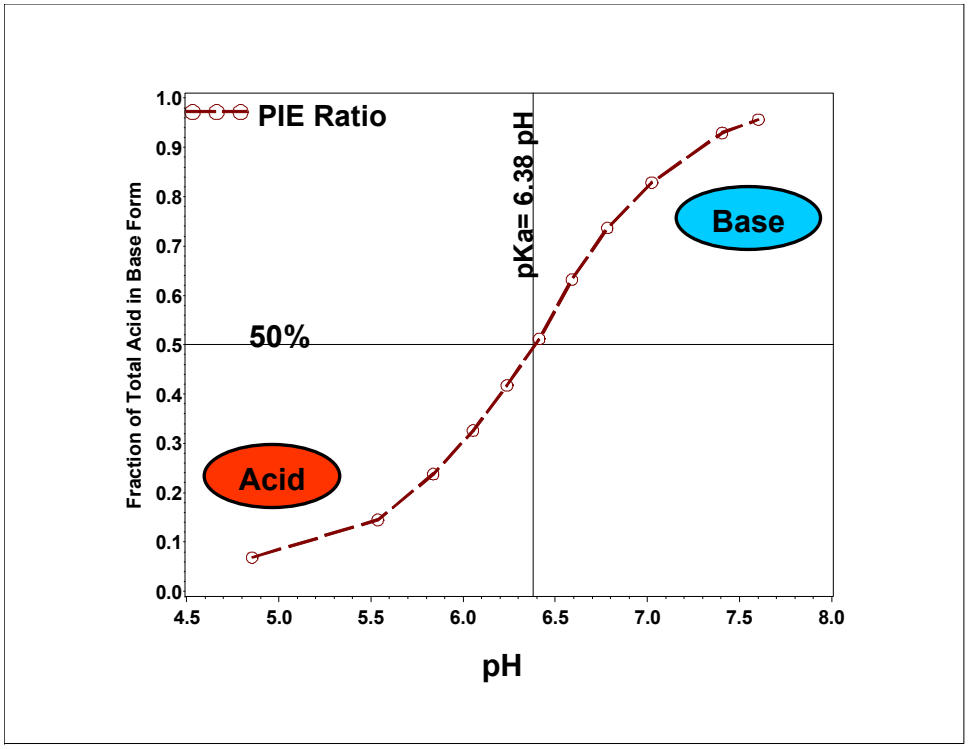

Figure E-2. Experiment 6 (N = 11), theoretical construct for estimating the pK_1 or pK_a of carbonic acid. The theoretical construct was completed by using a ratio of PIE based measurements (ratio, Eq. [E2]) to graph the fraction of total carbonic acid in base form versus pH to estimate the pK_1 or pK_a (Eq. [E1]) of the acid (estimated pK_a = 6.38 pH @ 20).

APPENDIX F

The majority of the Fifty-two lakes in this study had surface waters undersaturated with dissolved carbon dioxide.

As described in the *Introduction*, recent studies of lake metabolism have shown that most of the world's lakes surface waters are supersaturated with dissolved carbon dioxide (Sobek et al., 2005), suggesting that lakes may be a net source of carbon dioxide emission into the atmosphere (Sobek et al., 2005). However, most of the lakes in the *PIE in a fifty-two lake surface water survey* were not supersaturated with dissolved carbon dioxide. According to PIE based dissolved carbon dioxide measurements in Figure F-1, thirteen lake samples were oversaturated and thirty-nine lake samples were undersaturated with respect to the July 2007 ambient atmospheric global average of 362 μatm P_{CO2} (381 ppmv P_{CO2}; Tans, 2008). Therefore, most of these lakes are a sink for atmospheric carbon dioxide.

It is interesting to note that all the traditional direct and indirect dissolved carbon dioxide measurement methods used for the fifty-two lakes in Figure F-1, also showed that most of the fifty-two lakes were undersaturated with respect to ambient atmospheric P_{CO2}. Specifically, headspace based P_{CO2}, P_{CO2} by pH and laboratory DIC, P_{CO2} by pH and ANC (Gran titration), and P_{CO2} by pH and ANC (C_B and C_A) methods only found sixteen, two, three, and one lake samples, respectfully, that were oversaturated with respect to ambient atmospheric P_{CO2}.

These findings do not necessarily refute the supersaturation findings in Sobek et al. (2005). Considering that only 150 of the worlds lakes had direct measurements of carbon dioxide and 4582 of the worlds lakes have been indirectly measured (Table 1), more research is needed and many more lakes will have to be directly measured with PIE to build a better picture of why these particular lakes in this study were undersaturated with respect to atmospheric carbon dioxide.

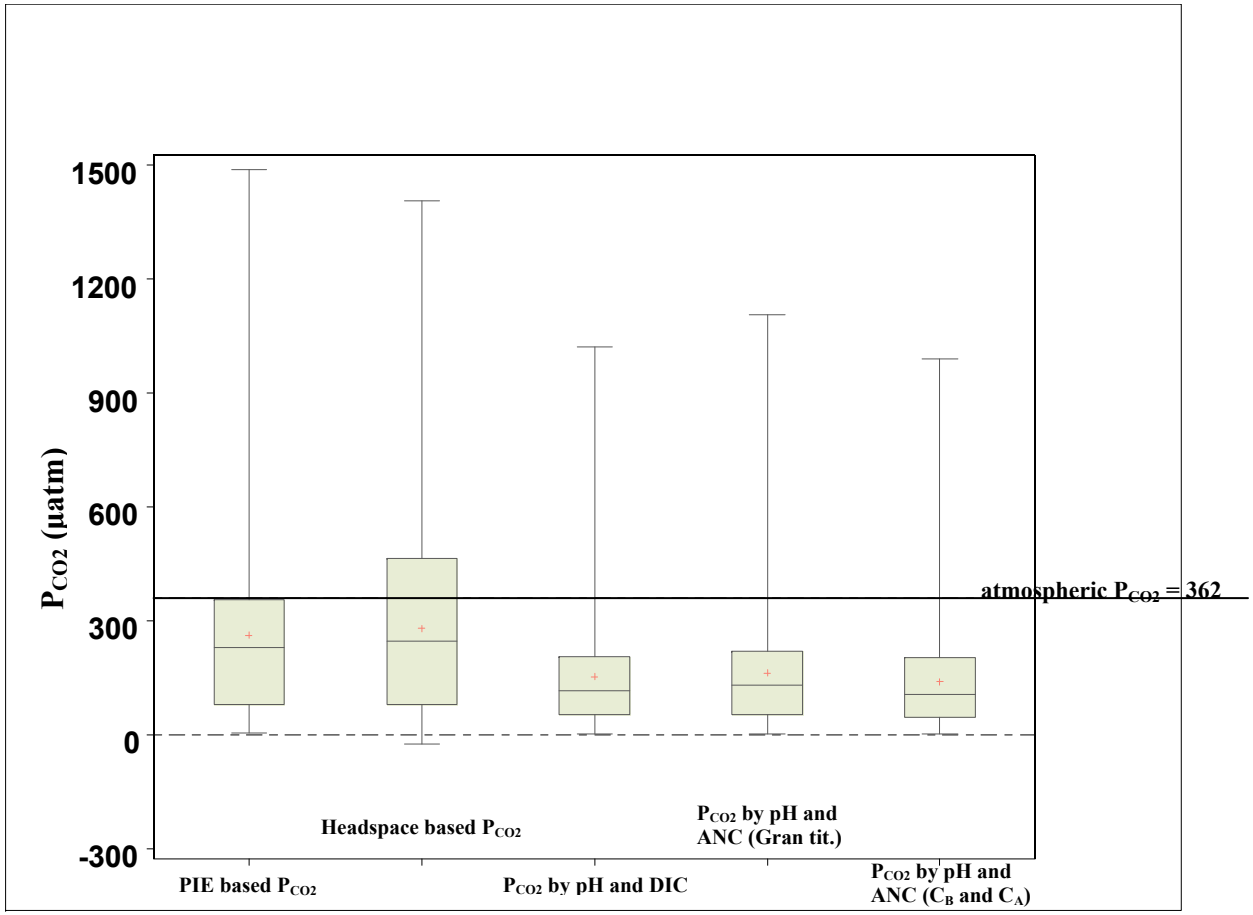

Figure F-1. PIE in a fifty-two lake surface water survey (N = 52), measured P_{CO2} by method, including PIE based P_{CO2}, headspace based P_{CO2}, P_{CO2} by pH and laboratory DIC, P_{CO2} by pH and ANC (Gran titration), and P_{CO2} by pH and ANC (C_B and C_A).